SOUND ABSORPTION IN ACOUSTICALLY TREATED DUCTS IN THE PRESENCE OF OBLIQUE WAVES

Peter A. Marino, Jr.

June, 1970

The Pennsylvania State University

The Graduate School

Sound Absorption in Acoustically Treated Ducts in the Presence of Oblique Waves

A Thesis in

Engineering Acoustics

by

Peter A. Marino, Jr.

Submitted in Partial Fulfillment
of the Requirements
for the Degree of

Master of Science

June, 1970

Date of Approval.

Gerhard Reethof
Alcoa Professor of Mechanical Engineering
Thesis Adviser

Richard O. Rowlands
Chairman of the Committee on Engineering Acoustics

ACKNOWLEDGEMENT

The author wishes to express his appreciation to Dr. Gerhard Reethof, Alcoa Professor of Mechanical Engineering, under whose guidance this thesis was conducted. Thanks are also due Dr. Eugen J. Skudrzyk, Professor of Physics, and Dr. Jiri Tichy, Associate Professor of Architectural Engineering, for their help in formulating the basic analysis.

This work was made possible by a grant from the National Aeronautics and Space Administration's Langley Research Center (NGR 39-009-121) whose financial support is gratefully acknowledged.

TABLE OF CONTENTS

LIST OF FIGURES

Figure Page

LIST OF TABLES

NOMENCLATURE

Symbol	Description
a	Length Dimension
B	Constant
c	Speed of Sound
f	Frequency
I	Intensity
J	$\sqrt{-1}$
k	Wave Number
L	Length Dimension
m	Integer Number
M	Integer Number
n	Integer Number
N	Integer Number
p	Integer Number
P	Pressure
s	Length Dimension
t	Time
x	Coordinate Axis
y	Coordinate Axis
z	Coordinate Axis
α	Angle Designation
β	Angle Designation
γ	Angle Designation
δ	Attenuation Constant

Symbol	Description
η	Angle Designation
θ	Angle Designation
κ	Phase Angle
Λ	Velocity Potential
λ	Wave Length
υ	Reflection Constant
T	Reflection Coefficient
ϕ	Angle Designation
Φ	Coefficient of Sound Pick Up
ψ	A Reflection Constant
ω	Angular Frequency

CHAPTER I

INTRODUCTION

The high intensity noise generation of jet engines needs no introduction. A visit to any of this country's major airports is enough to convince the observer that noise is one of the most unpleasant by-products of aeronautics. In the past, the technological advances that have led to the development of the contemporary jet engines have been made with little regard to the noise levels produced. Because the emphasis in the design of aircraft continues toward larger and more powerful engines, the noise generated by these engines approaches the intolerable point for both people and structures. In fact, with the advent of the supersonic transport, we may well be approaching the level of noise pollution that people will not accept. This in conjunction with the acoustics fatigue failures of aircraft structure is making noise one of the major limiting factors in the design and operation for all types of aircraft to be used in the future. (1)

It certainly is not postulated that intolerable noise is a necessary consequence of future aircraft engine development; therefore, one of the major tasks facing the engineer now and in the future is the control of this aerodynamic noise. One, however, cannot control that which he does not fully understand. Therefore, before any real results in noise abatement can be realized, a basic understanding of the mechanisms of the noise

sources and the propagation of the high intensity sound waves must be obtained.

There have been two methods of approach to resolving this noise problem. The first and most difficult method is that of eliminating the noise through a change in the design considerations of the actual components in the jet engines. A good summary and list of references in this area of investigation is given by Lawson, 1968. (2) This approach, as Morfey states, has two main stumbling blocks (a) finding which design parameters have a significant effect on the sound output of the fan, compressor, or any other noise generating component, and (b) how much must be given up in optimum component design and engine efficiency to obtain acceptable noise levels. (3) The second field of investigation is the actual absorption of the sound in the engine after it has been generated by one or a combination of the components. Despite the fact that there are numerous applications of attenuating and/or absorbing devices which, in fact, have been used in jet engines for many years, there is very little in the way of an edifying theory that would describe a design criteria for particular material configurations that could be used as satisfactory attenuators of the noise levels. (4) The main reason for this lack of information is that, in the past, absorptive liners have been designed on an ad hoc basis of inserting a piece of porous material into a portion of the engine with the intention of eventually absorbing the high sound levels. One of the reasons for this attitude in design has been a lack of basic research in

the attenuation of sound waves approximating that which is present in jet engine ducts. It was the purpose of this program to take an initial step by designing the necessary equipment and making an experimental investigation that could supply data to help fill this gap.

A study of the previous sound transmission investigations as applied to jet engines show that the majority of experimental data has been obtained by the propagation of plane waves down a uniform duct. In more cases than not, these transmission and insertion loss tests using plane waves have been conducted on absorptive materials not particularly applicable to jet engines. It has been shown by various investigators including J. M. Tyler and T. G. Sofrin (5) that higher order modes of transmission are of primary importance in jet engine noise evaluation. In particular, these higher modes in which Tyler and Sofrin were interested (called "spinning modes") are waves radiated from the front of axial compressors and fans. These higher modes of propagation result in much of the annoying noise generated to the ground by landing aircraft. Because of the significant contribution these "spinning modes" make to the noise pollution of our communities, it is highly desirable to attenuate these higher modes before propagating out of the jet engine.

The purpose of this study, then, is to investigate the transmission and attenuation of some of these higher order modes as they are propagated in a rectangular duct. Though a device is available that could be used to generate a "spinning mode" in

the duct (6), it was believed more beneficial to first study what effect simpler order modes of propagation might have on the relative sound absorption characteristics of sound absorbent materials. In order to conduct these tests, a modified traveling wave duct was constructed that was capable of accepting, as a lining, the various absorptive configurations to be tested as possible attenuators of the higher duct modes. These configurations were then tested for their insertion loss qualities when the wave modes were propagated down the duct. By using a lined duct configuration as mentioned above one simulates the physical reality of attenuating the discrete frequency noise propagating through the air intake of jet aircraft engines. It is hoped that the insertion loss results obtained from this study can later be applied to, and possibly simplify, the task of improving the methods of attenuating a "spinning mode" as it is propagating down a uniform duct or tube.

CHAPTER II

DESIGN OF EXPERIMENTAL MODEL

2.1 General Description

Straight ducts of constant cross section are frequently used as wave guides and sound conductors in acoustical experimentation. Ducts of this type can be used as impedance tubes for precise measurement of the resistive and reactive components of the normal acoustic impedance of a sound absorber (7), and they can be used as lined ducts to measure the insertion loss or attenuation of sound waves impinging on the walls at a grazing incidence. (8) The normal impedance and normal absorption coefficient, though of academic interest, are not directly applicable to the tests conducted under this program save for the use of these quantities in the standardization and classification of various samples used in the attenuation tests. Therefore, the bulk of experimentation has been conducted with the purpose of determining the effects of sound waves that are of grazing incidence with respect to the various samples under consideration.

The first use of the concept of a duct as an impedance tube and a wave guide seems to come from H. O. Taylor. (9) From this time on, the device has continuously been improved first by R. A. Scott (10) and by L. L. Beranek (7), and then more recently by this writer (11) and W. C. Sperry (8) to the point where an acoustic wave guide of this type can be used to obtain basic

acoustic data that could be applied directly to jet engines. The wave guide we have used in our tests is shown in Figure 1.

A microphone mounted probe tube was used in exploring the standing wave patterns and for measuring the sound pressure levels at various positions in the tube. The probe tube is connected to a small condenser microphone which is carried on the traversing mechanism shown in Figure 2. The position of the probe was varied by mechanically turning a lead screw on the traversing mechanism and the rotation of this lead screw allowed the microphone sensor to read at various locations in the duct. A scale on the side of mounting (Figure 3) was used to record the probe tube position in the duct.

The duct could be used as both a traveling wave and standing wave device depending on its end termination. To provide a traveling wave for making attenuation measurements, an anechoic termination was designed that would reduce the reflections of the propagating wave from the end of the duct. A satisfactory solution to this end reflection problem was a necessary step toward accurate attenuation measurements.

The sound source used to generate the incident waves was enclosed in a specially designed box so that it could be placed at any angle from 0° to 90° in relationship to the sample configurations on the side of the duct. By adjusting a slide bar, one can control the angle at which the sound source is placed, and this angle determines the direction of propagation in relationship to the absorbing samples lining the duct. The

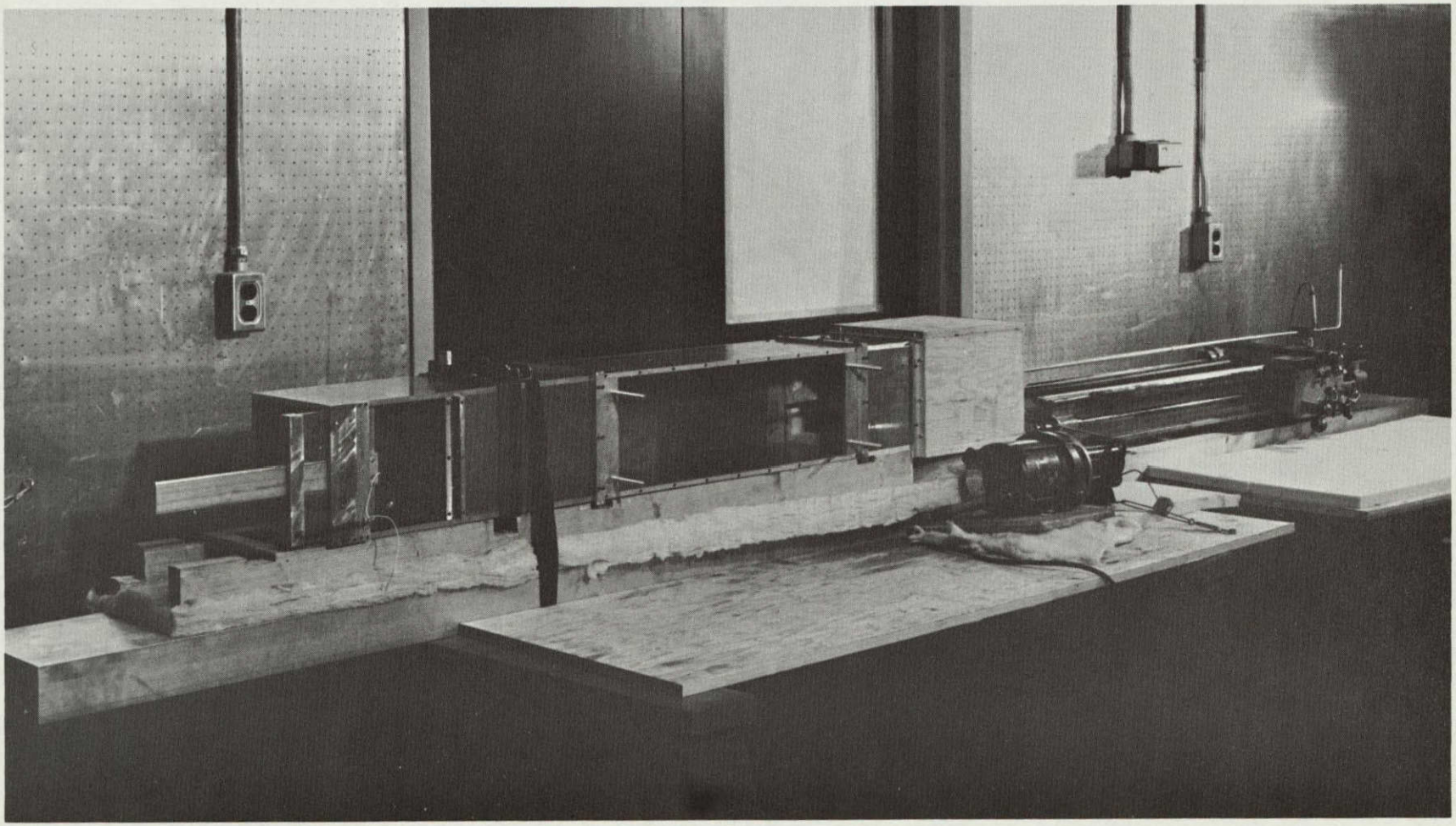

Figure 1 Experimental Model Used for Traveling and Standing Wave Tests

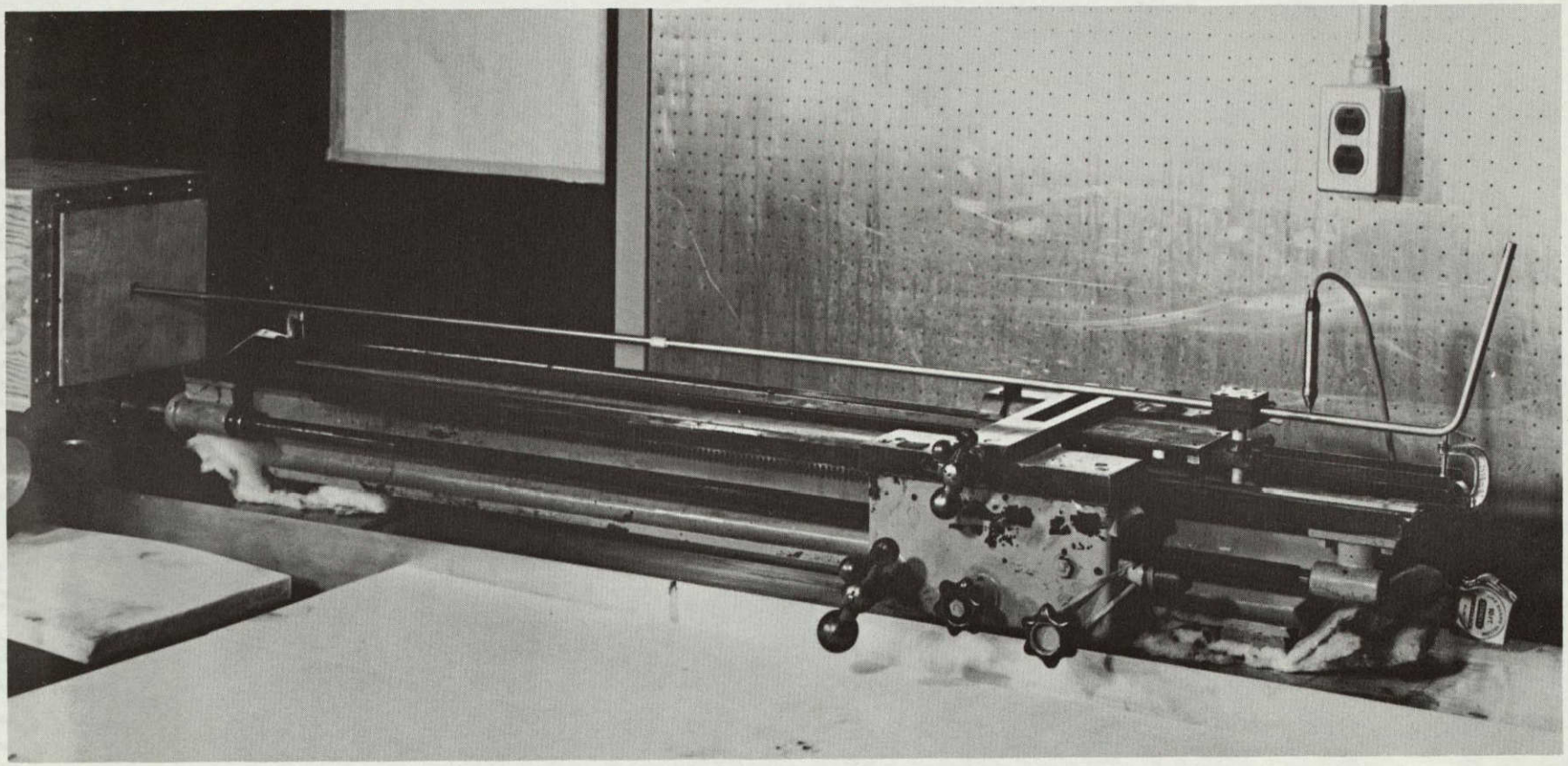

Figure 2 Traversing Mechanism

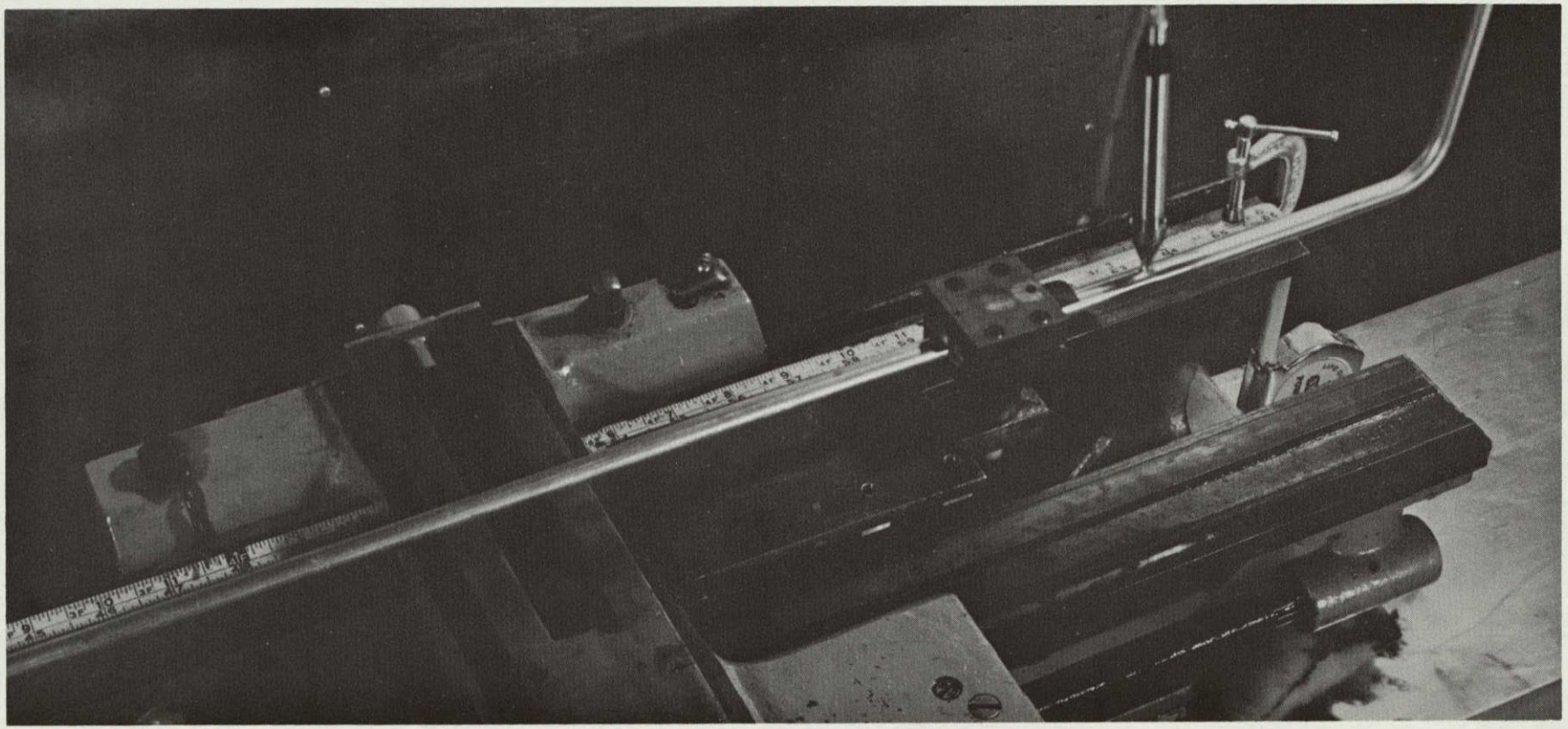

Figure 3 Scale Used to Measure Probe Position

reflected wave components present in the duct then represent higher modes of propagation. (12)

A flow resistance measuring device is used in conjunction with the traveling wave duct. The purpose of this device is to determine values of acoustical resistance for the sample configurations that were used as attenuating devices. The DC flow resistance is related to the ability of a material to absorb sound energy. The value of flow resistance must be optomized to a maximum absorption for each type of material tested. Many manufacturers supply DC flow resistance values for their products, but it has been the experience of this writer that the general values supplied are often unrepresentative of a particular piece of material. Therefore, it was deemed necessary to build a device that could be used to determine the resistance of the individual samples that were placed in the duct.

2.2 Duct Specifications

The duct described herein has been designed and built to meet the specific requirements that are most generally accepted for measuring sound absorption and transmission loss. This acceptance is based on the fact that field conditions can be made to closely simulate the incidence of sound and methods of mounting the samples.

Part of this design criteria is given in the recommendations of the "American Society for Testing of Materials" set forth in Reference 13. These design requirements will be briefly outlined below.

The first of these requirements to be met is that the tube must be straight and have rigid walls. The walls must be thick enough to eliminate any vibration that would cause dissipation of sound energy through them. A theoretical investigation of losses in the tube is given in Appendix A of this paper. A schematic of the duct is shown in Figure 4. This duct is made from 3/8-inch thick aluminum alloy. As can be seen from Figure 4, the main testing section is a total of 64 inches long and broken into four sections. Sections I and II are 8-inch long solid sections that can be used for microphone ports is necessary. In our tests, Section II held an anechoic termination, while Section I was just used to increase the tube length. Sections III and IV of the duct are the holders capable of accepting facing materials as branch sections. The overall duct configuration is square in cross section in order to facilitate the design and placement of the sound absorbing materials as seen in Figure 5.

The length and cross sectional inside dimension of the duct is dependent upon the frequency range of interest. The length must conform to the following relation.

$$\ell \geq \frac{1000}{f_{min}} \quad . \tag{2.1}$$

What is to be derived from Equation (2.1) is that for any frequency f and characteristic wave length λ, being generated as a standing wave, two pressure minimums are required to measure

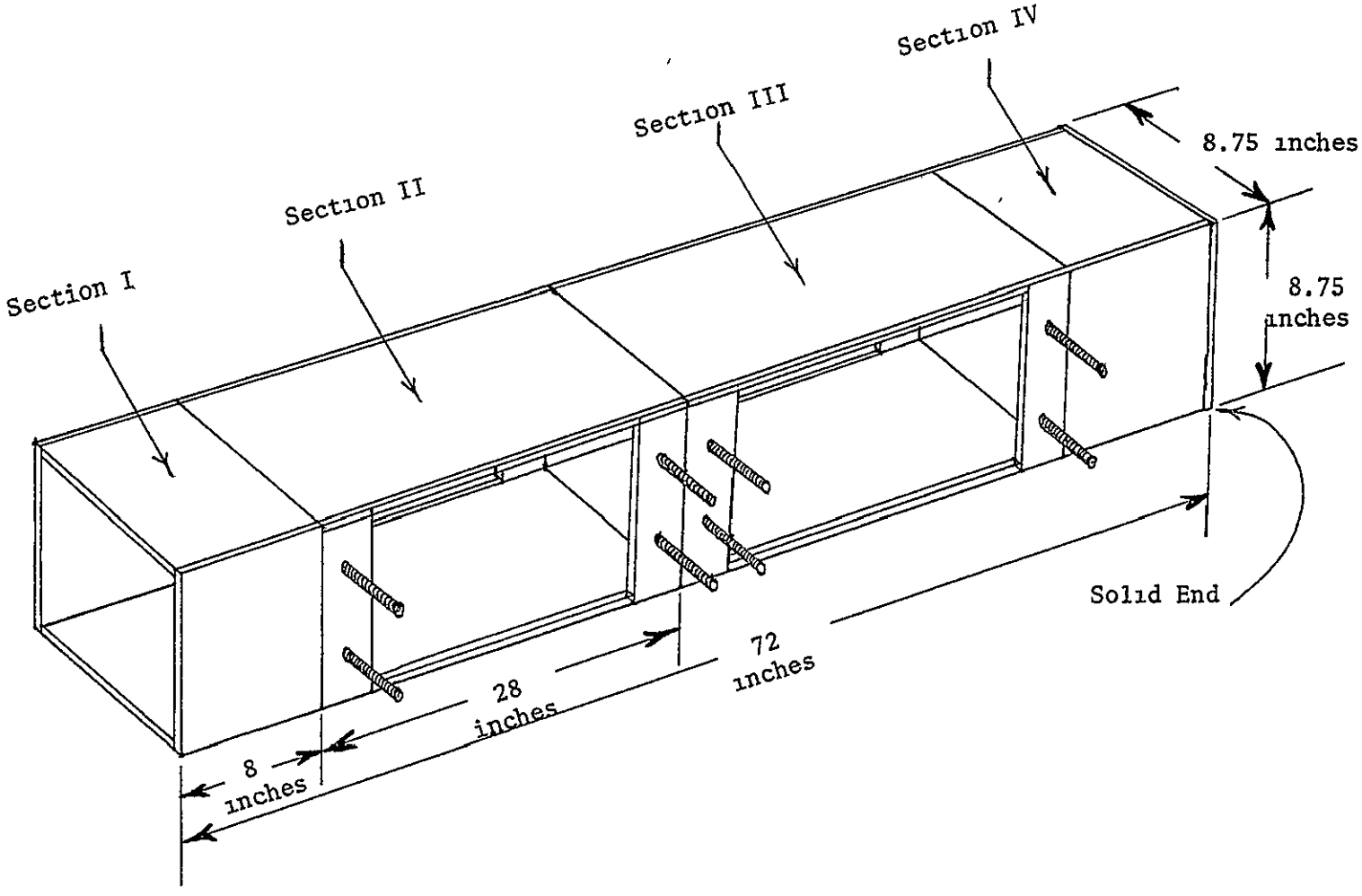

Figure 4 Schematic of Duct

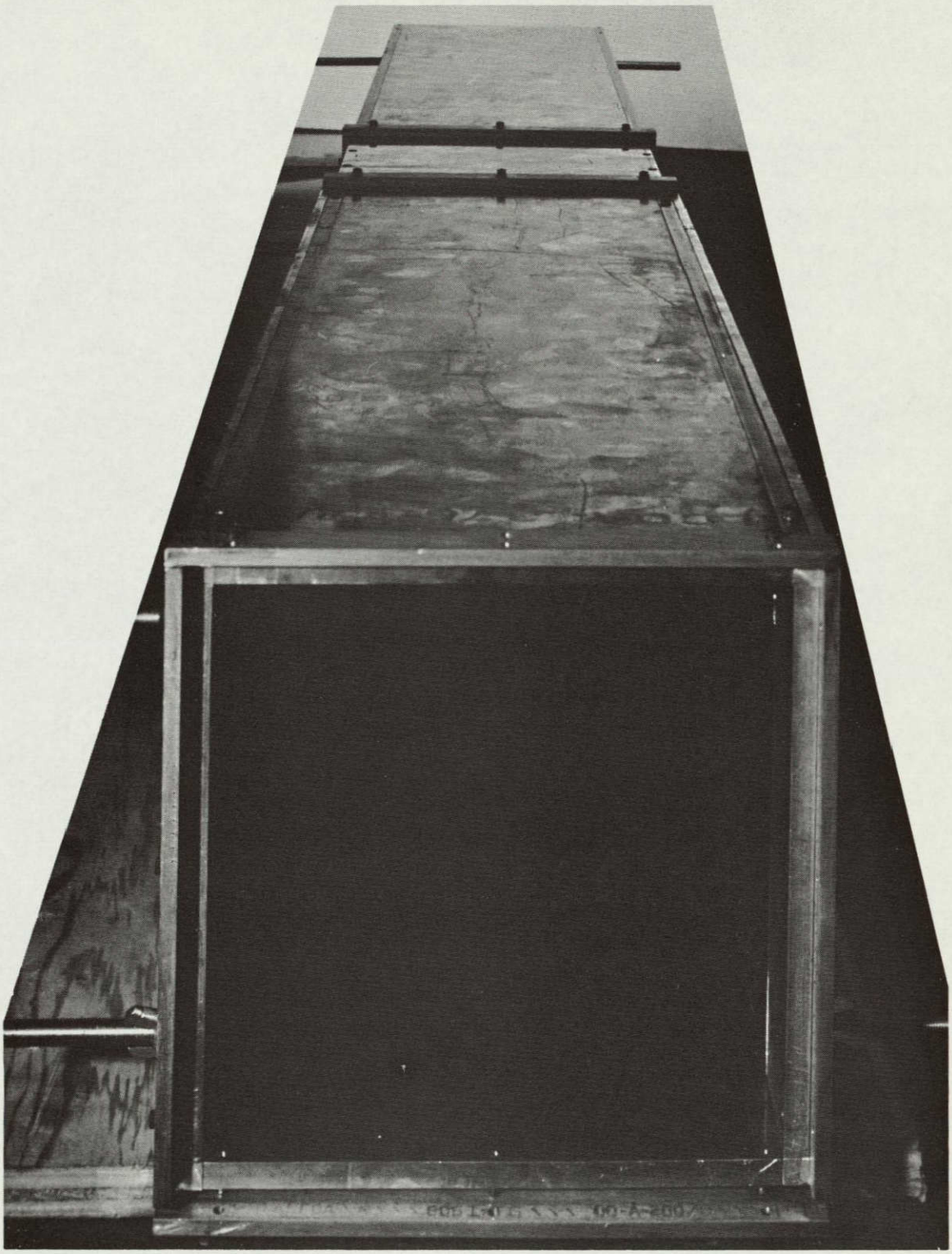

Figure 5 Duct Used for Tests

specific acoustic impedance. The length of the tube must allow for the propagation and measurement of these two minimums. For a duct of 64 inches in length, as ours is, the allowable frequency that can be used to measure normal specific acoustic impedance must not be less than 190 Hz.

The dimensions of the cross sectional area are determined by a relationship similar to Equation (2.1) except that parameters govern the maximum frequency one is able to propagate down the tube. The inside cross sectional dimension must conform to the following relation:

$$S \leq \frac{7000}{f_{max}} \quad . \tag{2.2}$$

Equation (2.2) is a relation used to avoid higher order modes in ducts when measuring normal acoustic impedance. Within the frequency range dictated by f_{max}, one can propagate a plane wave down the tube. For our tests, sound waves of frequency greater than f_{max} were used so that the transmission loss of these higher modes could be measured. However, for normal measurements of the acoustic impedance, the maximum frequency that would still give us a plane wave, as calculated from Equation (2.2), was approximately 1000 Hz. Actual measurements showed 1400 Hz to be a more representative figure.

It should be emphasized that although there is some leeway in the above design considerations, it is essential that one not significantly depart from any of the above conditions.

2.3 Probe Tube Specifications

The microphone probe tube is a long thin piece of 1/4-inch stainless steel tubing having a microphone mounted 6 inches from its end at a right angle to the axis of the tube. See Figure 6. With such a setup, one can measure the intensity in the sound field with less disturbance than if the microphone were used by itself to probe. One would ideally prefer to have the sound intensity, after being picked up at the probe tube tip, reach the microphone face without a change in level. However, a real probe will transmit energy through its walls. The problem in designing the probe, then, is to make the diameter of the tube large enough so that the signal transmitted down the tube to the microphone is much greater than the sound transmission through the walls while at the same time making the tube diameter small enough to allow no production of disturbance in the sound field. During theoretical and experimental investigations associated with the program outlined in Reference (11), it was found that a microphone probe tube with a cross sectional area not greater than 10 percent of the cross sectional area of the impedance tube will not cause a significant disturbance in the sound field. According to Reference (13), "the wall thickness of the probe tube shall not be less than approximately one-eighth of its diameter." The microphone probe tube used for these experiments was kept within the limits of the above mentioned specifications. However, in order to avoid a possible error in using a probe tube, a theoretical and experimental investigation of how much sound

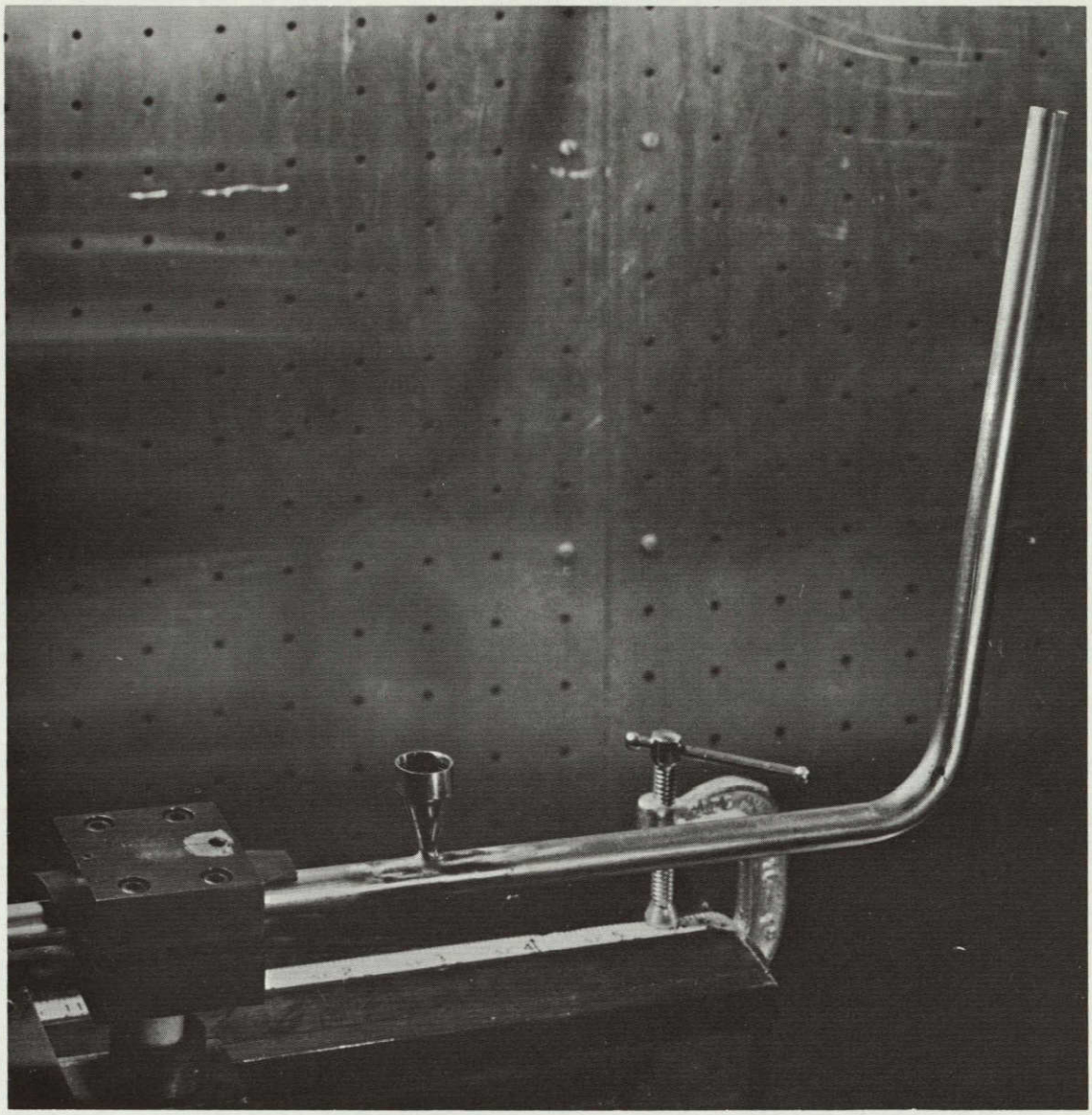

Figure 6 Microphone Mount

could be transmitted through the walls is presented in Appendix B. A last precaution was to pack the final 8 inches with fiber glass to prevent reflections from the end of the probe.

2.4 Mount for the Sound Source

The horn driver was mounted on a variable position plate at one end of the duct. This plate mounted in a box could be varied in position from lying parallel to the duct axis to a point where it was perpendicular to the duct axis. (See Figure 7.) The only precautions to heed in building this sound source holder is to avoid any transmission of the sound out of the back of the duct. By designing the sound source box with another movable plate, as shown in Figure 8, any transmission that occurred out of the rear of the box was negligible.

2.5 Anechoic Termination

Whenever a sound wave traveling down a duct reaches some discontinuity, part of the wave is reflected back towards the source. In a closed duct of some arbitrary termination, a standing wave is formed in the duct due to the discontinuity in the duct caused by the termination. For our tests, we want to reduce the terminating discontinuity to a minimum and generate a traveling wave. To generate a free traveling wave, one must either make the duct infinitely long or terminate it by a perfectly absorbing termination. Since the former solution is impractical, the latter method of approach was chosen.

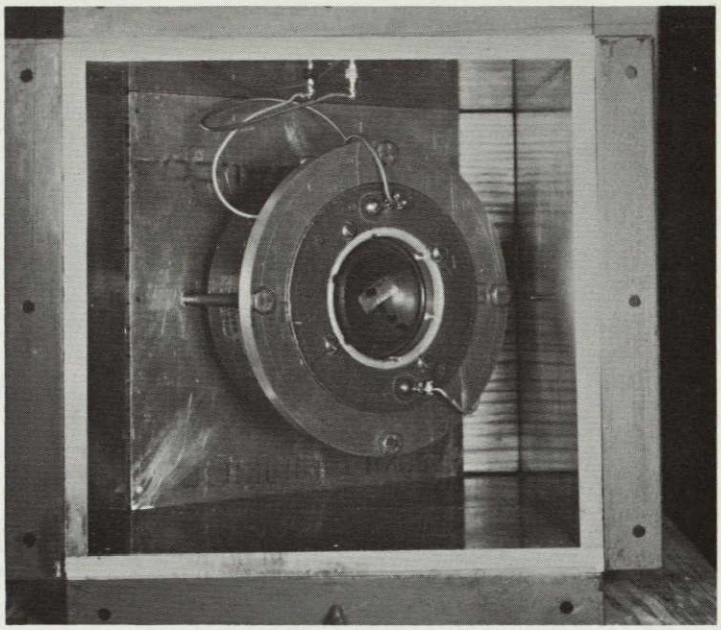

Figure 7 Variable Plate

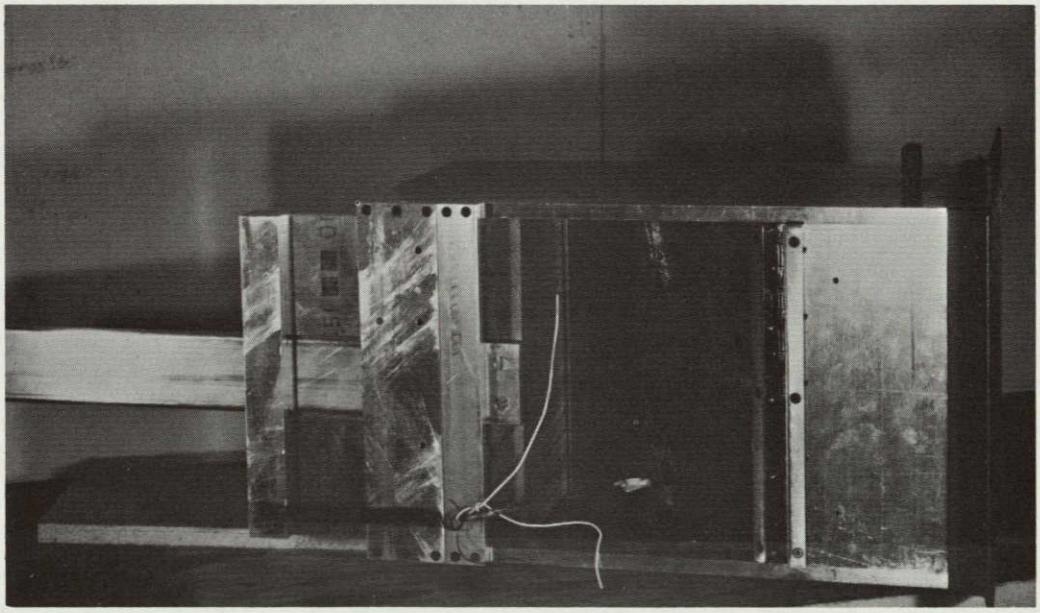

Figure 8 Speaker Box

The method used for testing the efficiency of these terminations was that of measuring the standing wave ratio formed in the duct as a result of the combining of the energy generated from the source and the energy reflected from the termination. The termination resulting in a standing wave ratio of zero over the frequency range of interest is the ideal case. British Standards Institute (14) advises that, for a plane wave source to be generating a free traveling wave in a duct, the standing wave ratio should not be more than 3 dB.

The anechoic termination finally decided upon was a modified wedge used in the design of an anechoic chamber. Of all the configurations tested, this wedge, shown in Figure 9, allowed the sound waves to terminate with a minimum of distortion over the broadest frequency range. As can be seen from the curve in Figure 10, the wedge used to terminate the duct fell well within the specifications set forth in Reference (14). For a comparison, the standing wave ratio of a high absorption piece of foam material with a solid backing is also plotted in this figure. Figure 11 shows the placement of the wedge in the terminating section of the duct.

2.6 End Plate to Measure Radial Pressure Distribution

To measure the transmission loss of a particular sample, one must measure the pressure amplitude along the axis of the tube. To insure the accuracy of the measurements, the variation of pressure with radial distance from the tube axis must be known.

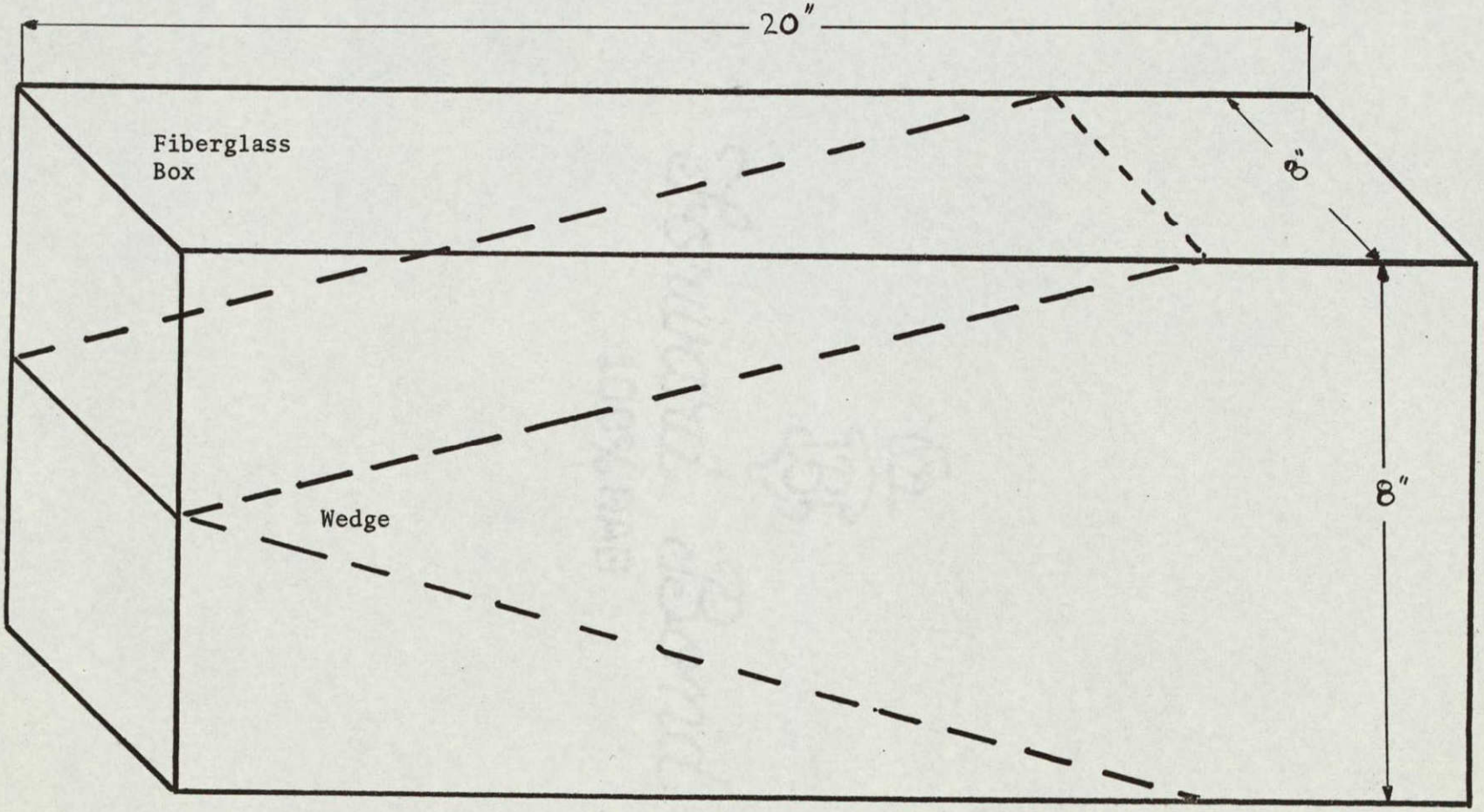

Figure 9 Schematic of Fiberglass Enclosure Used For Anechoic Termination

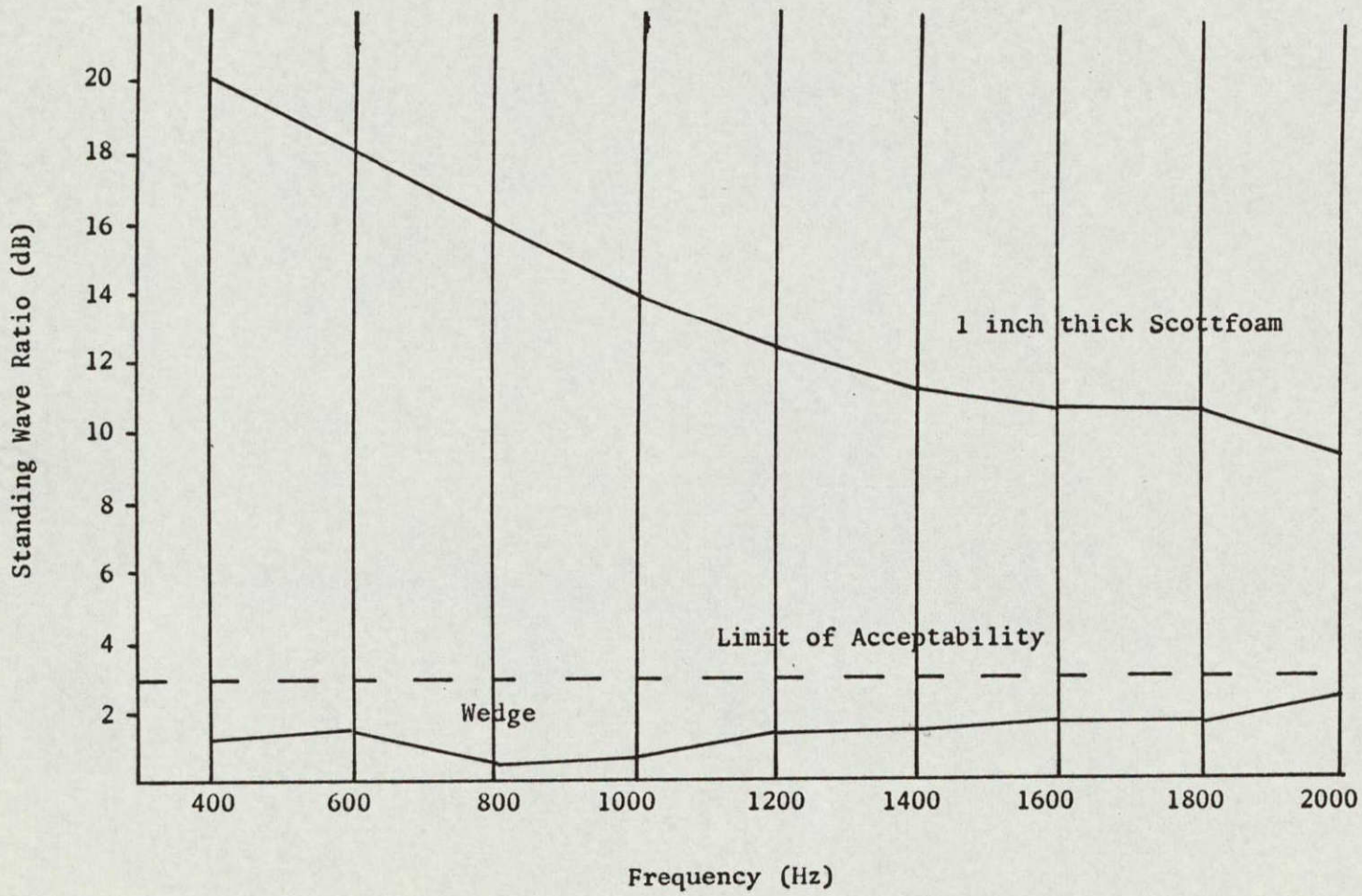

Figure 10 Effectiveness of the Anechoic Termination

Figure 11 Wedge Mounting for the Duct

If there is a significant variation in pressure amplitude along the radial dimensions, the transmission loss measurements cannot be made with just one probe tube traversing the centerline of the duct. Therefore, a series of tests for various frequencies and speaker inclinations to determine the pressure amplitude as a function of radial position were conducted using the specially designed end plate shown in Figure 12. Four frequencies (400 Hz, 1000 Hz, 2000 Hz, and 3000 Hz) and four speaker inclinations (20, 30, 60, and 90 degrees) were tested and the results were most encouraging. For each frequency and angle variation, the pressure amplitude was checked at three axial locations down the duct. Some of the results of these tests are illustrated in Figures 13 through 16. The only general effect that could be noted was that the radial variation of pressure amplitude increased as the test frequency increased and the angle of the speaker decreased. However, none of the variations were particularly noteworthy save for 30 degrees and 3000 Hz. The apparent variation at this condition cannot be explained. It is quite possible that these variations in pressure level are due to the cross modes present in the duct.

2.7 Sample Holder Configurations

Since the major portion of experimentation was concerned with measuring the insertion loss of various specimens lining the duct, a method of side mounting a large variety of configurations was desired. It was also found desirable to make normal impedance

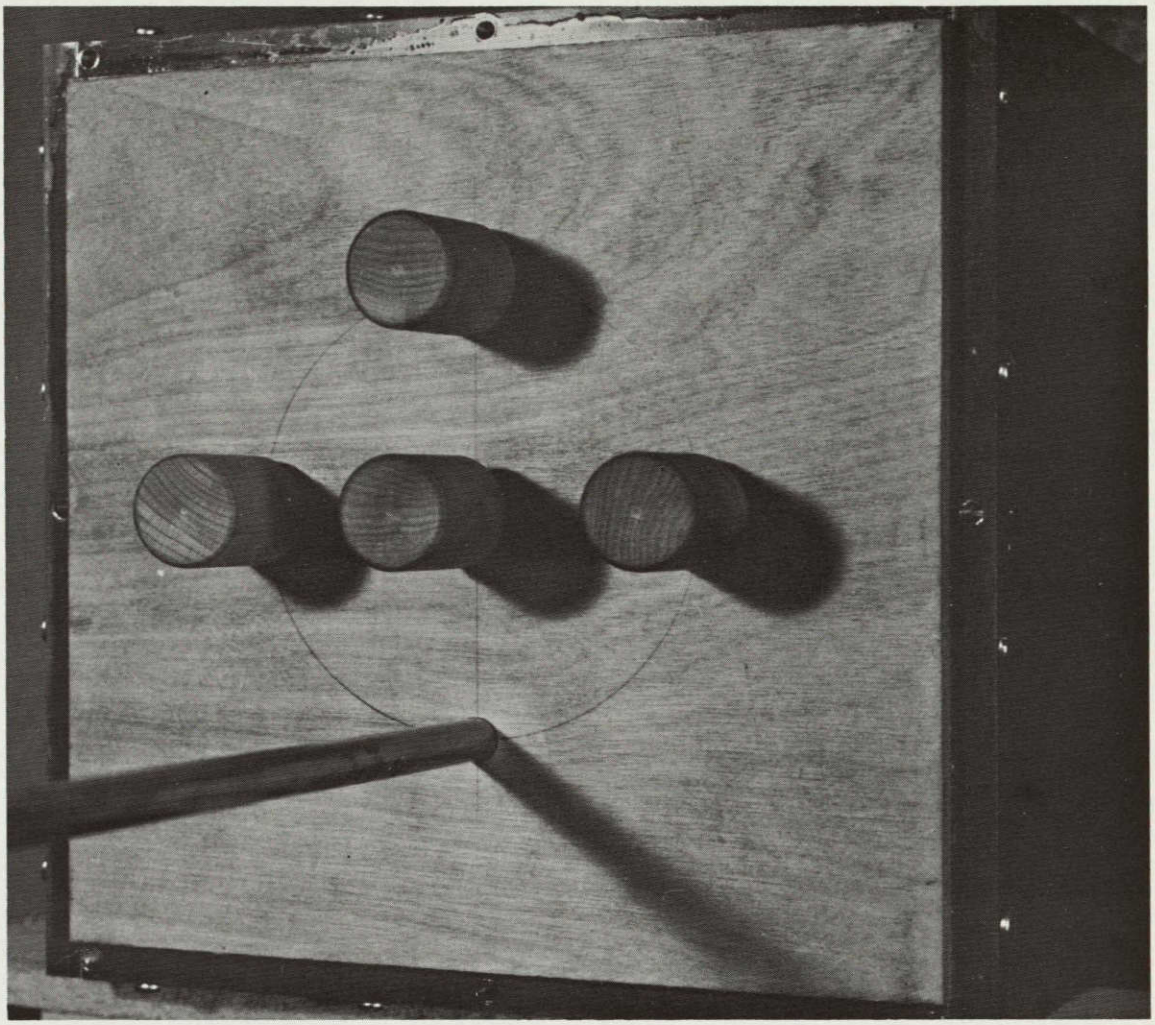

Figure 12 Plate to Measure Radial Pressure Distribution

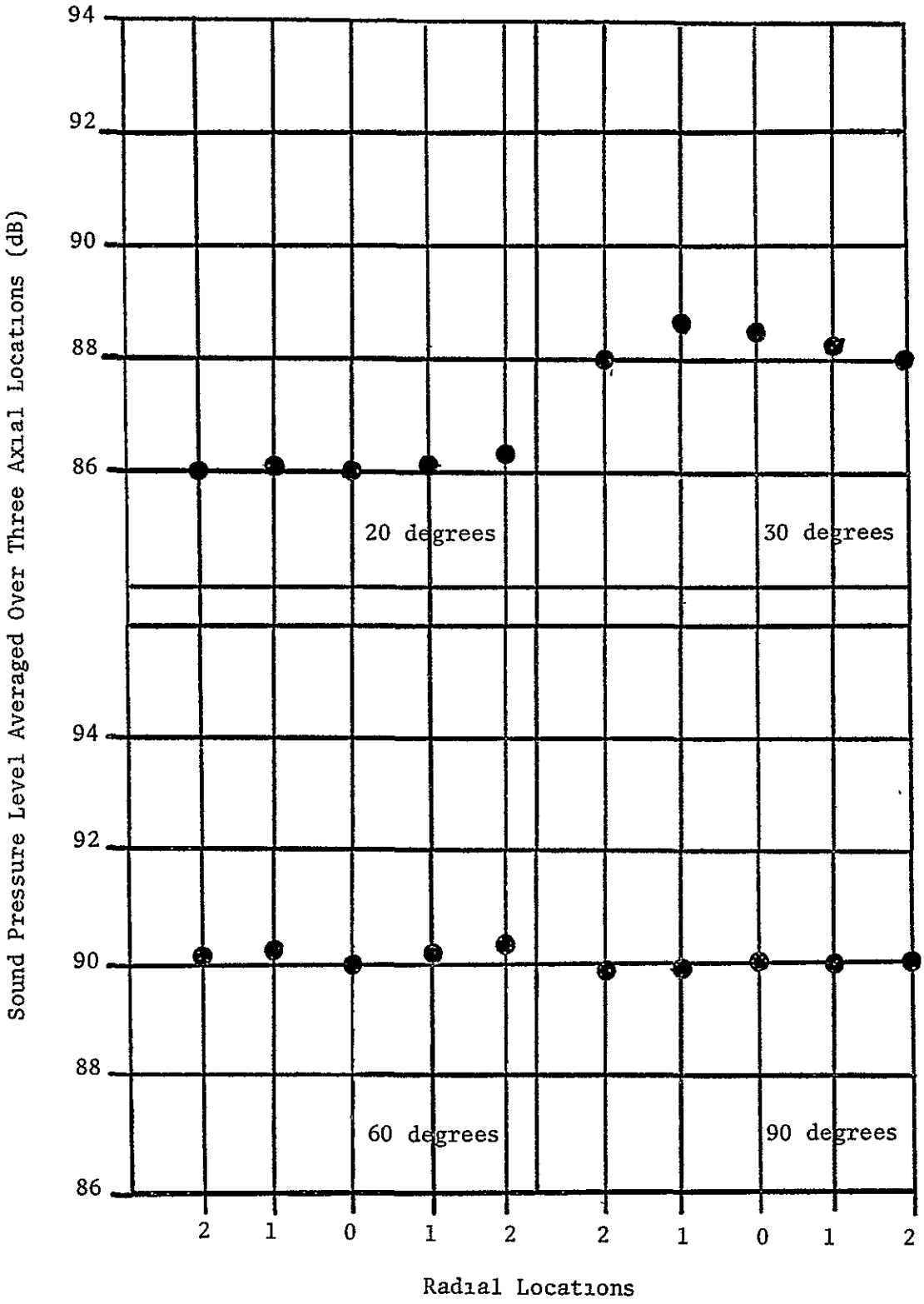

Figure 13 Radial Pressure Distribution For 400 Hz

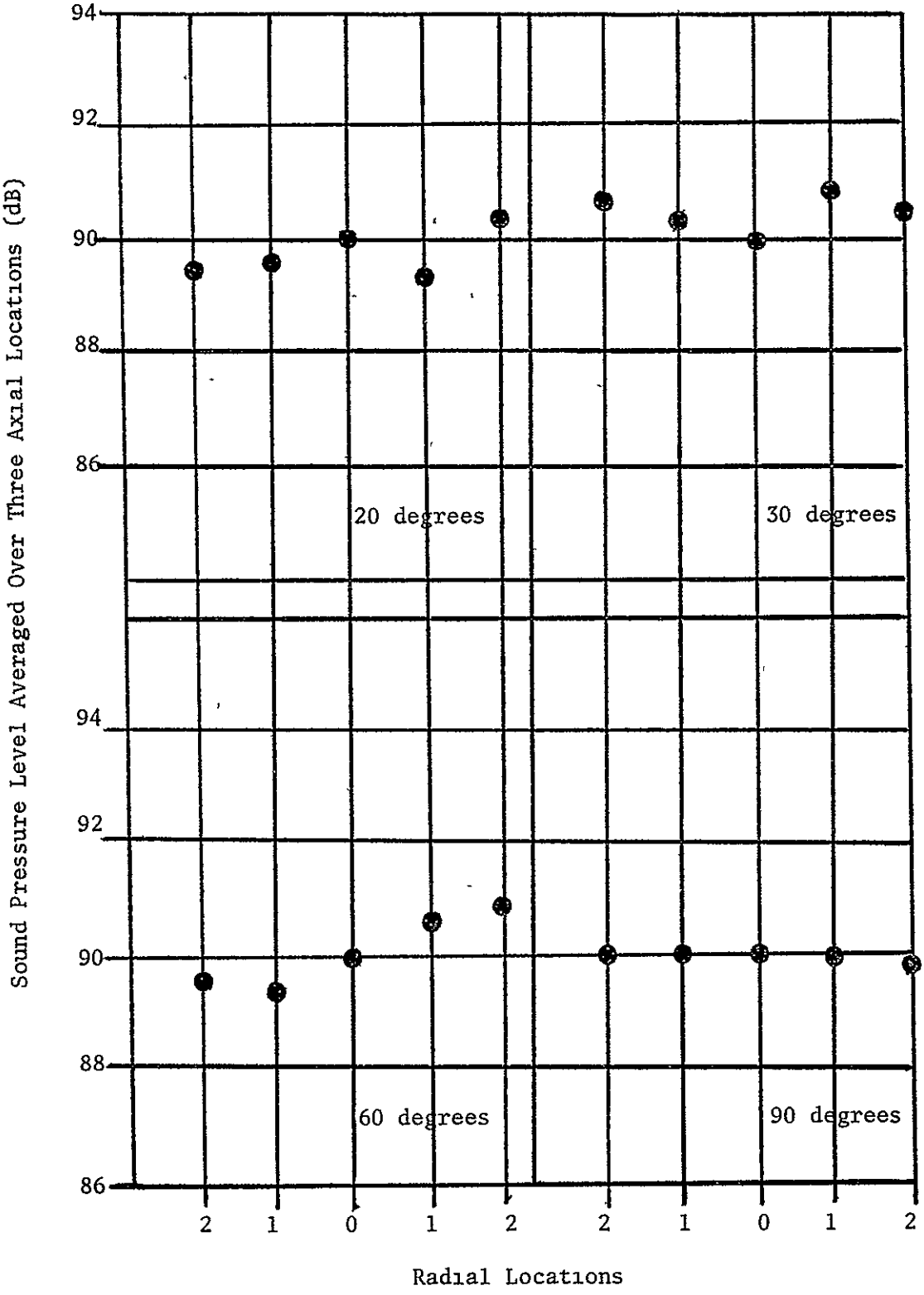

Figure 14 Radial Pressure Distribution For 1000 Hz

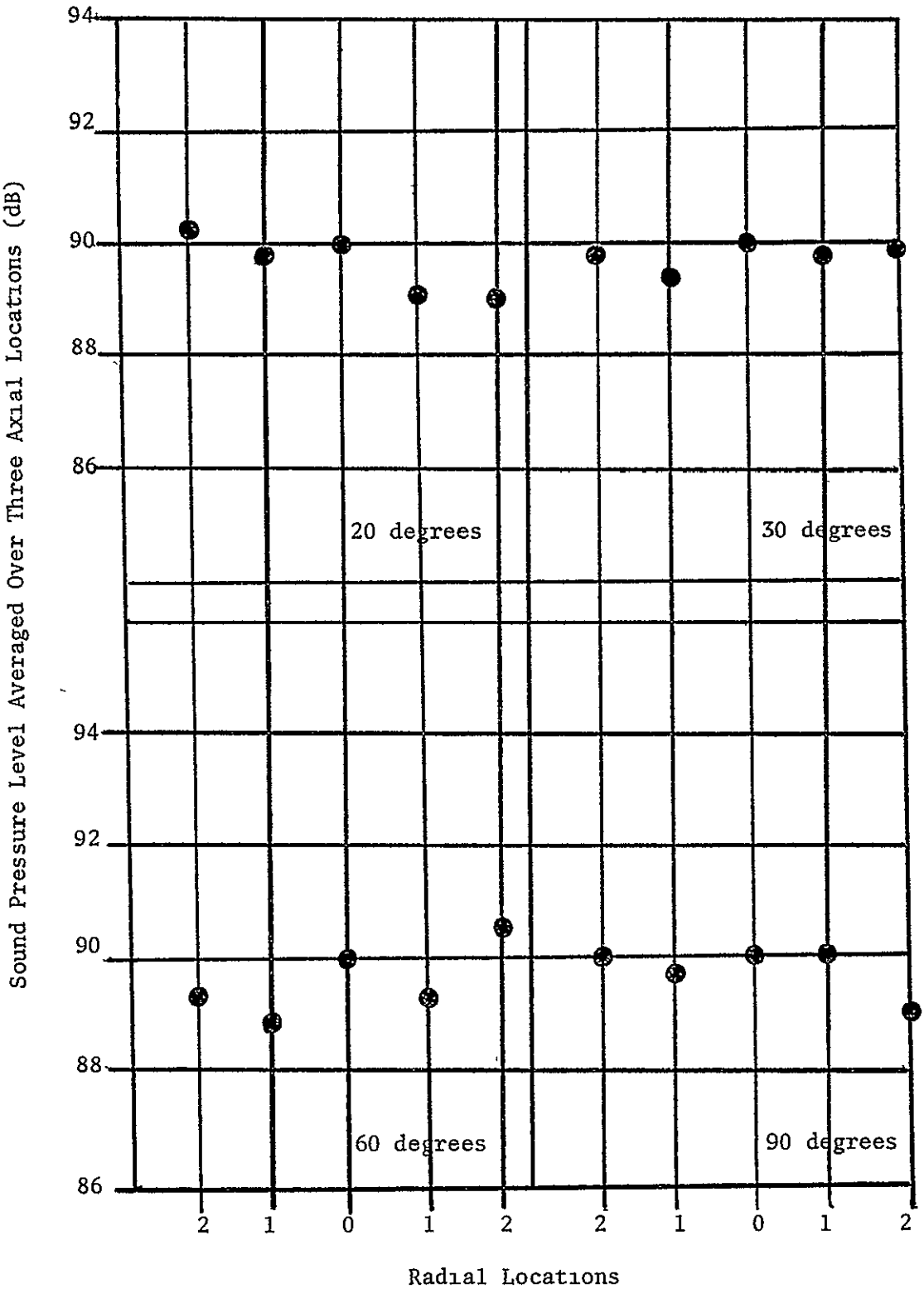

Figure 15 Radial Pressure Distribution For 2000 Hz

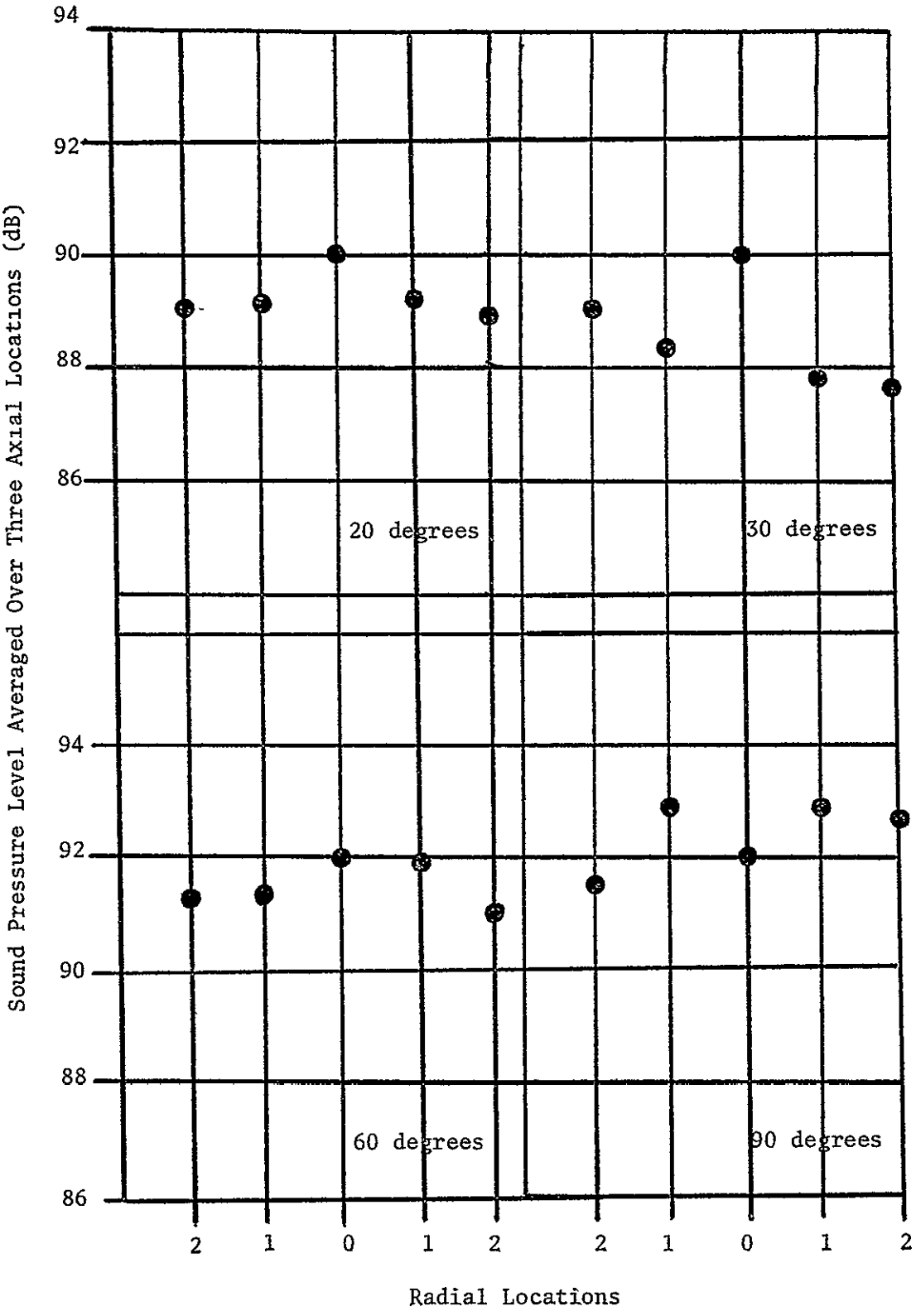

Figure 16 Radial Pressure Distribution For 3000 Hz

and absorption measurements on certain samples. Therefore, it was necessary to design the end of the tube so that specimens could be mounted at 90 degrees to its axis.

A typical acoustical treatment consists of three main components. the face design, the backing plate, and a core section. The core section can be either an air gap or some other acoustical treatment that is used to separate the face and back plate. Figures 17, 18 and 19 are general illustrations showing typical absorption treatments and specimen combinations tested. Figure 18 is of a porous acoustical treatment backed by a solid wall. For this design, the porous material was simply connected to a solid plate and placed into the duct so that its face was flush with the duct walls. If the thickness of the material was greater than the duct wall thickness, a sample holder box, similar to the one shown in Figure 17, was placed over the protruding position of material. The second design was that of a porous sample backed by a layer of air. To obtain this configuration for woven stainless steel as seen in Figure 18, spacer bolts were put through the material and screwed into the backing plate until the desired separation was reached. The sample plus the air gap was placed into the tube and a sample holder box was placed over any exposed portion of the air gap. The third general type of configuration was that of the Helmholtz resonator type. A wooden box with holes drilled in one of the faces along with a core of removable partitions backing the holes was used for this design (Figure 19). The partitions were made removable

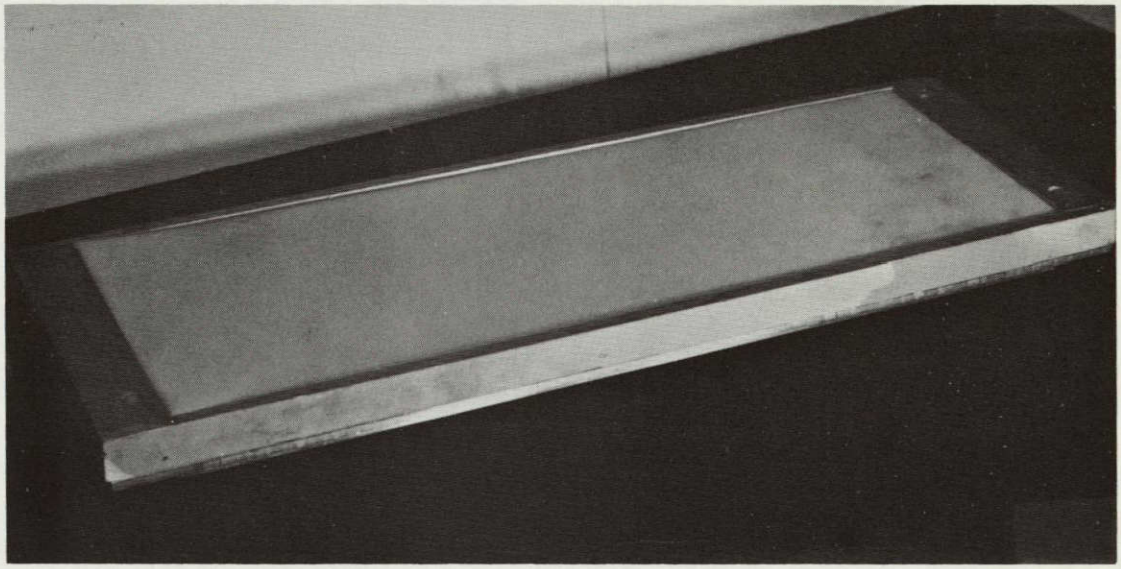

Figure 17 Scottfoam Mounted in a Sample Holder Box

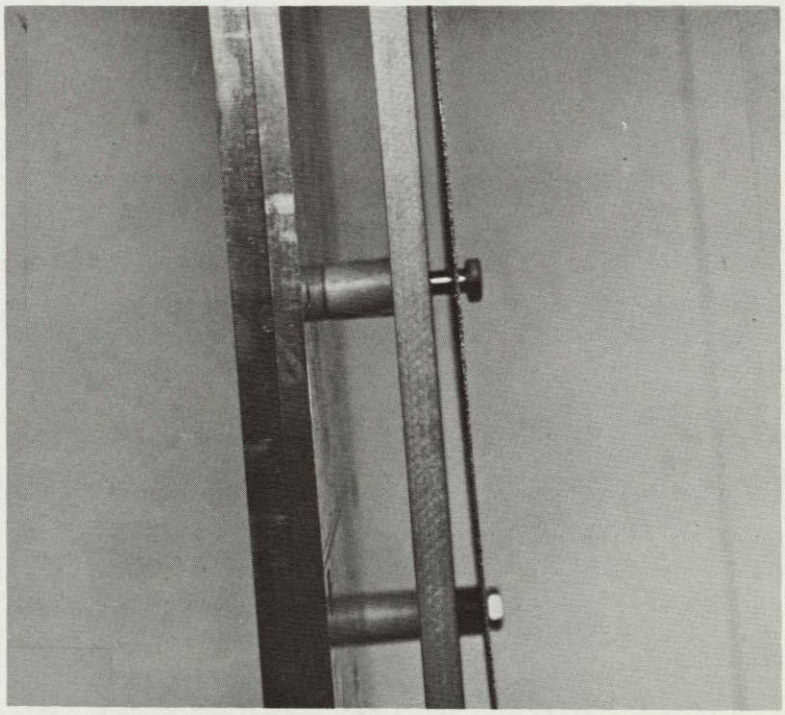

Figure 18 Feltmetal With Air Gap Configuration

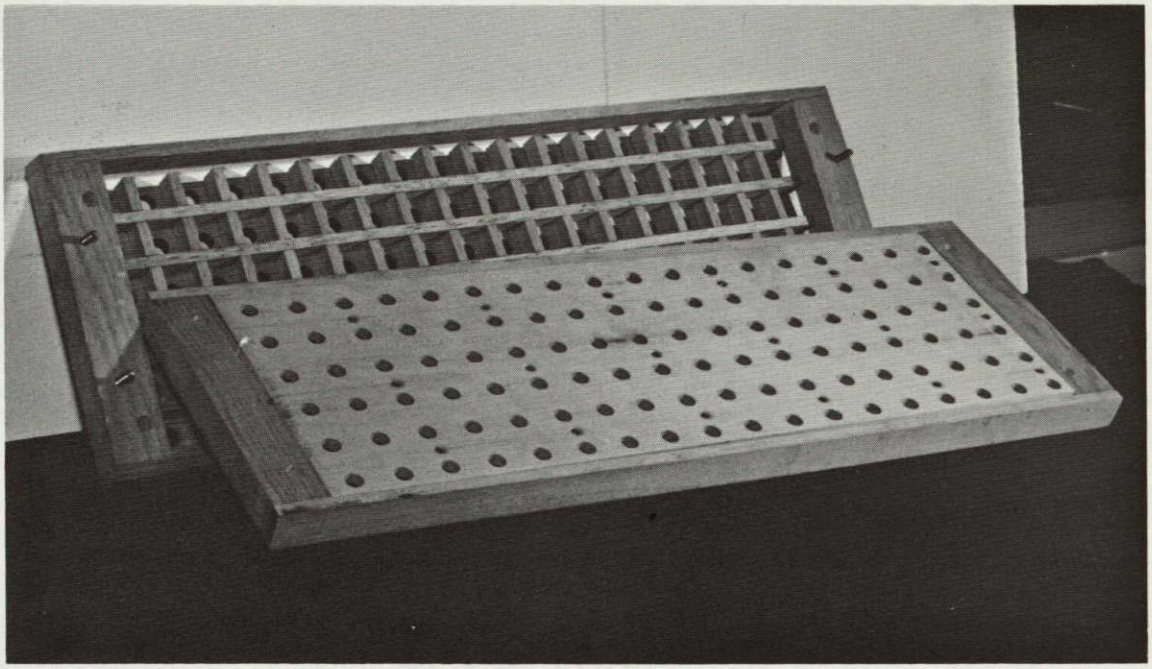

Figure 19 Perforated Facing With a Partitioned Air Backing

so that tests with and without them could be conducted. They were also made removable so another core, a porous material, for example, could be placed behind the resonator apertures.

All of this acoustical treatment was designed to be rectangular in cross section and compatible with the length of the side slots in the duct.

For the measurement of the normal absorption coefficients, the samples and their backing could be bolted directly into the end of the duct as shown in Figure 20. When a layer of air was in the core between the sample face and the solid plate, a box could be placed over the sample and the entire configuration bolted to the end of the duct.

2.8 Sample Evaluation

Materials considered to have the potential qualities of a lining material for jet engines were tested for their acoustical properties by two methods. The lining concepts considered were evaluated using a DC flow resistance apparatus and an acoustic impedance tube. The purpose of these evaluations is to develop a simple method of classifying and separating various configuration types of absorption materials.

2.8.1 Flow Resistance Technique. To determine the DC resistance properties of the materials the flow resistance apparatus shown in Figure 21 was built. The flow resistance of a pervious material is defined by

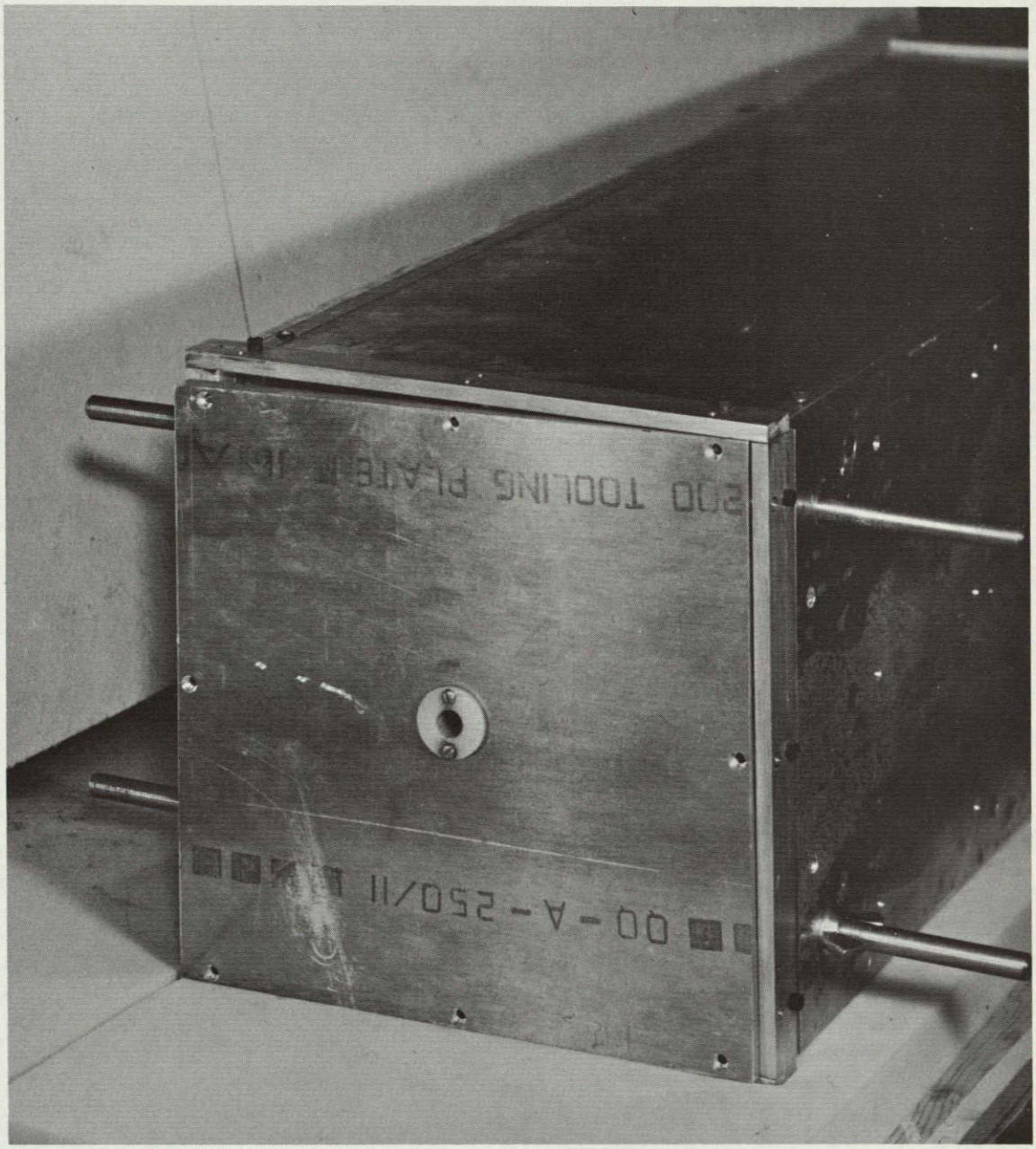

Figure 20 Plate Used for Standing Wave Tests

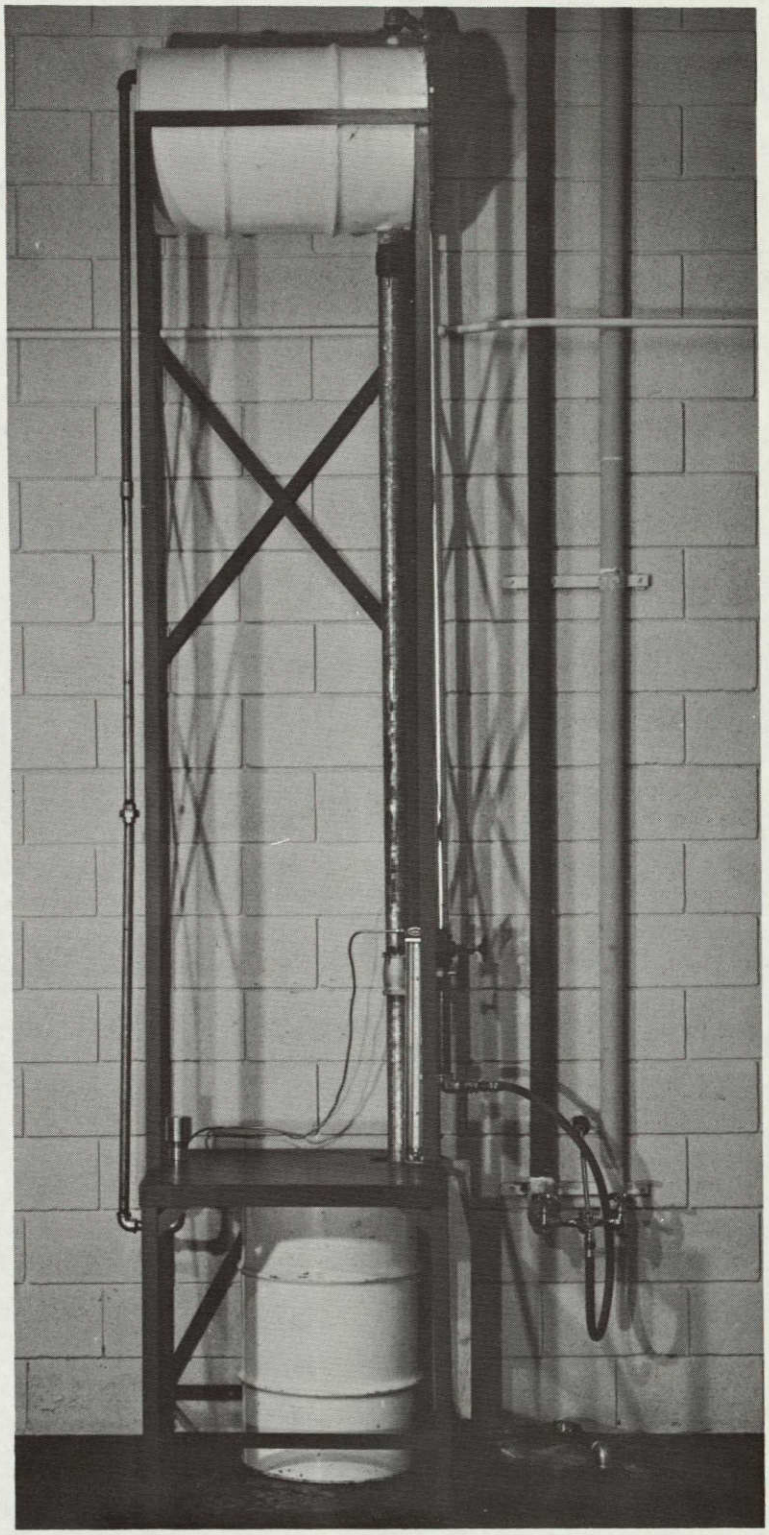

Figure 21 Flow Resistance Apparatus

$$R = \frac{\Delta p}{v} \quad , \qquad (2.3)$$

where Δp is the pressure differential across a sample of the material and v is the linear velocity through the sample. The procedure used for designing our device is similar to the one given by Beranek (15). The flow resistance is schematically illustrated in Figure 22. The sample of material is held in the sample holder. When water is steadily taken from the tank, air is sucked through the material at the same rate the water is removed from the tank. This causes a pressure drop across the sample and this pressure difference is measured on the manometer. By knowing the volume, velocity and the area of the sample, one can calculate the linear velocity from

$$v = \frac{U}{S} \quad , \qquad (2.4)$$

and the velocity along with the pressure drop in Equation (2.4) gives the flow resistance in the units of Rayls.

The most important piece of apparatus associated with the flow resistance device is the specimen holder. Our specimen holder is shown in Figure 23. A two-inch diameter piece of the material is placed on the mounting as shown in the figure and the top of the specimen holder is screwed down securing the material specimen in place. This type of securing reduces the leakage around the side of the sample necessary for accurate Δp readings.

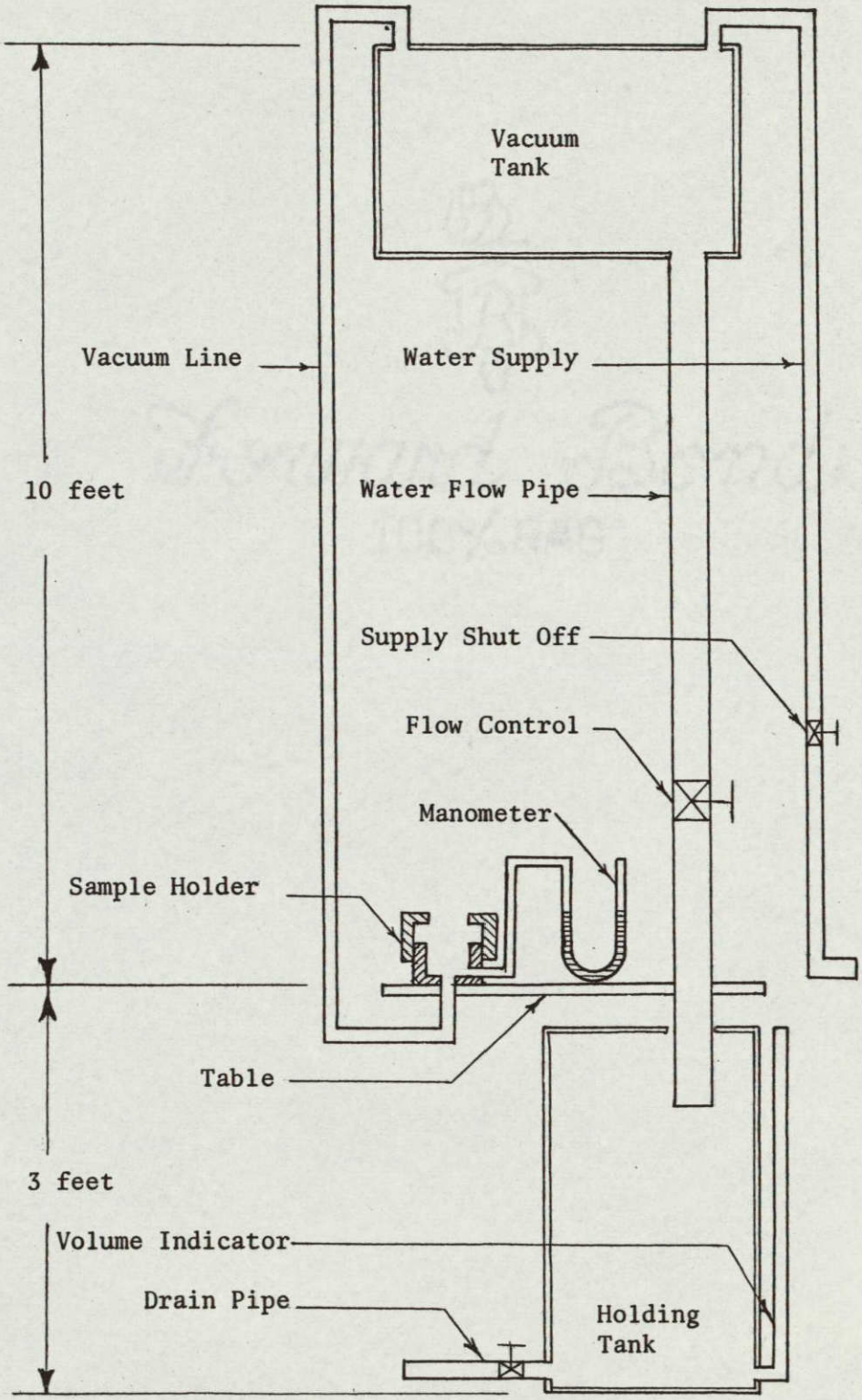

Figure 22 Flow Resistance Apparatus Schematic

Figure 23 Sample Holder

2.8.2 Impedance Tube Technique. For the normal acoustic impedance measurements, the duct used for the insertion loss measurements was converted to a standing wave tube. The theory of the use of a standing wave tube can be found in many references. (13)

As a brief explanation, the acoustic impedance is defined as the complex ratio of the acoustic pressure to the acoustic particle velocity at the surface of the sample. This complex impedance is made up of a real resistive component and an imaginary reactive component. In order to determine the acoustic impedance from duct measurements, we must determine the standing wave ratio, the distance from the face of the sample to the first minimum, and the distance between two successive minimums. Upon making these measurements, one can then calculate the impedance by the use of a Smith Transmission Line Calculator. If one is just interested in the normal absorption coefficient of a sample, he may determine this quantity by measuring only the difference in level between the maximum and minimum pressure amplitude in the standing wave. The normal absorption coefficient can then be obtained from Figure 24.

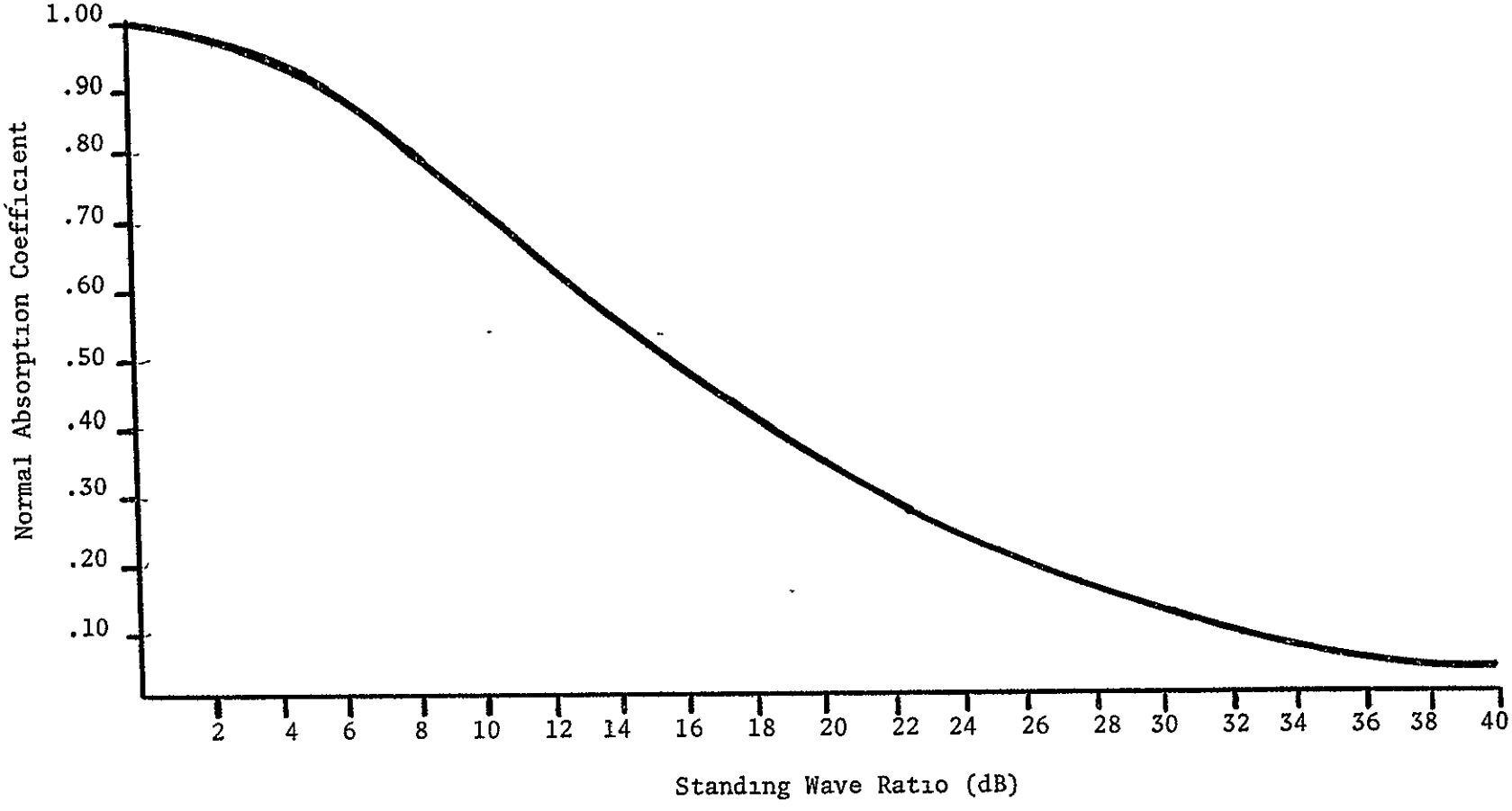

Figure 24 Relation of Normal Absorption Coefficient to Standing Wave Ratio

CHAPTER III

THEORETICAL BACKGROUND

Setting the sound source at arbitrary angles with respect to the duct axis generates waves which will reflect from side to side as they travel along. Consider, for example, the two-dimensional model shown in Figure 25. The reflected wave components in the geometrical description of this figure make up the higher modes of propagation between the two plates. The theoretical background in this Chapter is just the propagation of wavefronts inside the duct incident and reflecting from the duct walls. This is presented to give the reader some background on propagation of sound in ducts. It would be more realistic to theoretically consider the propagation in the tube by changing the boundary conditions to take into account the porous material lining; however, this is beyond the scope of this investigation and is recommended (in Chapter V) for consideration as a future project.

To better understand what is taking place in the duct, it is helpful to first consider a similar less complicated case the propagation of a wave in a duct of square cross section with the dimensions shown in Figure 26. (12)

The wave equation can be written in the form

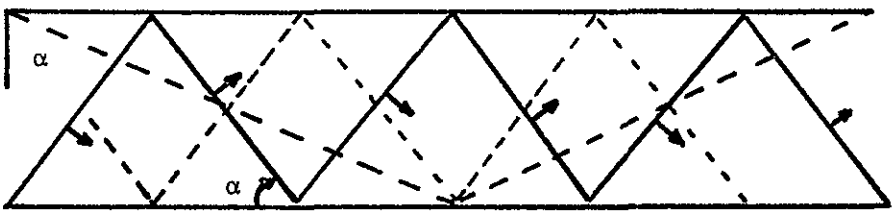

Figure 25 Reflected Wave Propagation

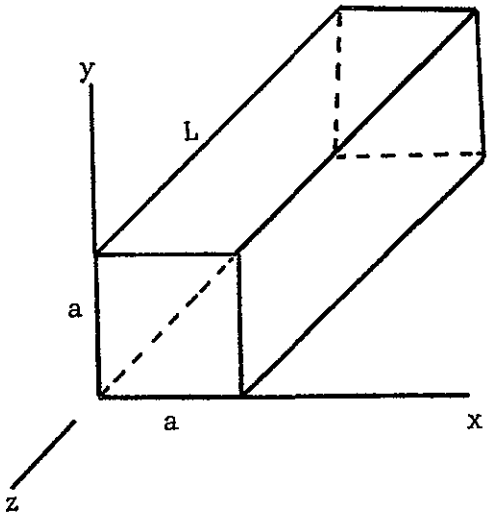

Figure 26 Duct of Square Cross Section

$$c^2\nabla^2\psi = \frac{\partial^2\psi}{\partial t^2} \quad , \tag{3.1}$$

where $\psi(x, y, z, t)$. By solving Equation (3.1), we find most quantities of interest in the acoustic field. If the oscillations are governed by some harmonic relationship, we can write an expression for ψ in the form of

$$\psi = \Lambda \exp(j\omega t) \quad , \tag{3.2}$$

where

$$\Lambda = \Lambda(x, y, z) \quad , \tag{3.3}$$

is solely a function of the coordinate system. A more concise equation can now be written to replace Equation (3.1).

$$\nabla^2\Lambda + \frac{\omega^2}{c^2}\Lambda = 0 \quad , \tag{3.4}$$

or

$$\nabla^2\Lambda + k^2\Lambda = 0 \quad , \tag{3.5}$$

where k is defined as the wave number

$$k = \frac{\omega}{c} \quad . \tag{3.6}$$

Equation (3.5) is the fundamental wave equation and the starting point for most acoustical problems associated with ducts. In

approaching this duct problem, the first step is to apply the boundary conditions of the square duct to Equation (3.5). On the rigid faces of the duct, the normal velocity of each component must vanish, i.e.,

$$\left.\frac{\partial \Lambda}{\partial x}\right|_{\substack{x = o \\ x = a}} = \left.\frac{\partial \Lambda}{\partial y}\right|_{\substack{y = o \\ y = a}} = \left.\frac{\partial \Lambda}{\partial z}\right|_{\substack{z = o \\ z = L}} = 0 \quad . \tag{3.7}$$

To solve for the values of Λ that satisfy these boundary conditions one can use the product method of separating the function Λ into the product of three separate functions. These three separate functions can each be shown to depend upon one of the variables of which Λ [Equation (3.3)] is a function. This is a standard method used in solving partial differential equations and can be found in any advanced mathematics text. (16) For our particular case, the function Λ is separated into the product of three quantities depending only on x, y, and z, respectively; i.e.,

$$\Lambda = F(x) \cdot G(y) \cdot H(z) \quad . \tag{3.8}$$

From this point, we may write the general solution which for our case transforms Equation (3.8) into the form

$$\Lambda = A_{mnp} \cos m \frac{\pi x}{a} \cos n \frac{\pi y}{a} \cos p \frac{\pi z}{L} \quad , \tag{3.9}$$

and if we allow

$$k_m = m \frac{\pi}{a} \quad ,$$

$$k_n = n \frac{\pi}{a} \quad , \tag{3.10}$$

and

$$k_p = p \frac{\pi}{a} \quad ,$$

then

$$\Lambda = A_{mnp} \cos k_m x \cos k_{ny} \cos k_{pz} \quad , \tag{3.11}$$

where the expression on the right side of the equal size is called the characteristic function and the values of k in Equation (3.10) are the eigenvalues. Substitution of the characteristic function into the wave equation yield for the wave number k

$$k^2 = \pi^2 \left(\frac{m^2}{a^2} + \frac{n^2}{a^2} + \frac{p^2}{L^2}\right) \quad , \tag{3.12}$$

where

$$k^2 = k^2_m + k^2_n + k^2_p = k^2_{mnp} \quad , \tag{3.13}$$

and

$$\begin{matrix} m \\ n \\ p \end{matrix} = 0, 1, 2 \ldots .$$

It is obvious from the above equation that

$$\frac{k_m^2}{k_{mnp}^2} \leq 1, \quad \frac{k_n^2}{k_{mnp}^2} \leq 1, \quad \frac{k_p^2}{k_{mnp}^2} \leq 1 \quad , \tag{3.14}$$

which is reminiscent of a cosine function, so if we let

$$\cos \phi = \frac{m}{a\left(\frac{m^2}{a^2} + \frac{n^2}{a^2} + \frac{p^2}{L^2}\right)^{1/2}} \quad , \tag{3.15}$$

$$\cos \theta = \frac{n}{a\left(\frac{m^2}{a^2} + \frac{n^2}{a^2} + \frac{p^2}{L^2}\right)^{1/2}} \quad , \tag{3.16}$$

$$\cos \gamma = \frac{p}{L\left(\frac{m^2}{a^2} + \frac{n^2}{a^2} + \frac{p^2}{L^2}\right)^{1/2}} \quad , \tag{3.17}$$

or

$$\cos \phi = \frac{k_m}{k_{mnp}}, \quad \cos \theta = \frac{k_n}{k_{mnp}}, \quad \cos \gamma = \frac{k_p}{k_{mnp}} \quad , \tag{3.18}$$

and

$$\cos^2 \phi + \cos^2 \theta + \cos^2 \gamma = 1 \quad . \tag{3.19}$$

Equation (3.18) tells us that the functions k_m, k_n, and k_p are components of the wave number k_{mnp} which forms the angles ϕ, θ, and γ with the coordinate axes. Thus, for a set of values of m, n, and p, we can determine a wave number which is the absolute value

of k_{mnp}. It is possible to determine all the natural frequencies of the duct under consideration by the expression

$$k_{mnp} = \frac{2\pi f_{mnp}}{c} \quad , \tag{3.20}$$

or

$$f_{mnp} = \frac{c}{2} \sqrt{\frac{m^2}{a^2} + \frac{n^2}{a^2} + \frac{p^2}{L^2}} \quad . \tag{3.21}$$

It is fairly obvious that, for any eigenvalue of k_{mnp}, there will be a combination of plane waves. The direction of these waves are dependent upon the components k_m, k_n, and k_p of the vector of the eigenvalue. We can see from Equations (3.2) and (3.7) that

$$\psi = A \exp (j\omega t) \quad , \tag{3.22}$$

and

$$\psi = A_{mnp} [\cos k_m x \cos k_n y \cos k_p z] \exp (j\omega t) \quad . \tag{3.23}$$

If we now use the definition of the cosine

$$\cos \alpha = \frac{\exp (j\alpha) + \exp (-j\alpha)}{2} \quad , \tag{3.24}$$

we can write Equation (3.23) as

$$\psi = A_{mnp} \{ [\frac{\exp (jk_m x) + \exp (-jk_m x)}{2}]$$

$$[\frac{\exp (jk_n y) + \exp (-jk_n y)}{2}]$$

$$[\frac{\exp (jk_p z) + \exp (-jk_p z)}{2}]\} \exp (j\omega t) \quad , \quad (3.25)$$

or rewriting

$$\psi = \frac{A_{mnp}}{8} \Sigma [\exp j(\omega t \pm k_m x \pm k_n y \pm k_p z)] \quad , \quad (3.26$$

or, from Equations (3.15), (3.16), and (3.17),

$$\psi = \frac{A_{mnp}}{8} \Sigma \exp j(\omega t \pm x k_{mnp} \cos \phi$$

$$\pm y k_{mnp} \cos \theta \pm z k_{mnp} \cos \gamma) \quad , \quad (3.27)$$

or it can be simply written as

$$\psi = \frac{A_{mnp}}{8} \Sigma \exp j(\omega t - k_{mnp} \xi) \quad , \quad (3.28)$$

where

$$\xi = \pm x \cos \phi \pm y \cos \theta \pm z \cos \gamma \quad . \quad (3.29)$$

From expressions (3.28) and (3.29), there are eight possible

combinations of plane waves for each value of k_{mnp}. The general solution for the natural oscillations now can be written in the form

$$\psi = \sum_{m=o}^{\infty} \sum_{n=o}^{\infty} \sum_{p=o}^{\infty} \Lambda_{mnp} \exp(j\omega t) \quad . \tag{3.30}$$

The waves that are making up the normal modes begin at some point (z = 0) on the face of the duct with direction cosines described by Equations (3.15), (3.16), and (3.17). They then propagate reflecting off the walls that make up the duct. When all the waves reach the end of the volume, they return to the starting face and begin to describe its same path over again. Each path length traveled by a wave corresponds to a definite discrete value of frequency which is one of the natural frequencies of the volume physically interpreted through the eigenvalues. To carry this analysis a bit further, adding the anechoic termination shown in Figure 9 has the effect of making the duct infinite. The next step in the investigation of sound propagation will be the investigation of the sound waves as they travel down this infinite tube.

The rectangular duct becomes infinite when the length L along the z axis becomes infinite also. As seen in the previous section, the equation

$$\nabla^2\Lambda + k^2\Lambda = 0 \quad , \tag{3.5}$$

is used as the starting point. A solution similar to that shown in Equation (3.8) can also be applicable for this configuration. The general solution will then have the form

$$A = A_{mnp} \cos k_m x \cos k_n y \quad . \tag{3.31}$$

There is only $\cos k_m x$ and $\cos k_n y$ in this term because just the velocities on the x = a face and the y = z face are again zero. There is also a propagation in the z direction but the only wave motion is in the positive z direction and can be accounted for by an $\exp(-k_p z)$ term. So then the general expression analagous to Equation (3.30) has the form

$$\psi(x, y, z, t) = \sum_{m=o}^{\infty} \sum_{n=o}^{\infty} B_{mn} \cos k_m x \cos k_n y$$

$$\exp[j(\omega t - k_p z)] \quad . \tag{3.32}$$

As before, upon substitution into the wave equation, we see that the wave number k can be written in terms of k_m, k_n, and k_p; i.e.,

$$k^2 = k^2_m + k^2_n + k^2_p \quad . \tag{3.33}$$

However, for our case, where we have a sound wave propagating with a frequency f at z = 0, the value of k is given as $k = \frac{\omega}{c}$ which, as

can be seen from Equation (3.33), implies that k_p can only have values defined by the following condition:

$$k_p = \sqrt{k^2 - (k^2_m + k^2_n)} \quad , \tag{3.34}$$

or

$$k_p = \sqrt{\frac{\omega}{c} - (k^2_m + k^2_n)} = k_{mn} \quad . \tag{3.35}$$

The wave process in the tube is only excited by oscillations of these modes (m, n) if

$$k > \sqrt{k^2_m + k^2_n} \quad , \tag{3.36}$$

or if

$$f_{mn} > \frac{c\sqrt{k^2_m + k^2_n}}{2\pi}$$

and this is the cut off frequency below which mode propagation can not exist. Writing the cut off frequency in terms of tube geometry, we get

$$f_{mn} = \frac{c}{2}\sqrt{\frac{m^2}{a} + \frac{n^2}{a}} \quad . \tag{3.38}$$

If we regard the propagation of the waves in the z-direction as the sum of plane waves which are propagated at an angle to the z-axis and reflected from the sides, we may write the direction

cosines of these waves as

$$\cos \phi = \frac{k_m}{k} \quad , \tag{3.39}$$

$$\cos \theta = \frac{k_n}{k} \quad , \tag{3.40}$$

and

$$\cos \gamma = \frac{k_{mn}}{k} \quad . \tag{3.41}$$

From this, Rzchevkin shows (17) that a general expression for the velocity potential can be written which is similar to Equation (3.26).

$$\psi_{mn}(x, y, a, t) = \frac{B_{mn}}{4} \sum_{4} \exp j(\omega t \pm k_m x \pm k_n y \pm k_{mn} z) \quad , \tag{3.42}$$

or it can be rewritten as

$$\psi_{mn} = \frac{B_{mn}}{4} \sum_{4} \exp j[\omega t - k(\pm x \cos \phi \pm y \cos \theta - z \cos \gamma)] \quad , \tag{3.43}$$

which we can write as

$$\psi_{mn} = \frac{B_{mn}}{4} \exp j(\omega t - k\xi) \quad , \tag{3.44}$$

where

$$\xi = \pm \cos \phi \pm y \cos \theta - z \cos \gamma \quad . \tag{3.45}$$

This general expression characterizes four possible plane waves which can be determined by the signs associated with ξ. If we take the signs into account in Equation (3.43), the wave can be represented by four waves or rays which are reflected from the four sides of the tube after leaving the $z = 0$ position from the directional angles given in Equations (3.39), (3.40), and (3.41). Figure 27 shows a two-dimensional representation of this wave propagation down a duct.

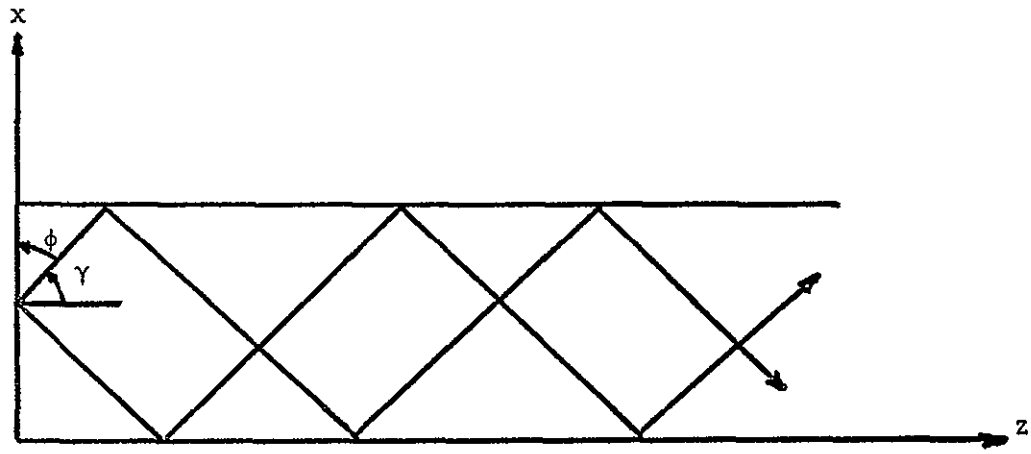

Figure 27 Two Dimensional Wave Propagation

CHAPTER IV

EXPERIMENTAL RESULTS

4.1 Introduction

The overall objective of this program was the testing of metallic and non metallic materials that could be considered as potential acoustic treatments for jet engines. These treatments were tested for their flow resistance and normal incidence absortivity characteristics so that some sort of standardization of acoustic properties could be determined. Along with determining the properties of the materials, each of the specimens was placed in a duct as acoustic side branches and waves of various angles of incidence were made to impinge on the lining causing a grazing incidence effect. The insertion loss of each of these treatments was measured and plotted as a function of frequency and incidence angle. It was hoped that when attenuation results were obtained, they could be used in conjunction with the flow resistance and absorption results to help obtain a system of choosing suitable lining material.

4.2 Flow Resistance Results

The flow resistance tests were conducted with two general categories of resistive materials. Of these two material types, one was a soft porous foam manufactured by the Scott Paper Company called Scottfoam, and the other was a woven stainless steel material called Feltmetal. Six different configurations of these

two materials were flow tested for their resistive properties. The DC flow resistance of a sample can be directly related to its acoustic resistance, and can therefore be used to reflect the sample's absorptive properties. Manufacturers at times supply flow resistance specifications with their products, however, these values reflect results obtained from one specimen of material at a specific flow velocity. This, of course, is not a realistic way to take acoustic data. Therefore, we decided to conduct our own tests on each of our particular samples.

Two separate samples were taken from each of these lining materials and tested over a wide range of flow velocities. Figures 28 and 29 show the measured DC flow resistance values of the two Feltmetal samples. Figure 28 shows FM 123 Feltmetal which is a woven stainless steel mesh configuration of 0.040 inch thickness to which the manufacturer gives a specific flow resistance value of 50 Rayls. Figure 29 shows the results obtained from Feltmetal FM 134 which has a quoted flow resistance of 35 Rayls. In both cases, our tests indicate the expected variation of flow resistance with velocity. There is a maximum deviation of 40 percent from the manufacturer's value of flow resistance. Our results indicate the 50 Rayls and 40 Rayls could be considered representative values of our two samples of FM 123 and FM 134, respectively.

Figure 30 through 33 indicate the results of the flow resistance tests on the four Scottfoam configurations. Scottfoam configurations are normally characterized by thickness and porosity. Our tests were conducted on two porosities each at two thicknesses.

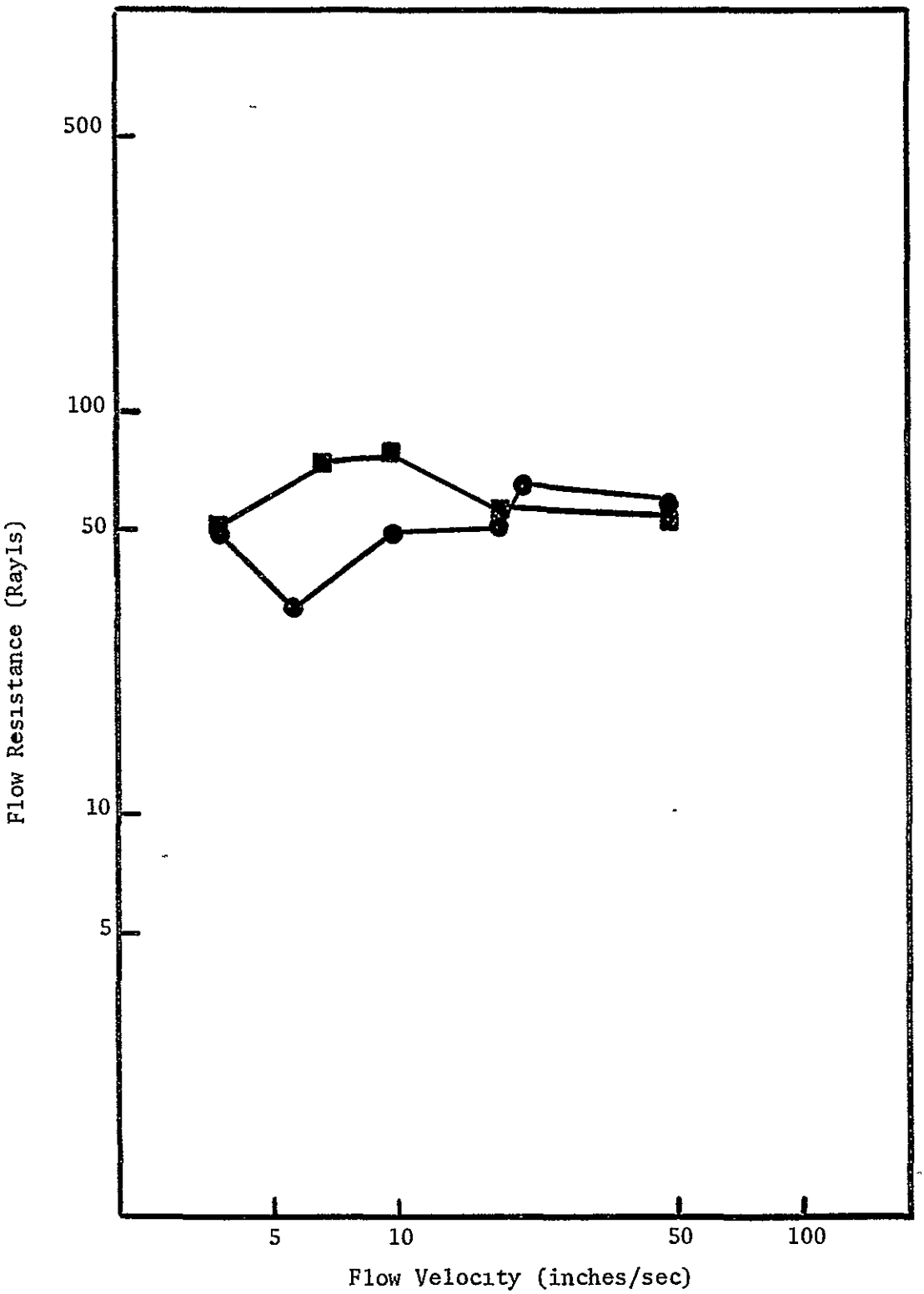

Figure 28 Flow Resistance of FM 123 Feltmetal

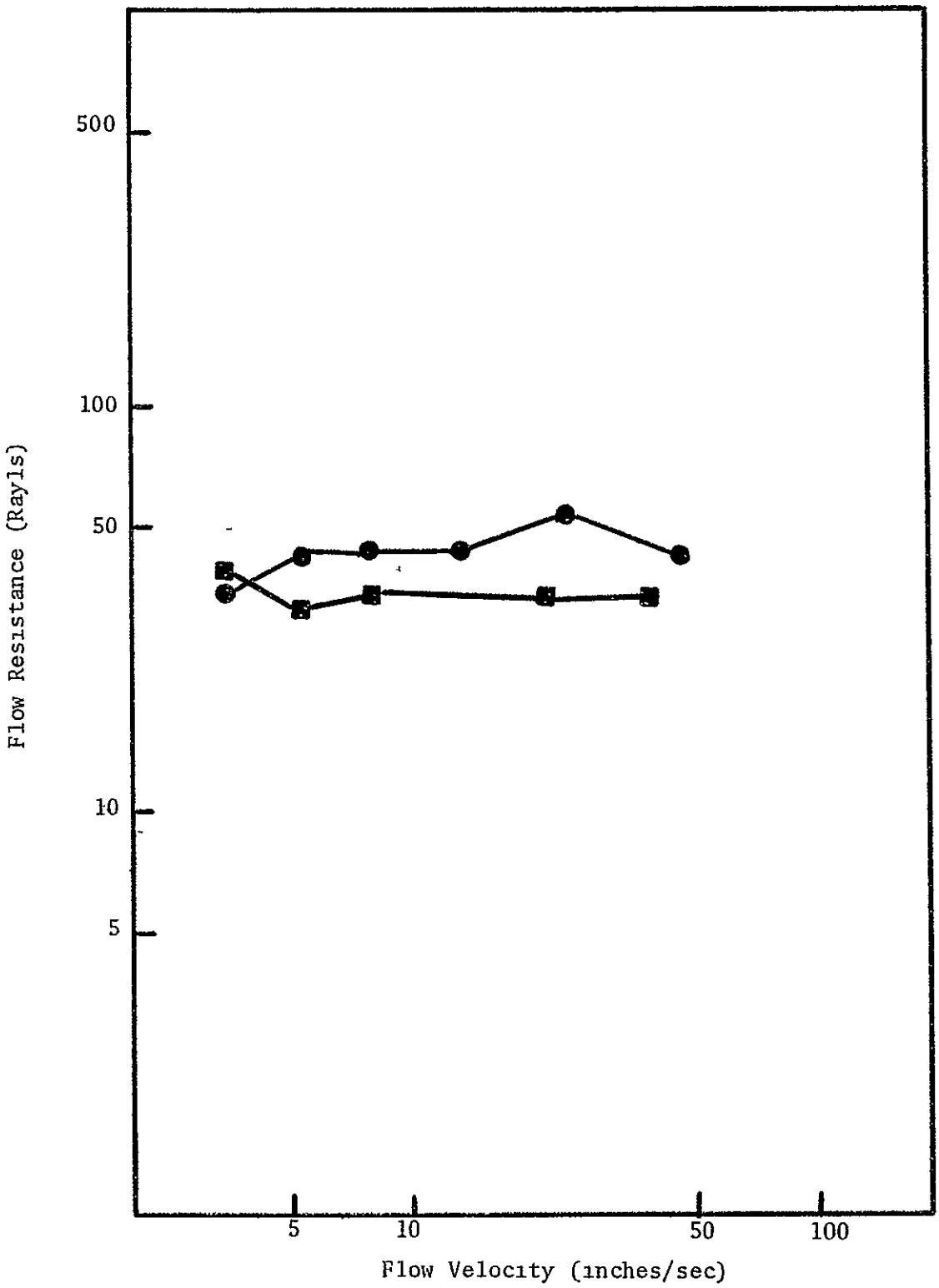

Figure 29 Flow Resistance of FM 134 Feltmetal

The porosity is represented by the number of pores per inch the value of which has a great effect on the flow resistance values of each sample. Figures 30 and 31 are results of Scottfoam containing 80 pores per inch. Both figures show a large fluctuation of flow resistance with flow velocity. These variations can be accounted for in two ways. First, by nature of their make up, the specimens probably do not have the same unit porosity. Secondly, these specimens are very flexible and as the flow velocity increases, the samples tend to buckle distorting the results. However, our results indicate 10 Rayls as a representative value of 1/2-inch thick sample and 18 Rayls representative for the 1-inch thick sample. One might suppose that the thicker sample would have the higher flow resistance, and the above results indicate this; however, Figure 32 and 33 do not reflect the anticipated thickness effect. These figures show flow resistance results on 100 pore per inch Scottfoam which indicate no change of flow resistance with thickness since the average value for 1/2-inch thick and 1-inch thick samples is 9 Rayls. These results can be attributed to the high porosity of the sample, and the sample's inherently low flow resistance.

4.3 Normal Incidence Absorption

The six material types used in the DC flow resistance tests along with a perforated facing configuration were used to form fourteen different acoustic absorbing devices. We placed these fourteen configurations at the end of the duct and tested them for their effectiveness as absorbing devices by measuring their normal absorption coefficient.

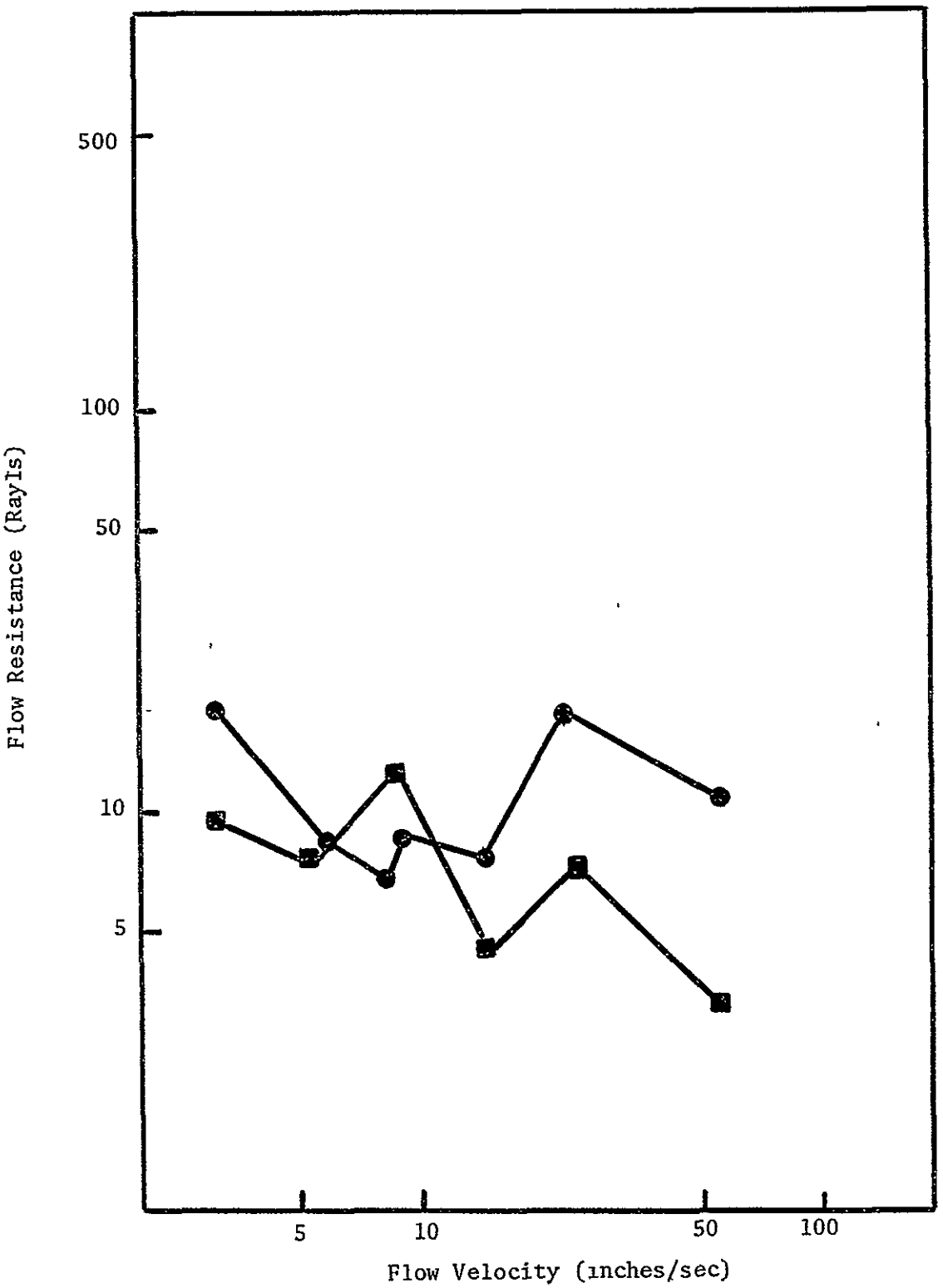

Figure 30 Flow Resistance of Scottfoam 1/2 Inch Thick 80 Pores/Inch

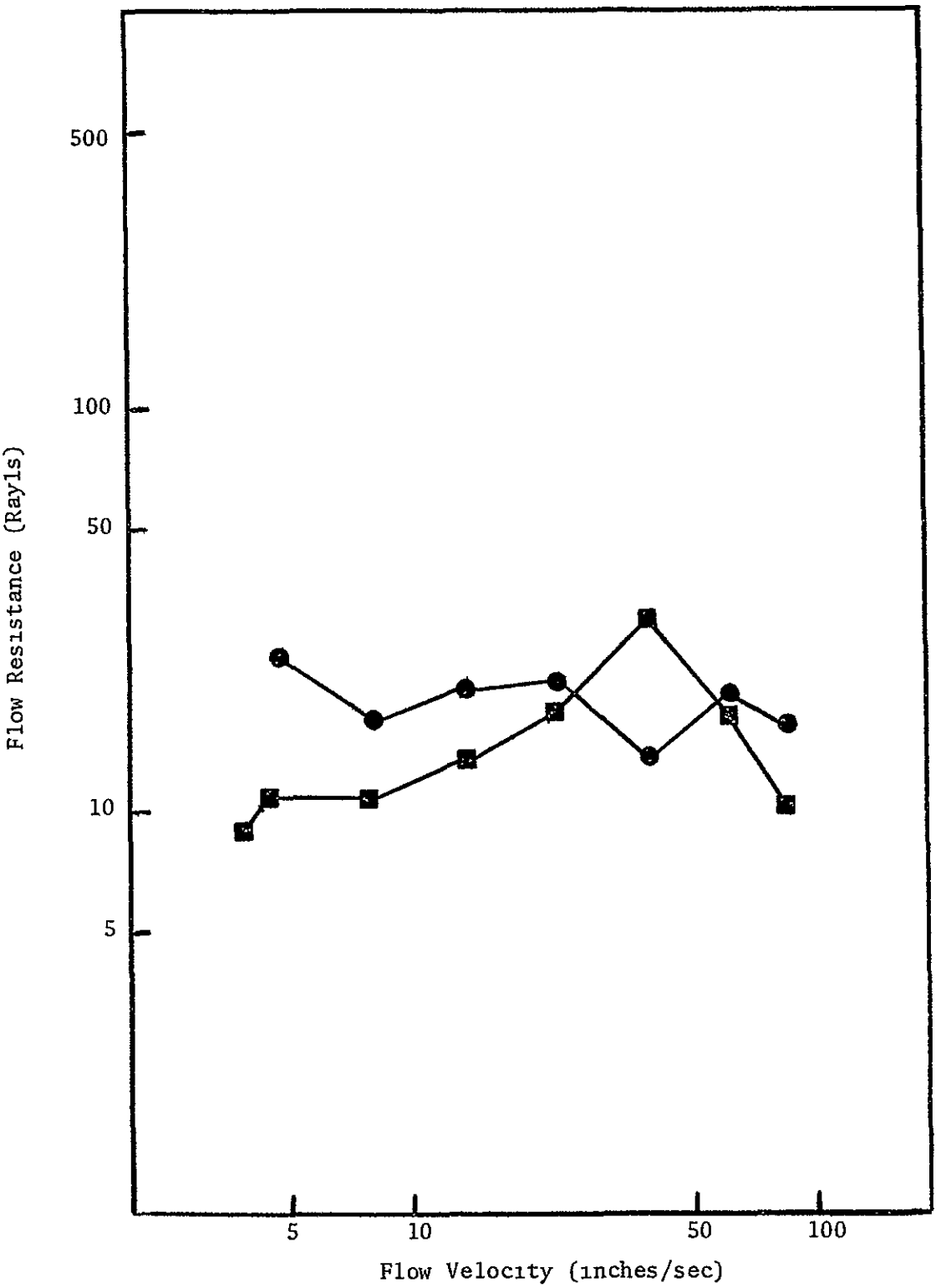

Figure 31 Flow Resistance of Scottfoam
1 Inch Thick 80 Pores/Inch

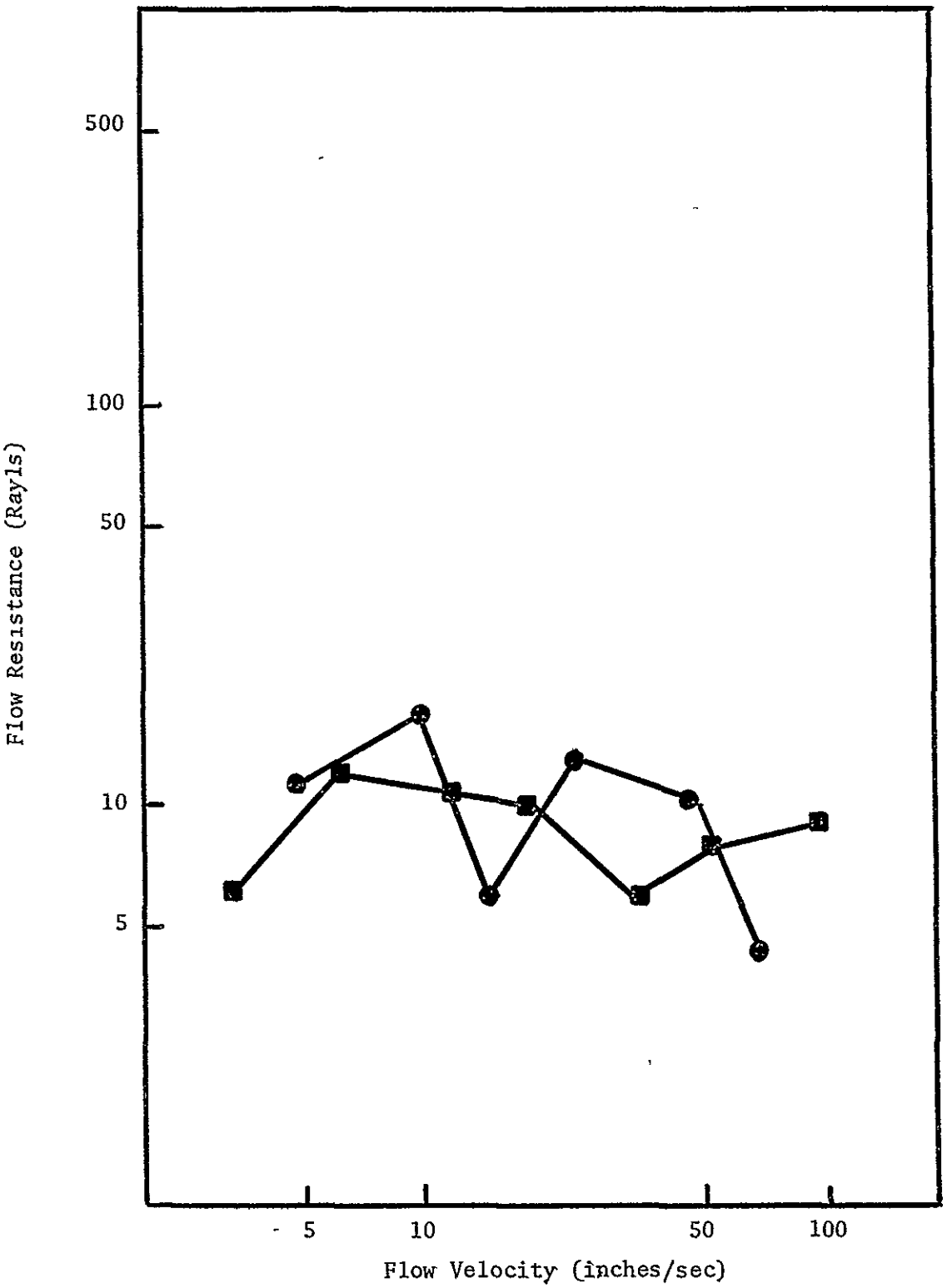

Figure 32 Flow Resistance of Scottfoam 1/2 Inch Thick 100 Pores/Inch

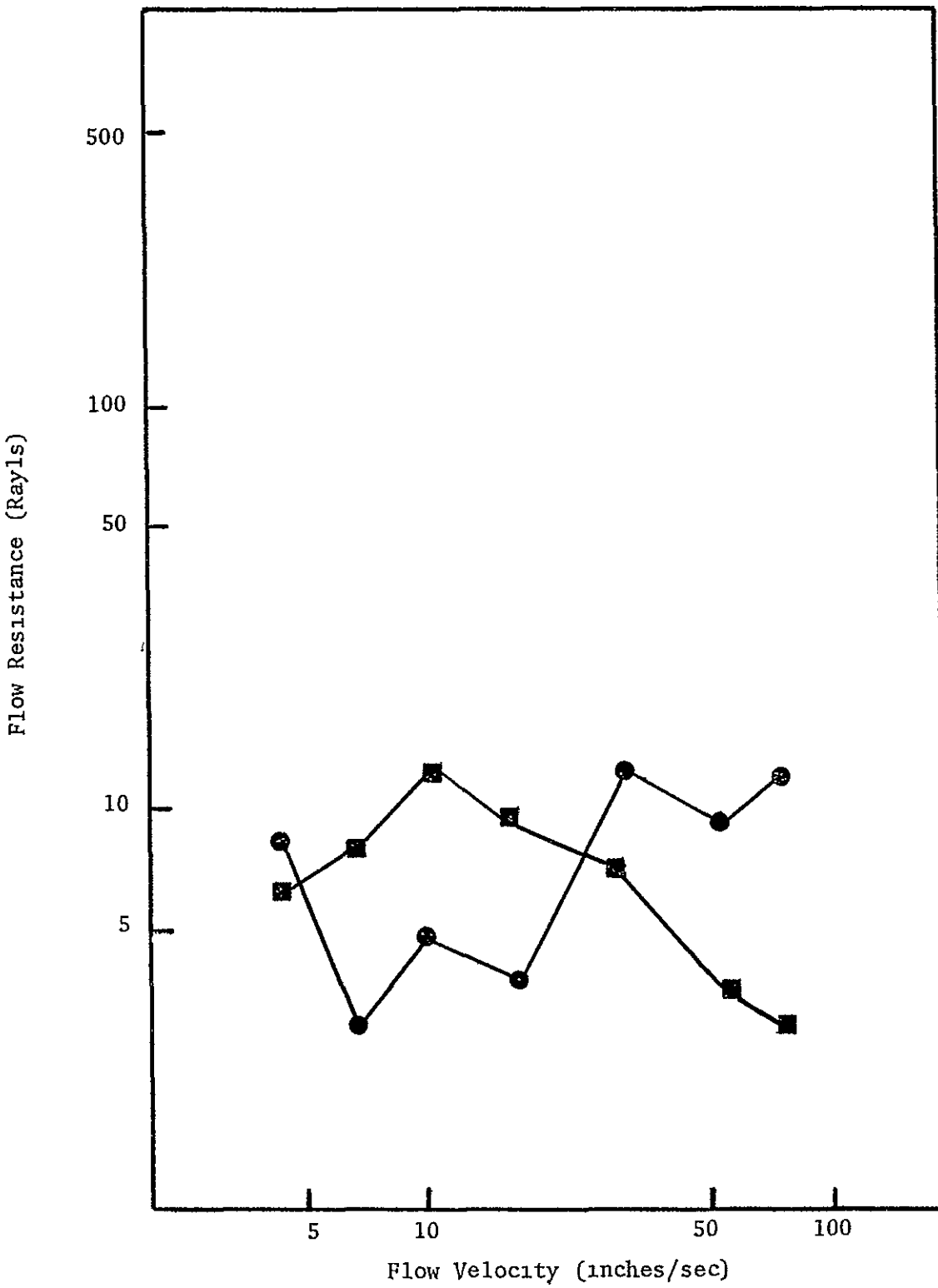

Figure 33 Flow Resistance of Scottfoam 1 Inch Thick 100 Pores/Inch

Figures 34 through 37 show the absorption coefficient versus frequency curves of devices using 80 pore per inch Scottfoam as the facing material. In the four cases shown, the absorption is still increasing with frequency within our range of frequencies. For frequencies up to 2000 Hz, the 1-inch thick facing material has better absorption characteristics than the thinner Scottfoam. As seen in Figures 35 and 37, the air core placed between the facing material and the solid plate increases the absorption for both thicknesses and almost identical trends were obtained for high porosity (100 pore per inch) Scottfoam. Figures 38 through 41 show the results obtained for the configurations using the high porosity specimen as a facing material. Both the thickness and the use of an air core increased absorption in the frequency range of interest. When these results are compared to the results of the 80 pore per inch tests, we see that the higher porosity has a slightly better absorption versus frequency curve up to 2000 Hz. These results are a result of the higher porosity material having a larger facing reactance than the configurations with 80 pore per-inch facing material.

Figures 42 and 43 show the absorption versus frequency curves for the two configurations tested using perforated plates for facing. From Figure 42, we see the results obtained using a perforated plate .375-inch thick having a hole diameter of .500 with a 10 percent open area backed by .625-inch partitioned air gap. This resonator configuration seems to have a resonance frequency around 950 Hz where it has its maximum absorption.

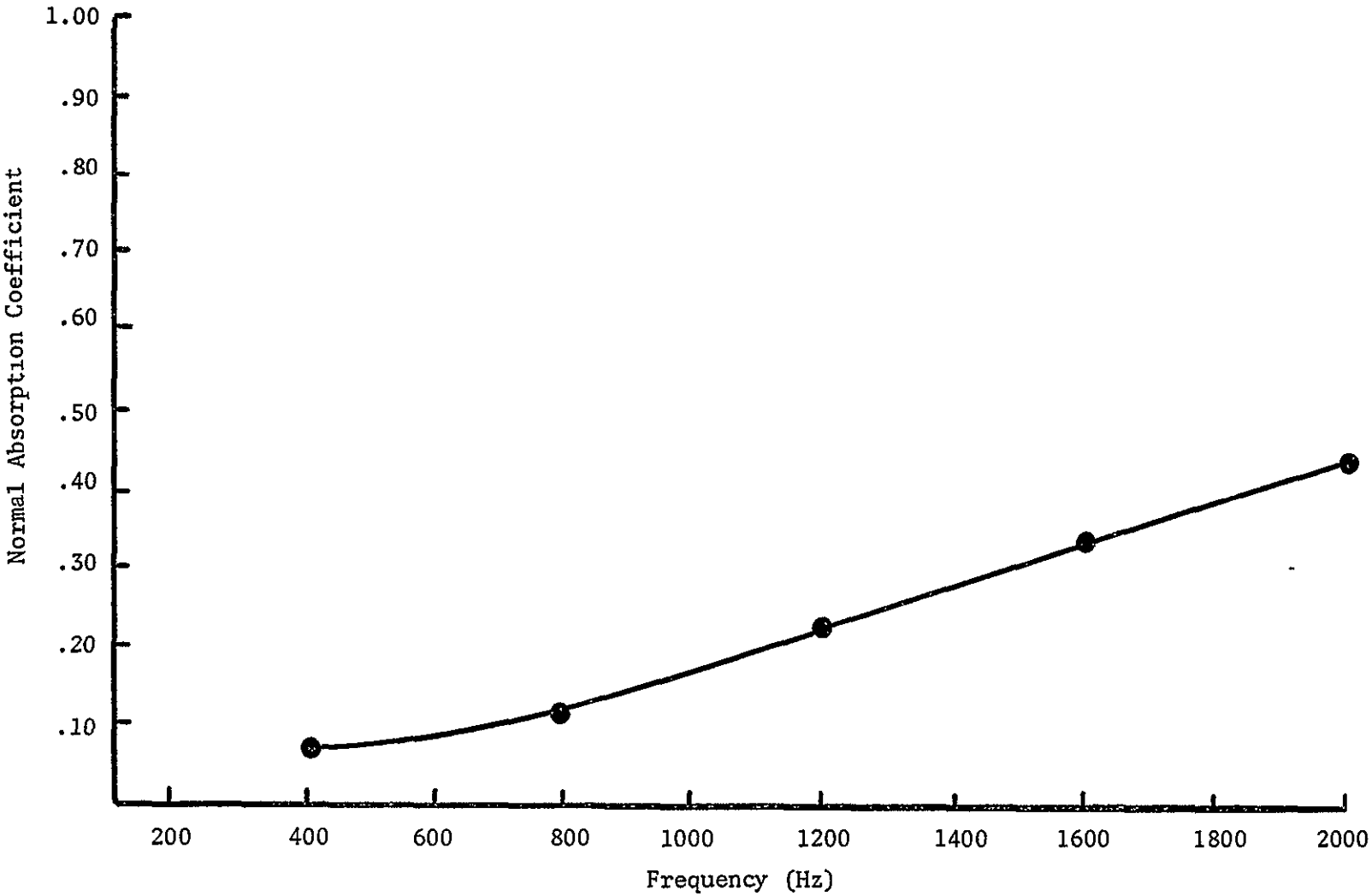

Figure 34 Normal Absorption Coefficient Versus Frequency For Solid Back Scottfoam 1/2 Inch Thick 80 Pores/Inch

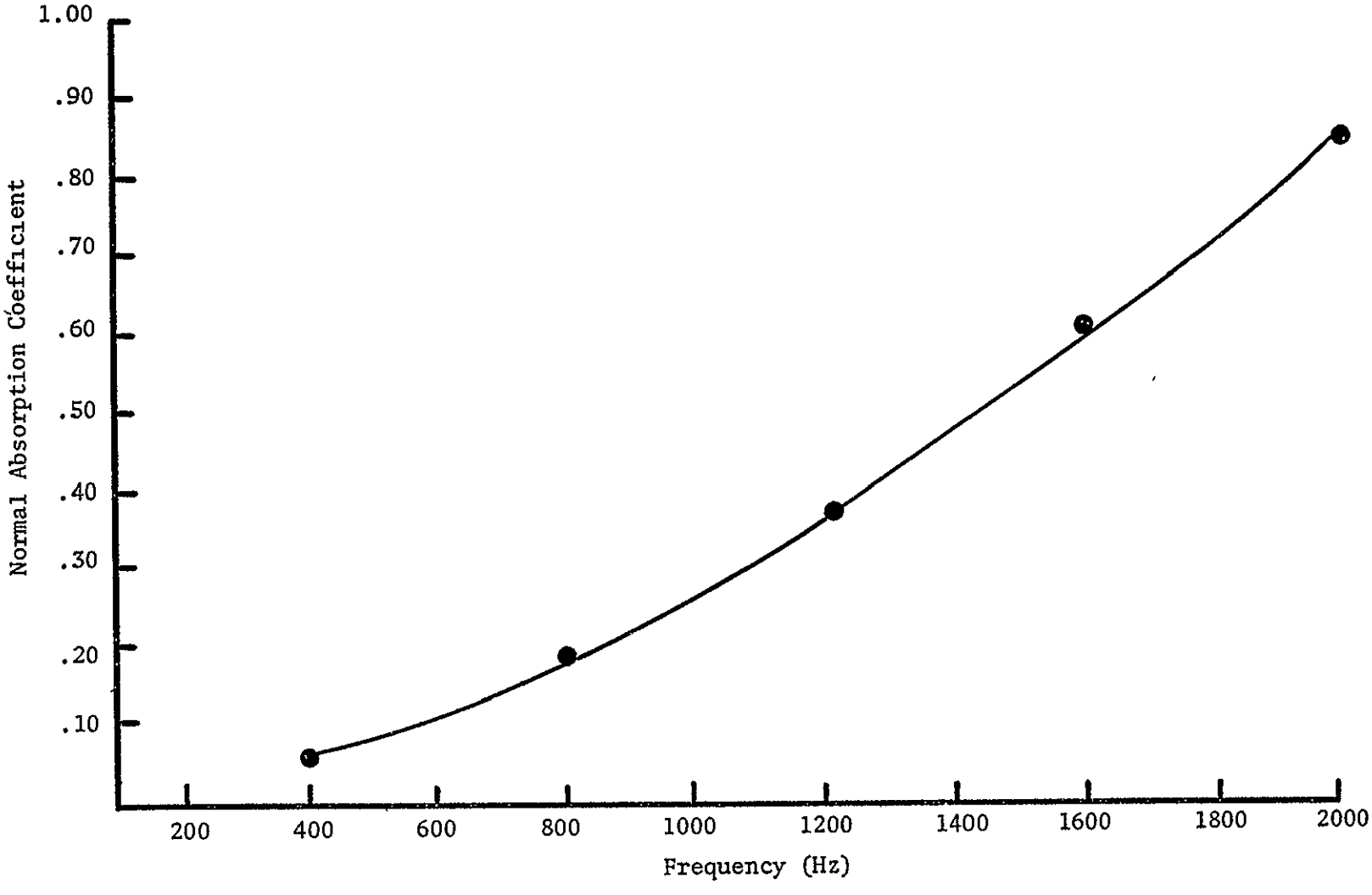

Figure 35 Normal Absorption Coefficient Versus Frequency For Air Backed Scottfoam 80 Pores/Inch 1/2 Inch Thick

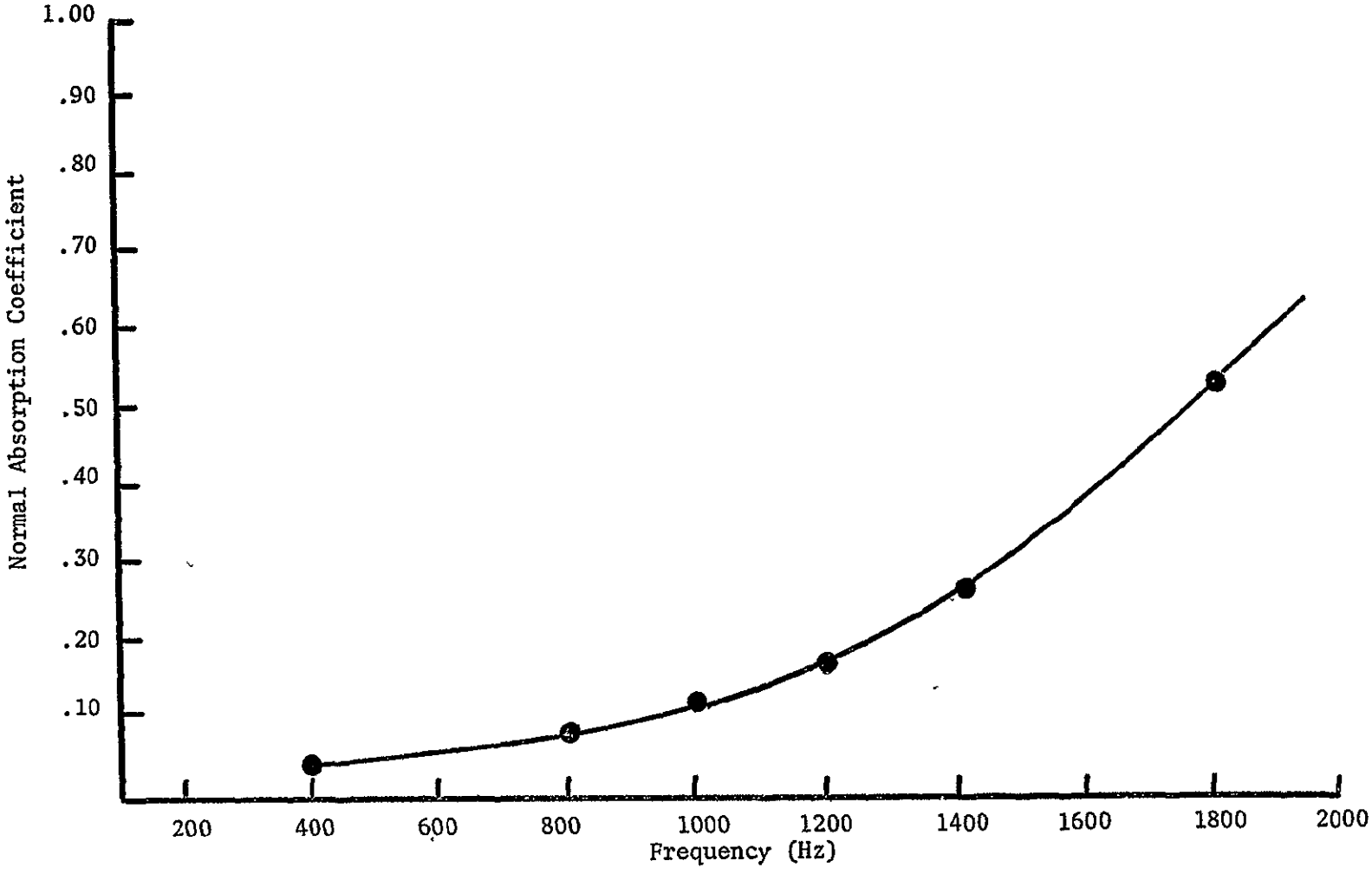

Figure 36 Normal Absorption Coefficient Versus Frequency For Solid Backed Scottfoam 1 Inch Thick 80 Pores/Inch

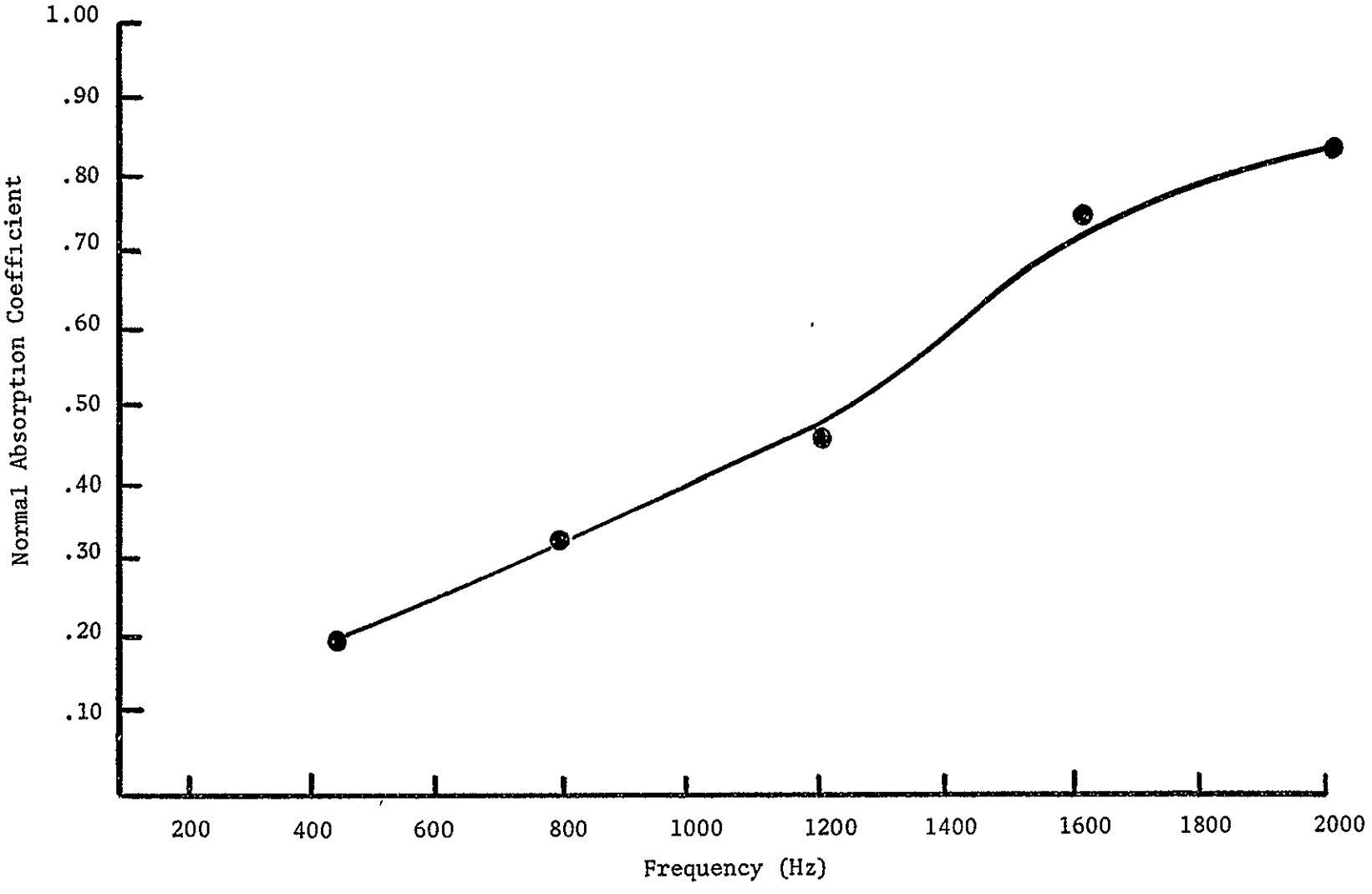

Figure 37 Normal Absorption Coefficient Versus Frequency For Air Backed Scottfoam 1 Inch Thick 80 Pores/Inch

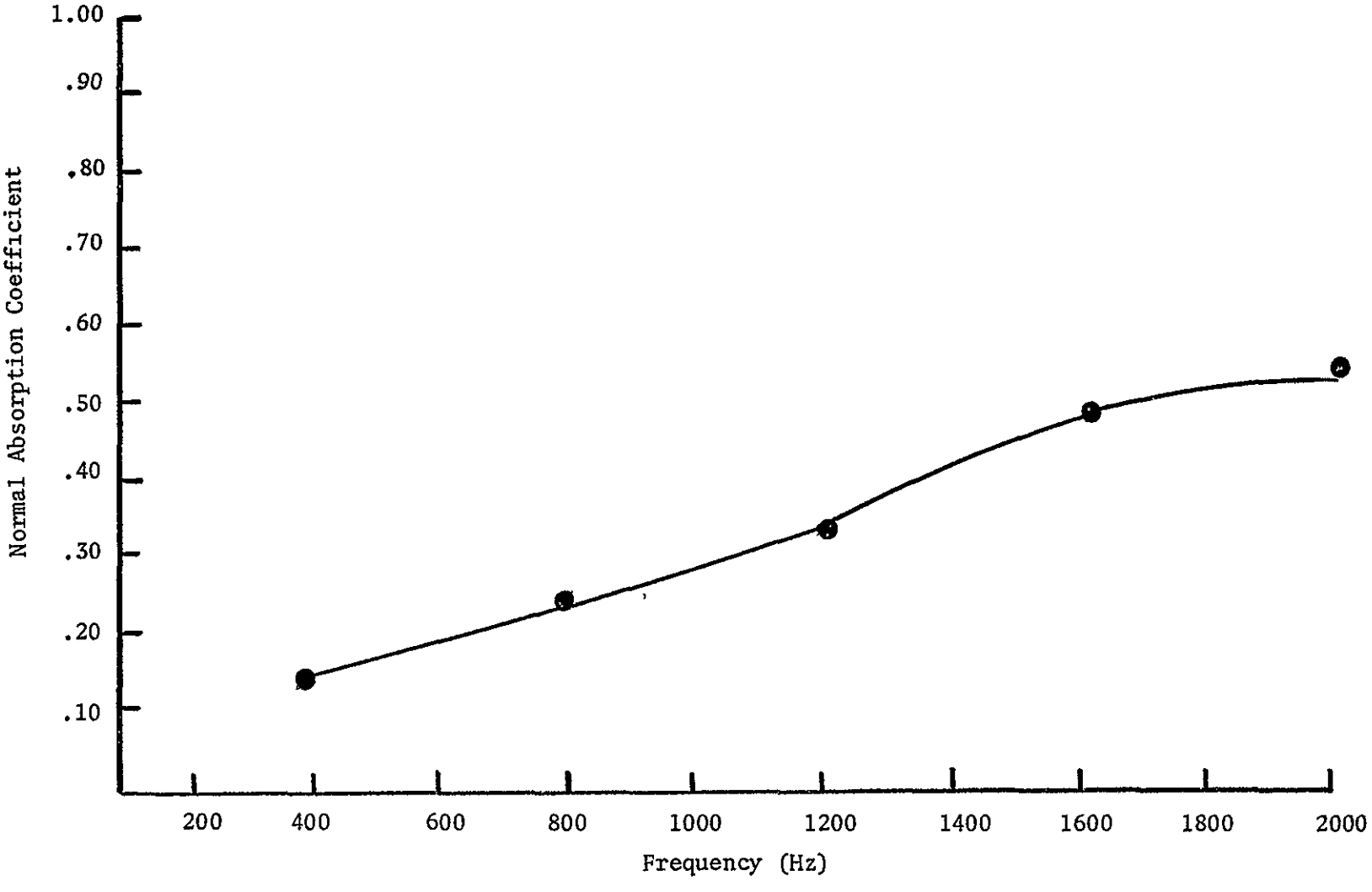

Figure 38 Normal Absorption Coefficient Versus Frequency For Solid Backed Scottfoam 1/2 Inch Thick 100 Pores/Inch

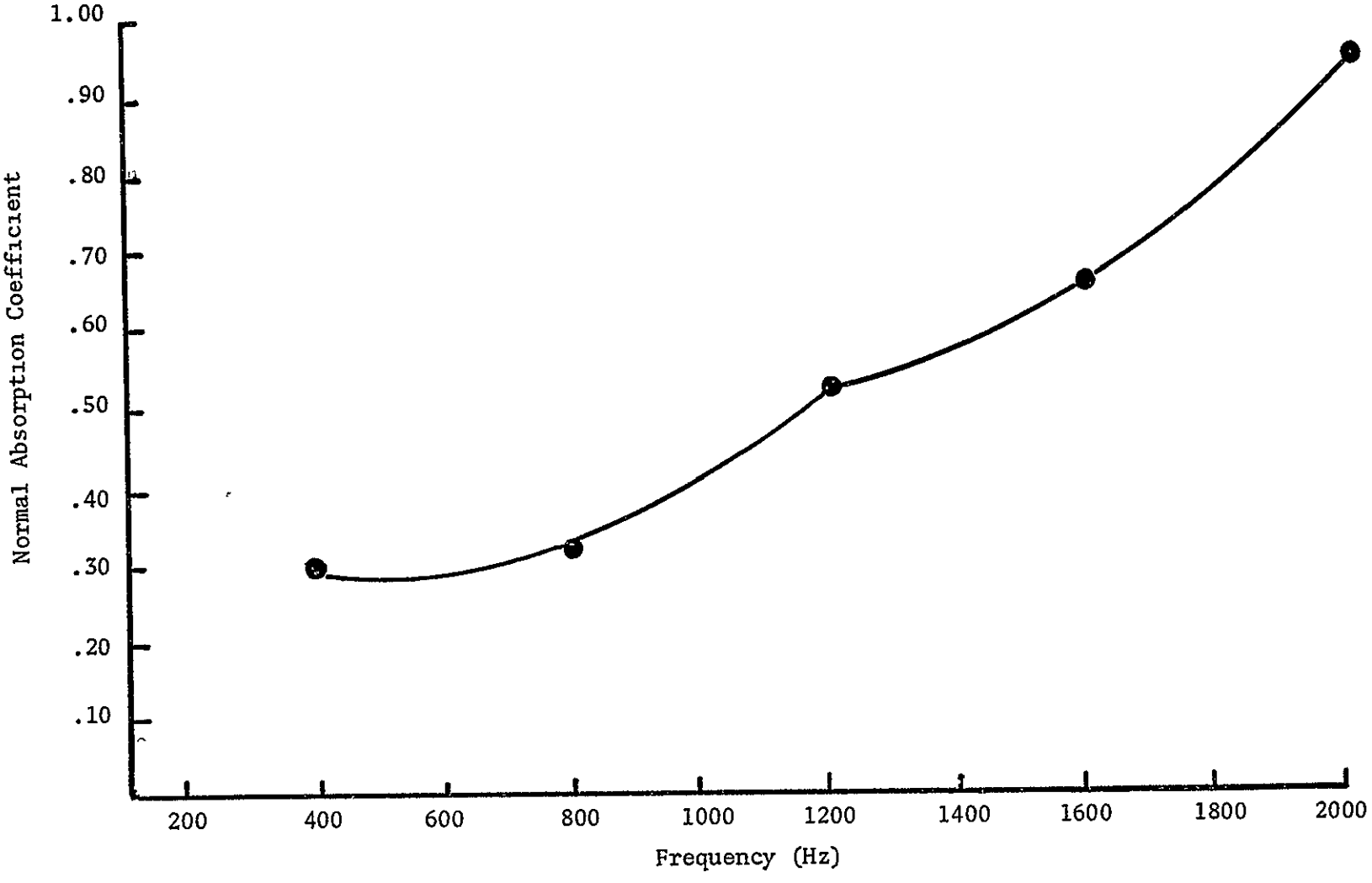

Figure 39 Normal Absorption Coefficient Versus Frequency For Air Backed Scottfoam 1/2 Inch Thick 100 Pores/Inch

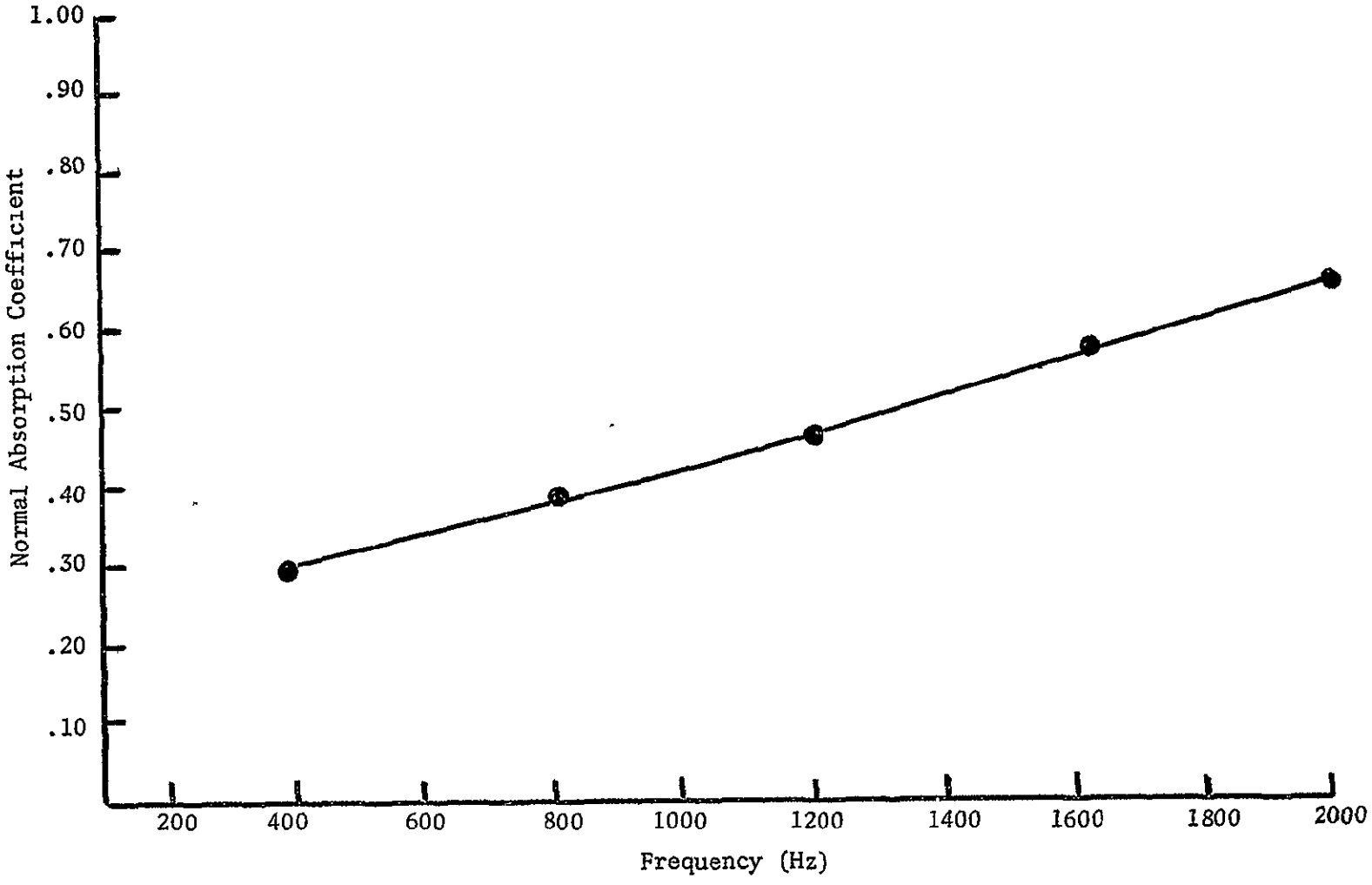

Figure 40 Normal Absorption Coefficient Versus Frequency For Solid Backed Scottfoam 1 Inch Thick 100 Pores/Inch

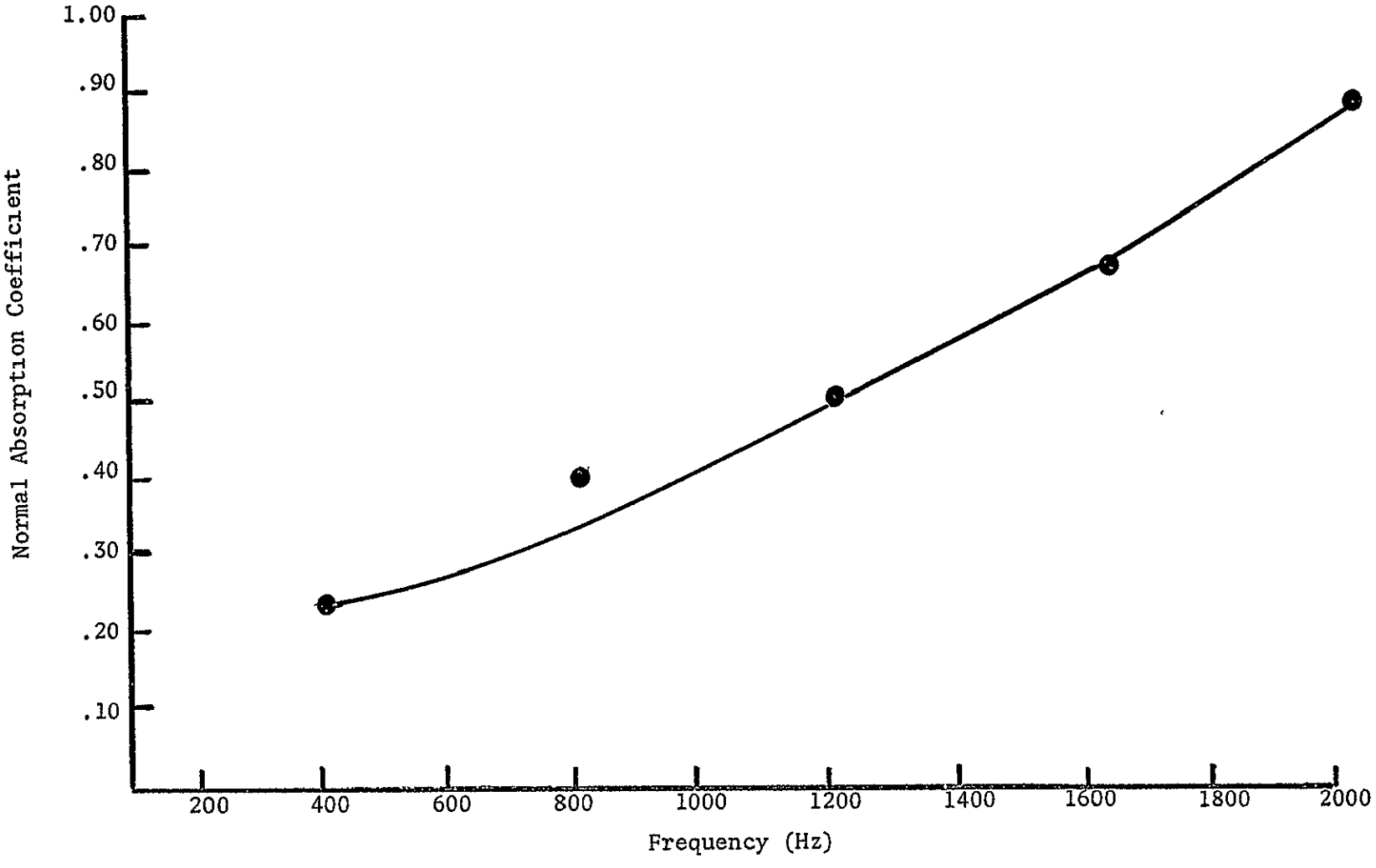

Figure 41 Normal Absorption Coefficient Versus Frequency For Air Backed Scottfoam 1 Inch Thick 100 Pores/Inch

Figure 43 shows the absorption characteristics of this same perforated plate with 1/2-inch thick, 80 pore per inch Scottfoam as a core material. The results indicate a widening of the absorption bandwidth to the point at which at higher frequencies the resonator configuration is still an effective absorber.

The last four configurations tested were absorbing devices using the woven stainless steel mesh Feltmetal as the facing material and Figures 44 through 47 indicate the results of these tests. As we see from Figures 44 and 45, the Feltmetal backed by a solid wall is not very effective for absorbing sound up to 2000 Hz. However, the addition of an air gap of 1/2 inch significantly increased the absorption characteristics in this frequency range. There is not a major difference between the FM 123 and the FM 134, but the FM 134 is a better absorber to 2000 Hz.

4.4 Grazing Incidence Absorption

The specimens tested for grazing absorption properties consisted of twelve of the fourteen specimens tested during the normal incidence tests. Each test was conducted with the absorbing devices placed on two sides of the duct as side branches and by comparing the sound pressure levels at various points in the duct with the sound pressure level at these same points in an untreated duct. For example, a wave was propagated down the untreated duct and the sound level measured at various locations, the duct was then lined with the absorbing branch section and the sound pressure level recorded again. The difference in sound

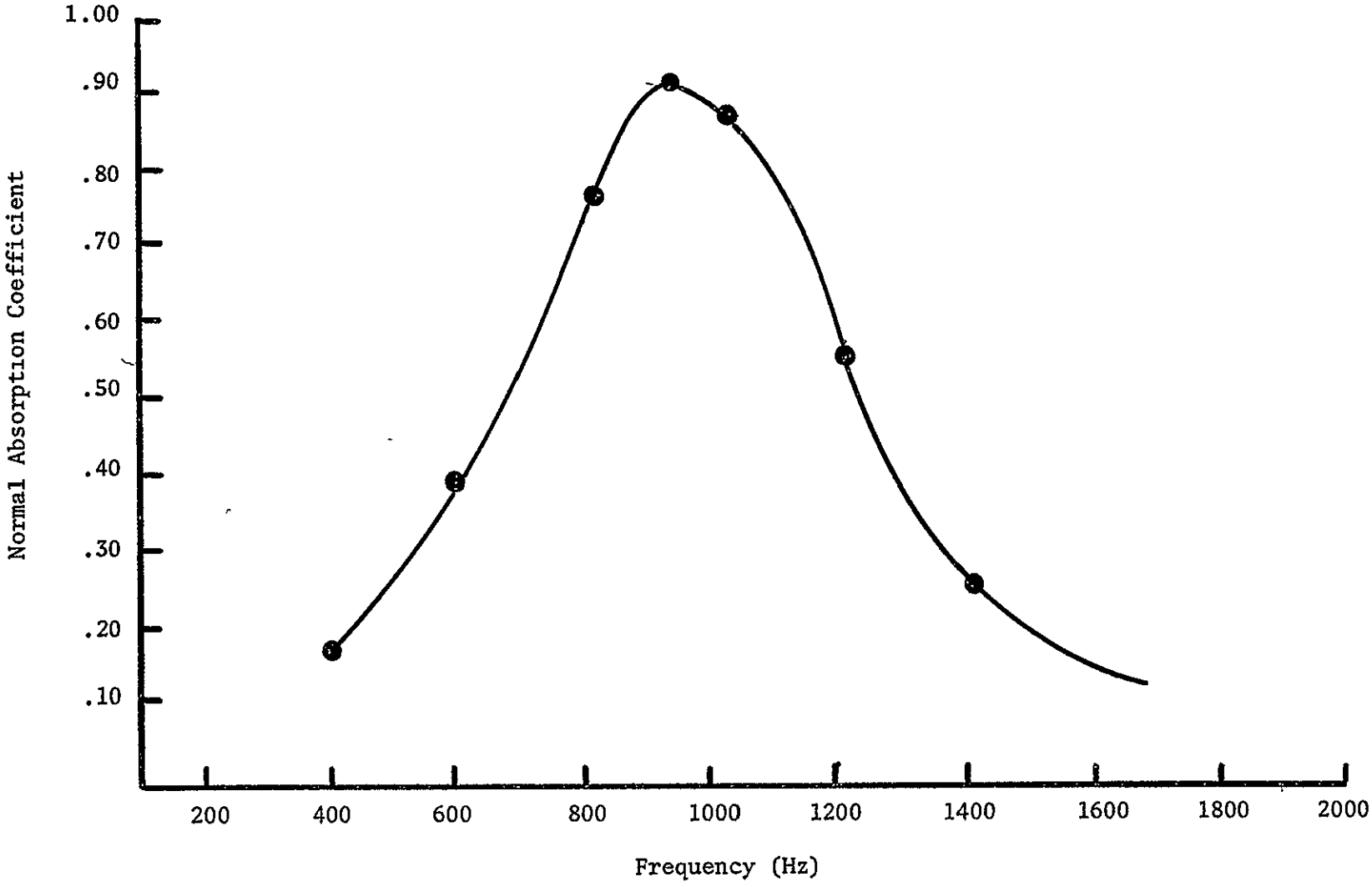

Figure 42 Normal Absorption Coefficient Versus Frequency For Resonator With Partitioned Air Backing

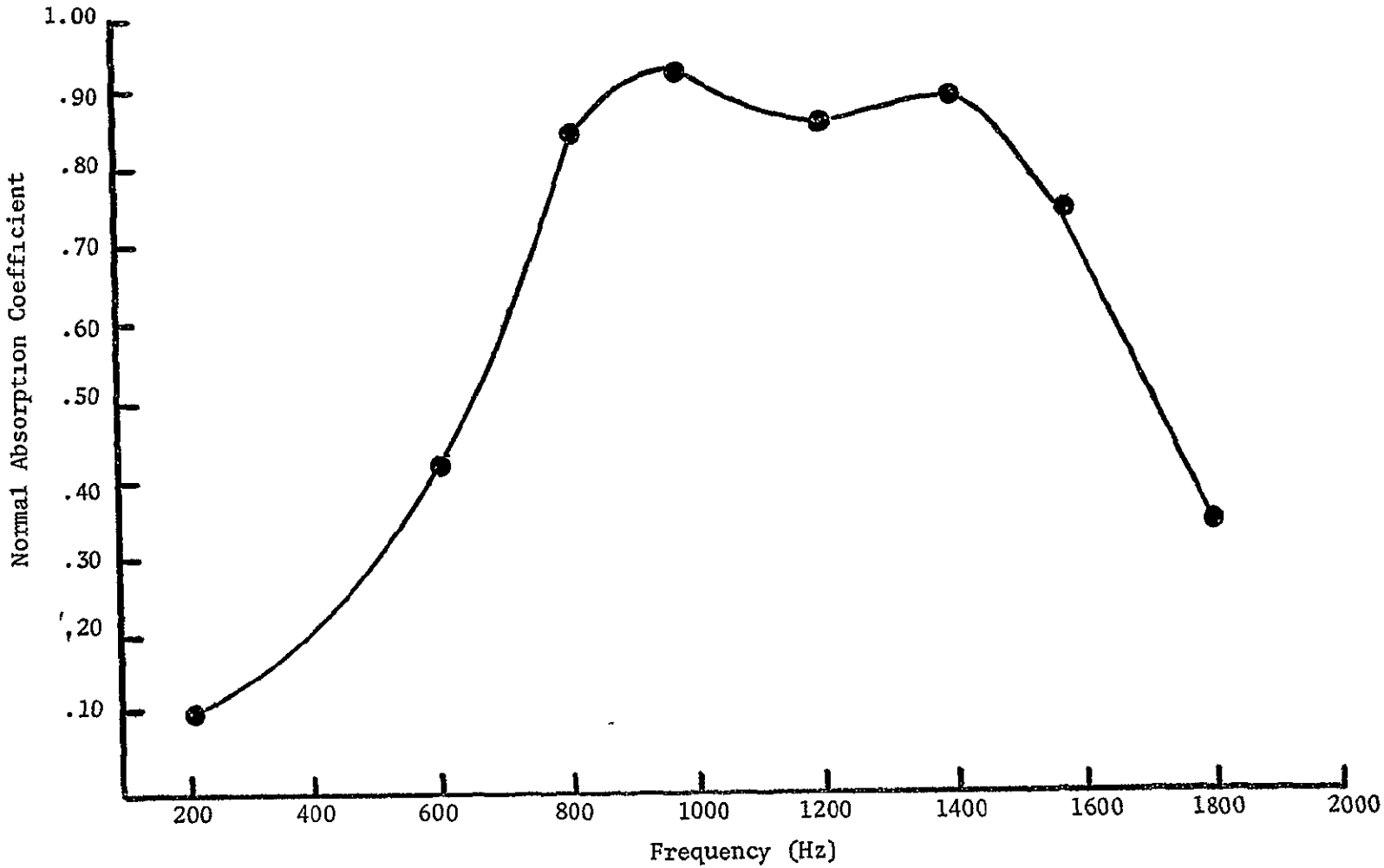

Figure 43 Normal Absorption Coefficient Versus Frequency For Resonator With Foam Backing

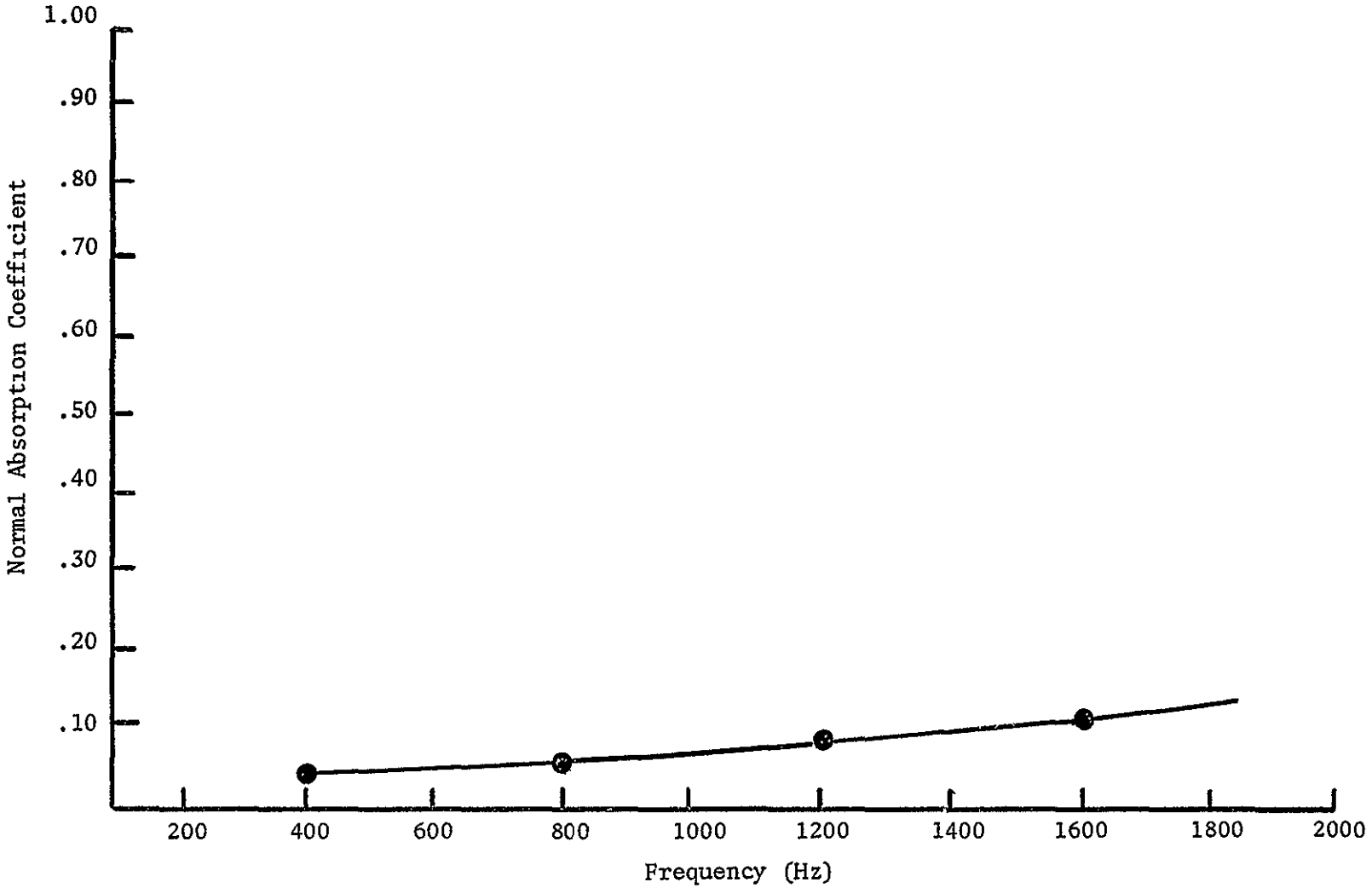

Figure 44 Normal Absorption Coefficient Versus Frequency For Feltmetal FM 123 With Solid Backing

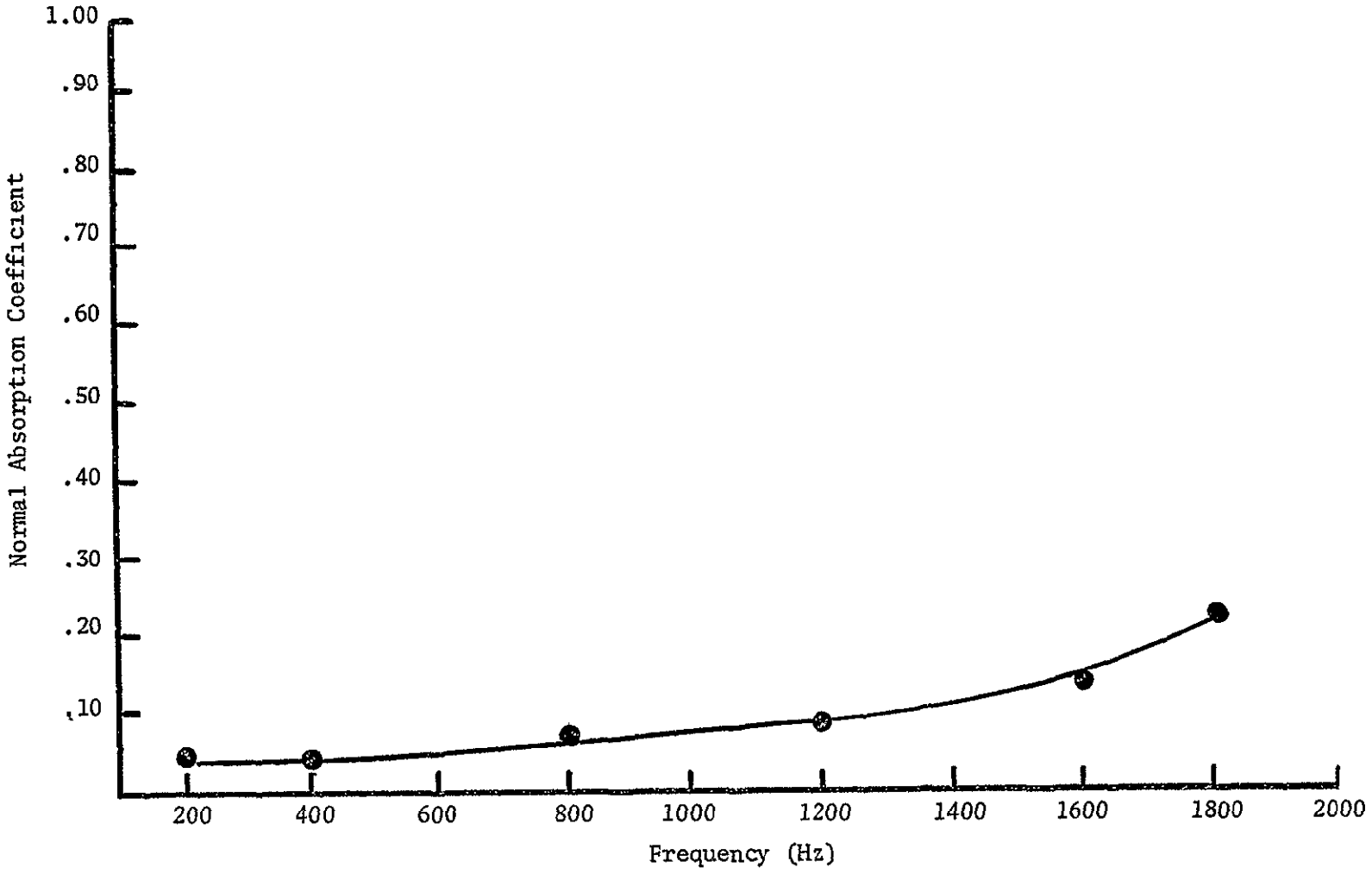

Figure 45 Normal Absorption Coefficient Versus Frequency For Feltmetal FM 134 With Solid Backing

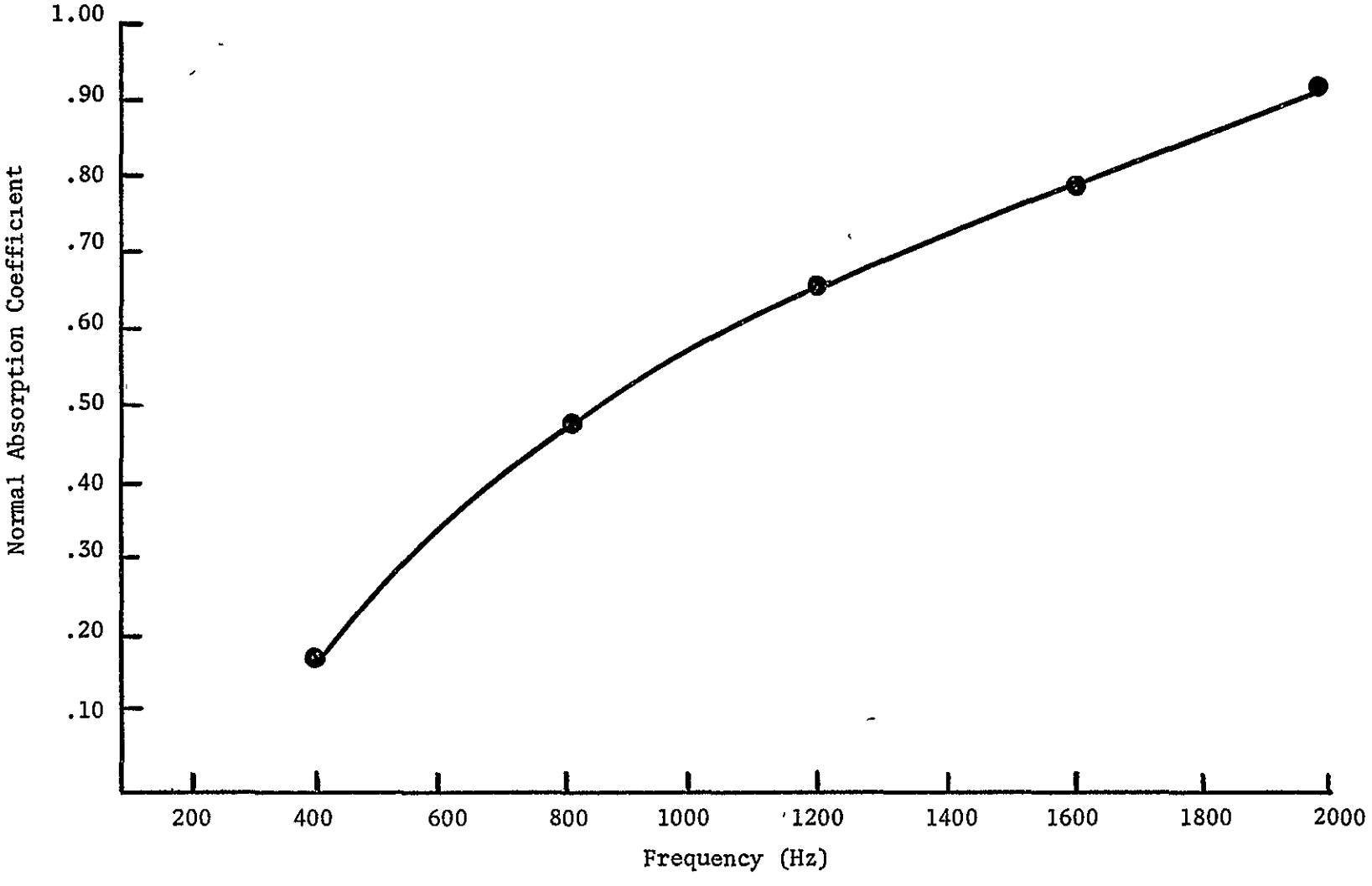

Figure 46 Normal Absorption Coefficient Versus Frequency For Feltmetal FM 134 With Air Backing

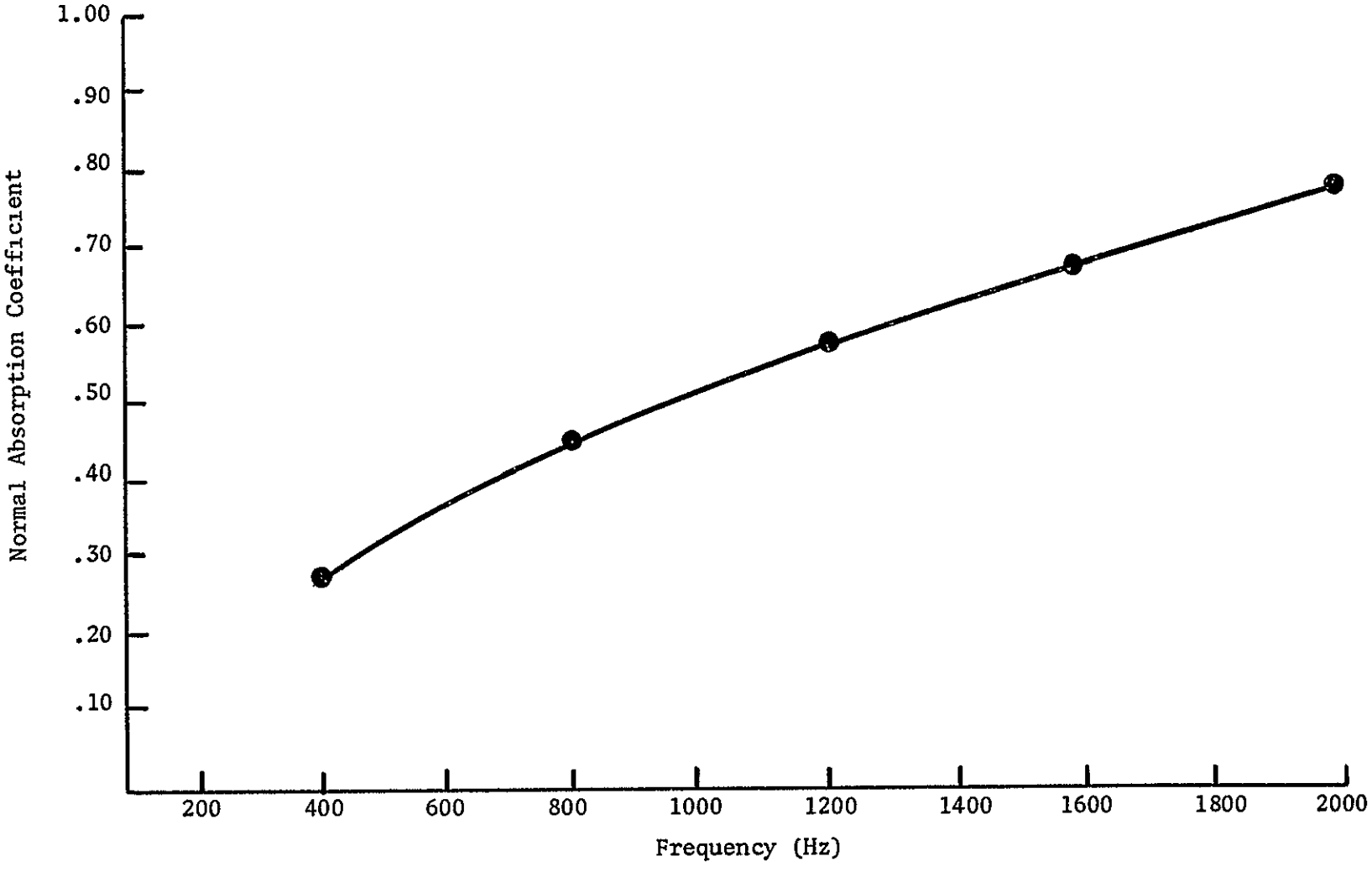

Figure 47 Normal Absorption Coefficient Versus Frequency For Feltmetal FM 123 With Air Backing

pressure level between the former and the latter is plotted as the effective transmission loss. This effective transmission loss was measured for grazing incidence waves impinging at angles for 10 to 90 degrees in odd multiples over a frequency range of 400 to 2000 Hz. Some data was taken at 2200 Hz and appears in the results but most of the results were obtained for frequencies up to 2000 Hz.

The results of the various grazing incidence tests on absorbing devices using 80 pore per inch Scottfoam as a facing material are shown in Figures 48 through 50. As we see in Figures 48 and 50, the 1/2-inch and 1-inch thick, 80 pore per inch Scottfoam with solid backing is a relatively good attenuator. Its sound absorbing properties generally decrease with increasing angle and the overall effective transmission loss increases with frequency. Figure 49 shows the results of the 1/2-inch thick sample of Figure 48 backed by a 1-inch air gap. The air gap core has spread the incidence effect over a wider range of transmission loss; for example, with solid backing, there was a maximum increase of 6 dB attenuation going from 90 degree to 10 degrees incidence while now this maximum transmission loss has increased to 9 dB as a result of the use of the air gap. The air gap also increased the transmission loss at each discrete frequency for each individual angle tested.

Figures 51 through 53 are the results using the 100 pore per inch Scottfoam in the absorbing devices. The trends noticed in the previous three figures are also noted in these three. The

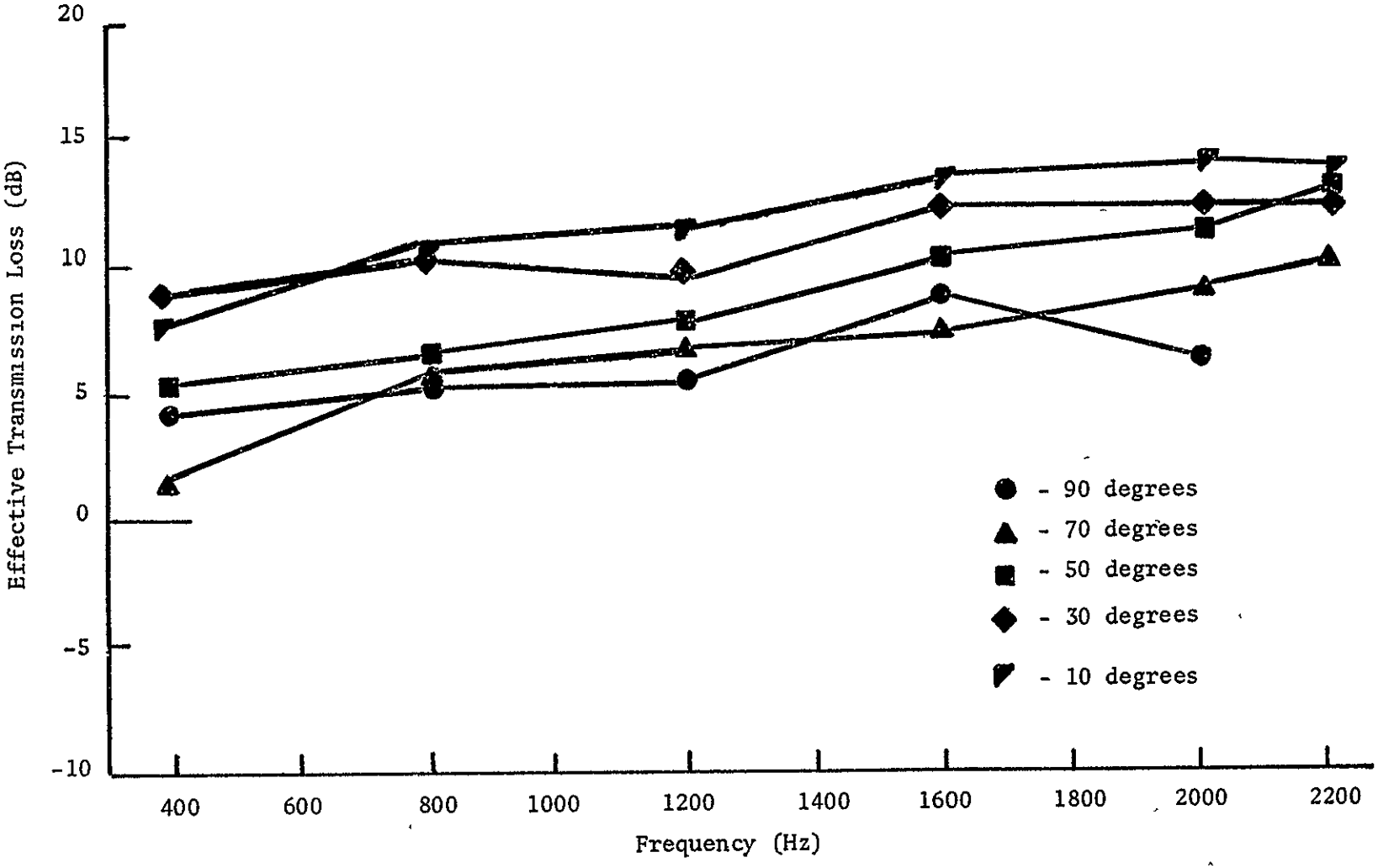

Figure 48 Grazing Absorption as a Function of Incident Angle. Scottfoam 80 Pores/Inch 1/2 Inch Thick With Solid Backing.

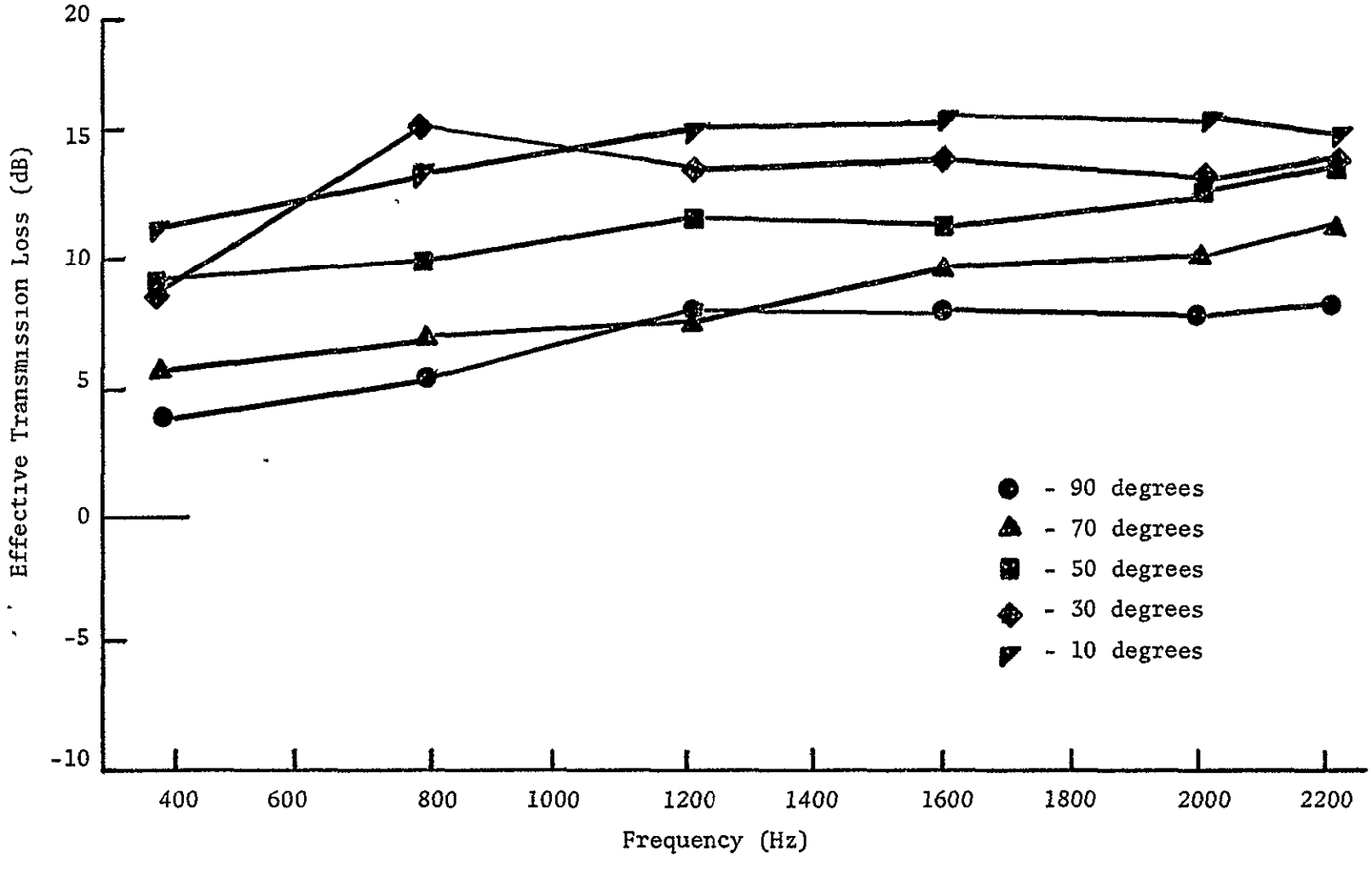

Figure 49 Grazing Absorption as a Function of Incident Angle.
Scottfoam 80 Pores/Inch 1/2 Inch Thick Air Backed

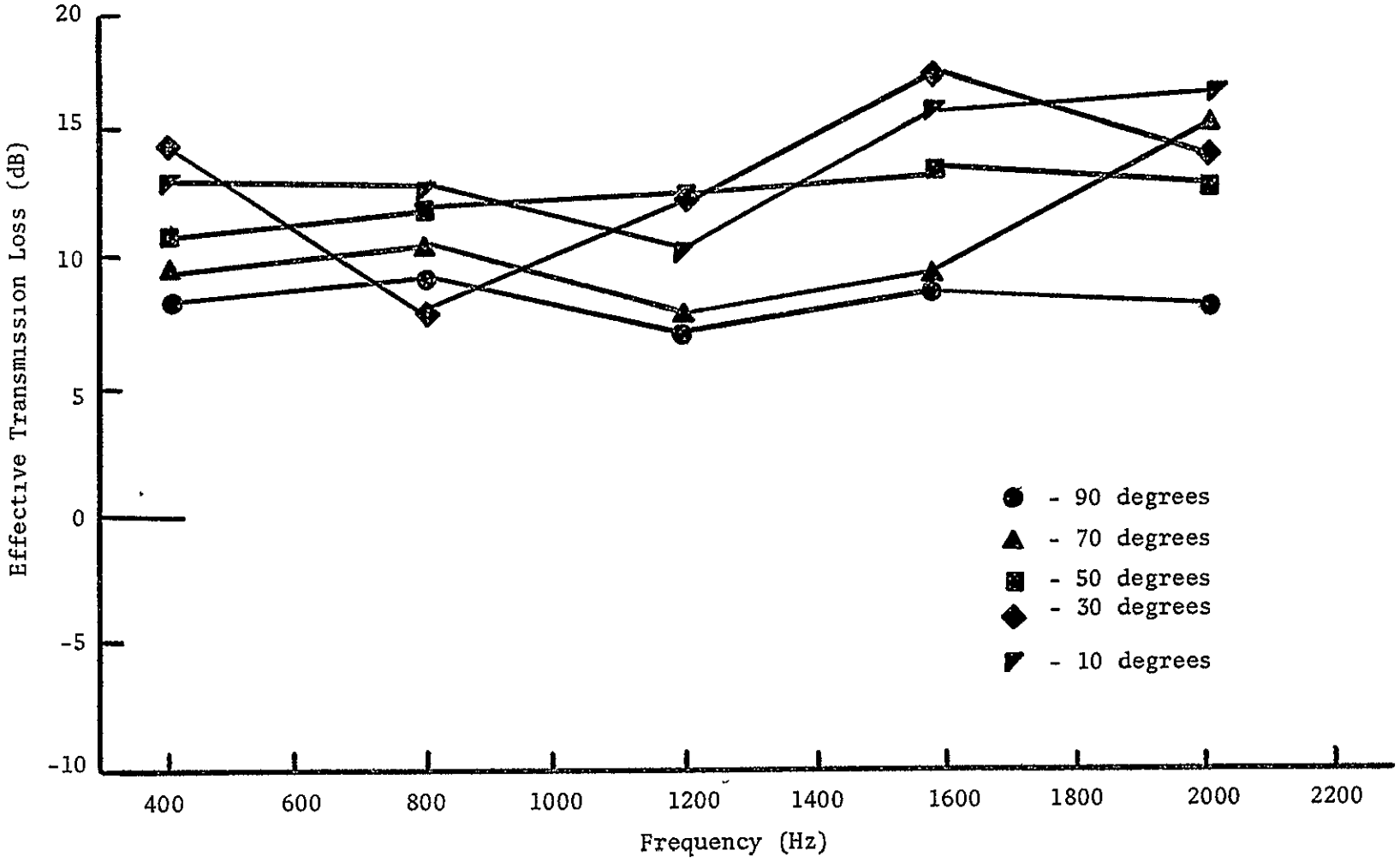

Figure 50 Grazing Absorption as a Function of Incident Angle.
Scottfoam 80 Pores/Inch 1 Inch Thick Solid Backing

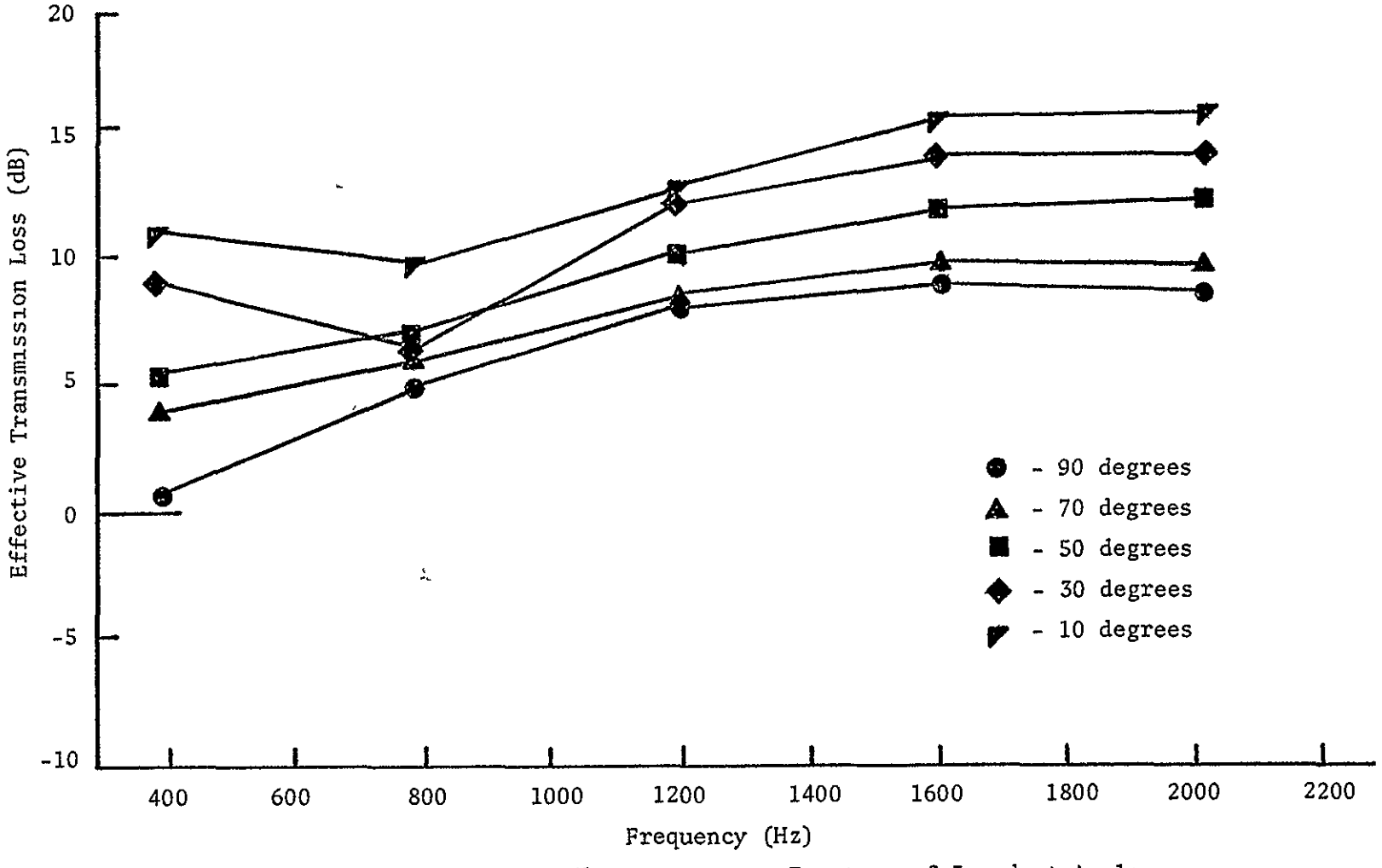

Figure 51 Grazing Absorption as a Function of Incident Angle. Scottfoam 100 Pores/Inch 1/2 Inch Thick With Solid Backing

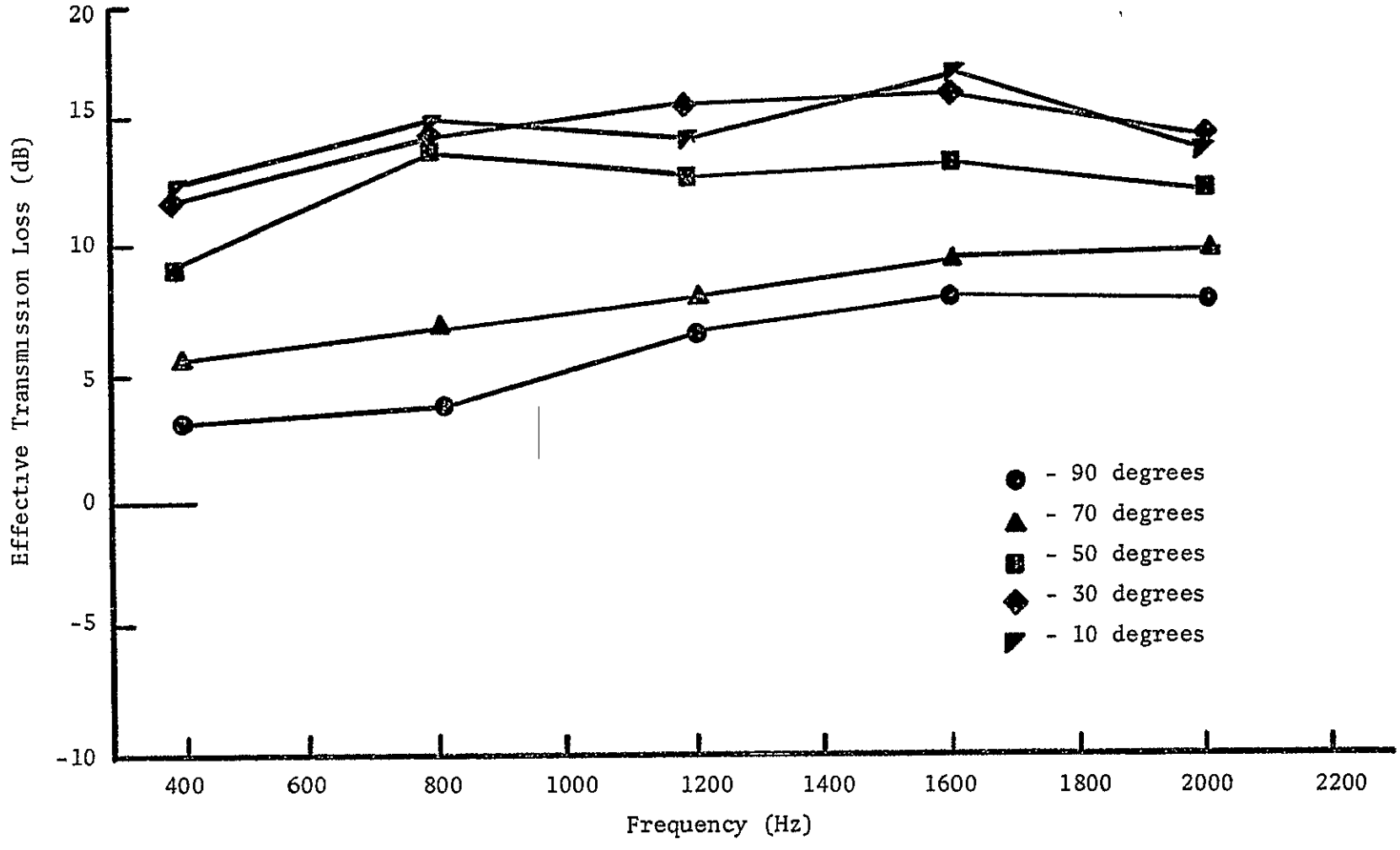

Figure 52 Grazing Absorption as a Function of Incident Angle.
Scottfoam 100 Pores/Inch 1/2 Inch Thick with Air Backing

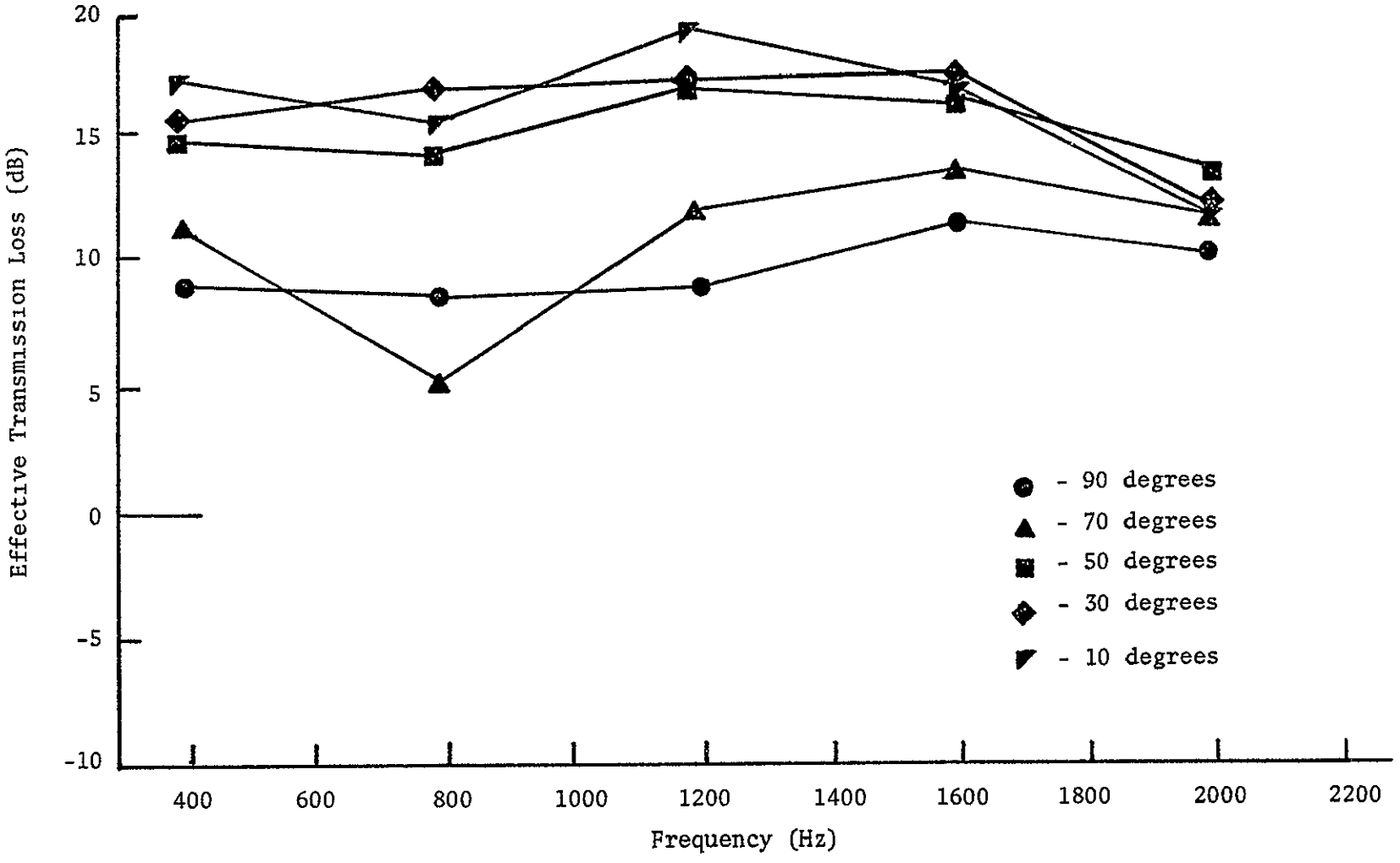

Figure 53 Grazing Absorption as a Function of Incident Angle.
Scottfoam 100 Pores/Inch 1 Inch Thick Solid Backing

air gap seems to spread the data out increasing the attenuation of the lower impingement angles by a larger amount than the higher angles. A further comparison will be carried out in the next section.

Figures 54 through 57 illustrate the results of configurations with Feltmetal specimens as facing material. The overall trend shows the effective transmission loss increasing with decreasing angle of incidence and increasing frequency. Solid backed Feltmetal is not a very effective absorbing device at any angle of incidence. Figure 56 shows solid backed FM 123 reacting no better than a solid wall as a sound absorber. The air core helped considerably for all angles tested. It again spread out the effective transmission loss as a function of incidence angle, and it increased the absolute value of the effective transmission loss for every angle.

The final grazing absorption tests were conducted on resonator configurations. The first, a partitioned air backed perforated face, showed very little effective transmission loss. In fact, as can be seen in Figure 58, there was no discernable effect of incident angle. For low frequencies, attenuation could be considered constant at all angles of incident below 70 degrees. At the high frequencies (above 1200 Hz) the data is bunched together for every angle. When the 80 pore per inch Scottfoam core was added to the resonator configuration, there was a spreading out of the data and an increase of effective transmission loss with decreasing angle of incidence. See Figure 59.

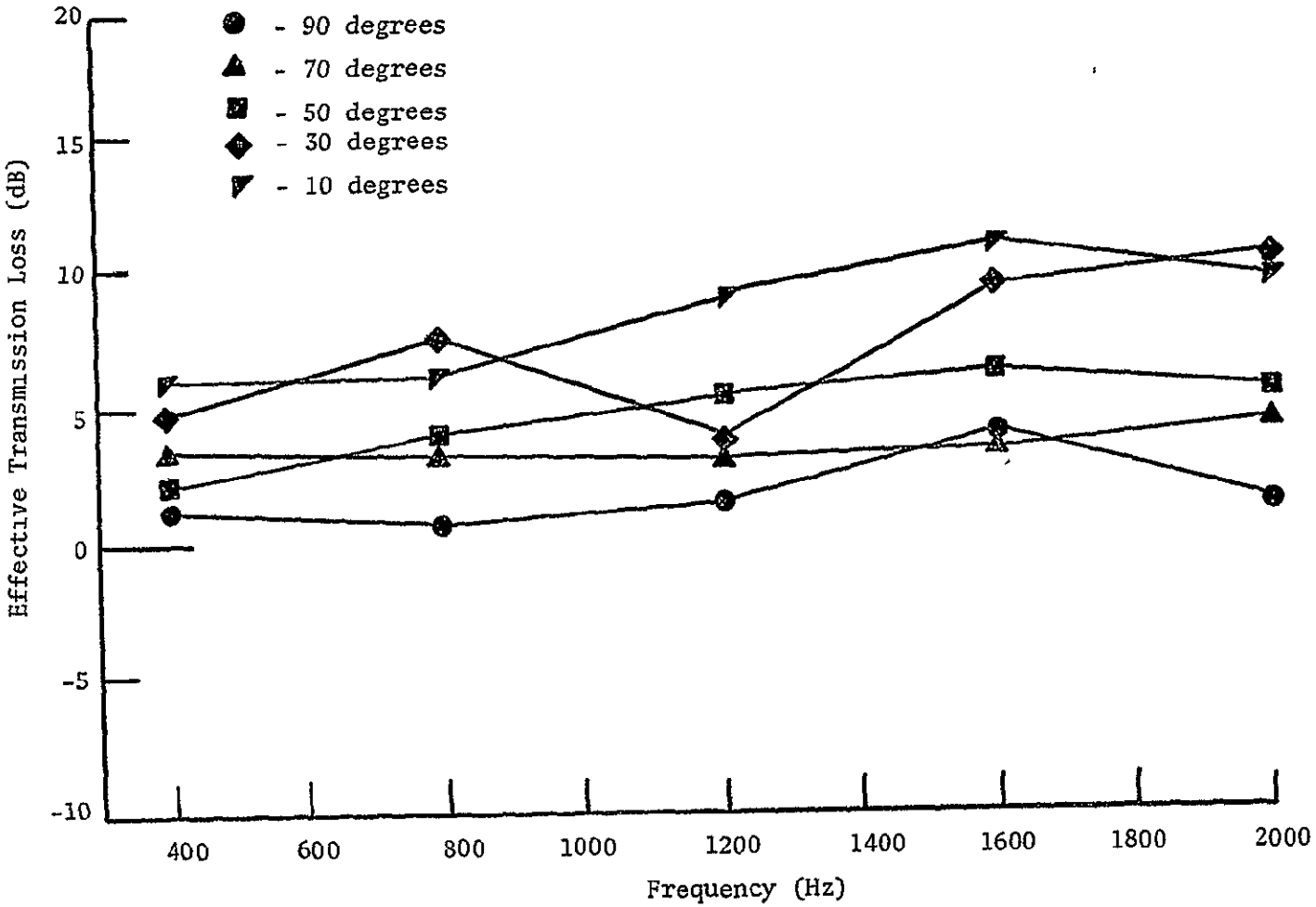

Figure 54 Grazing Absorption as a Function of Incident Angle. Feltmetal FM 134 With Solid Backing

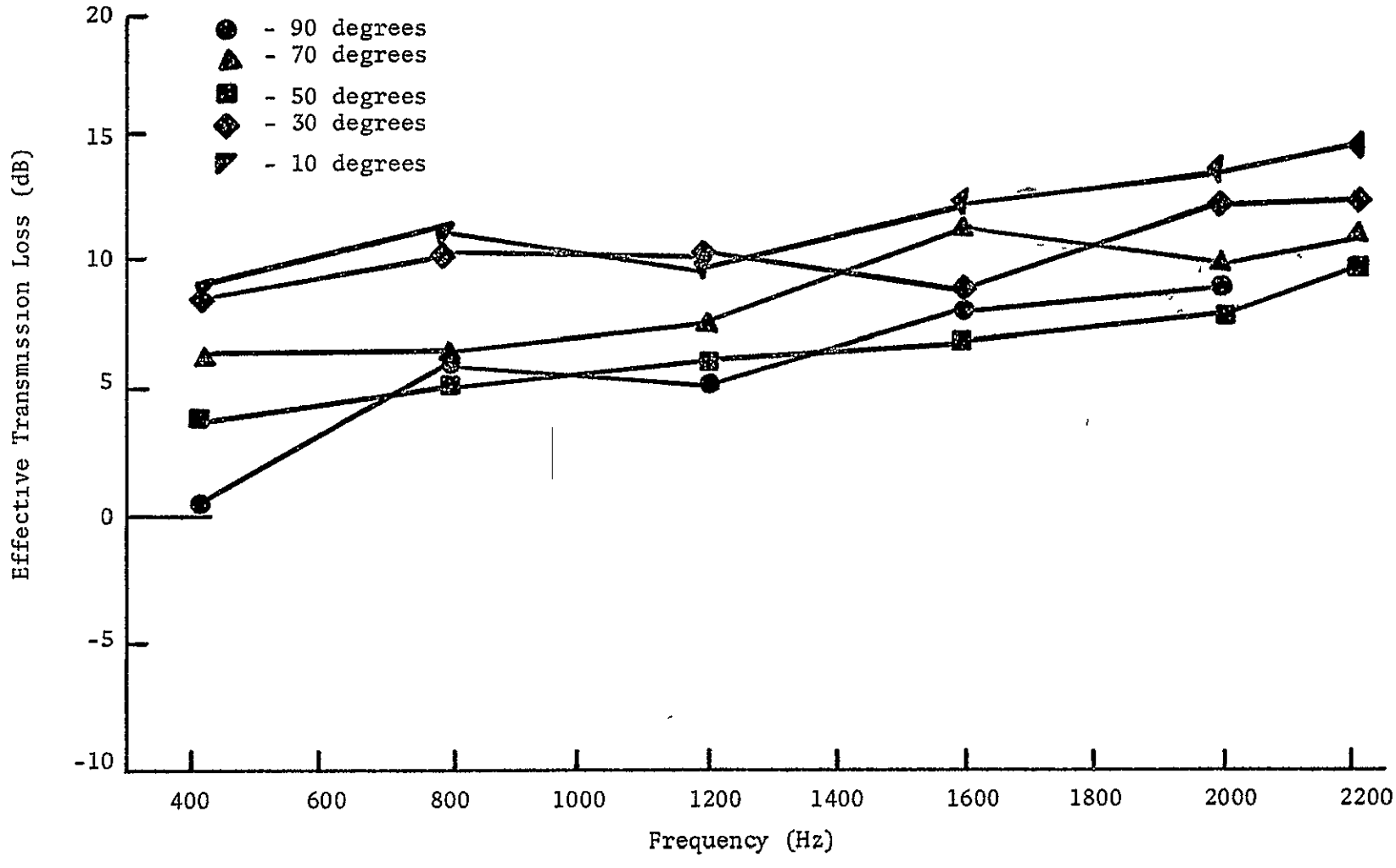

Figure 55 Grazing Absorption as a Function of Incident Angle.
Feltmetal FM 134 With 1 Inch Air Gap

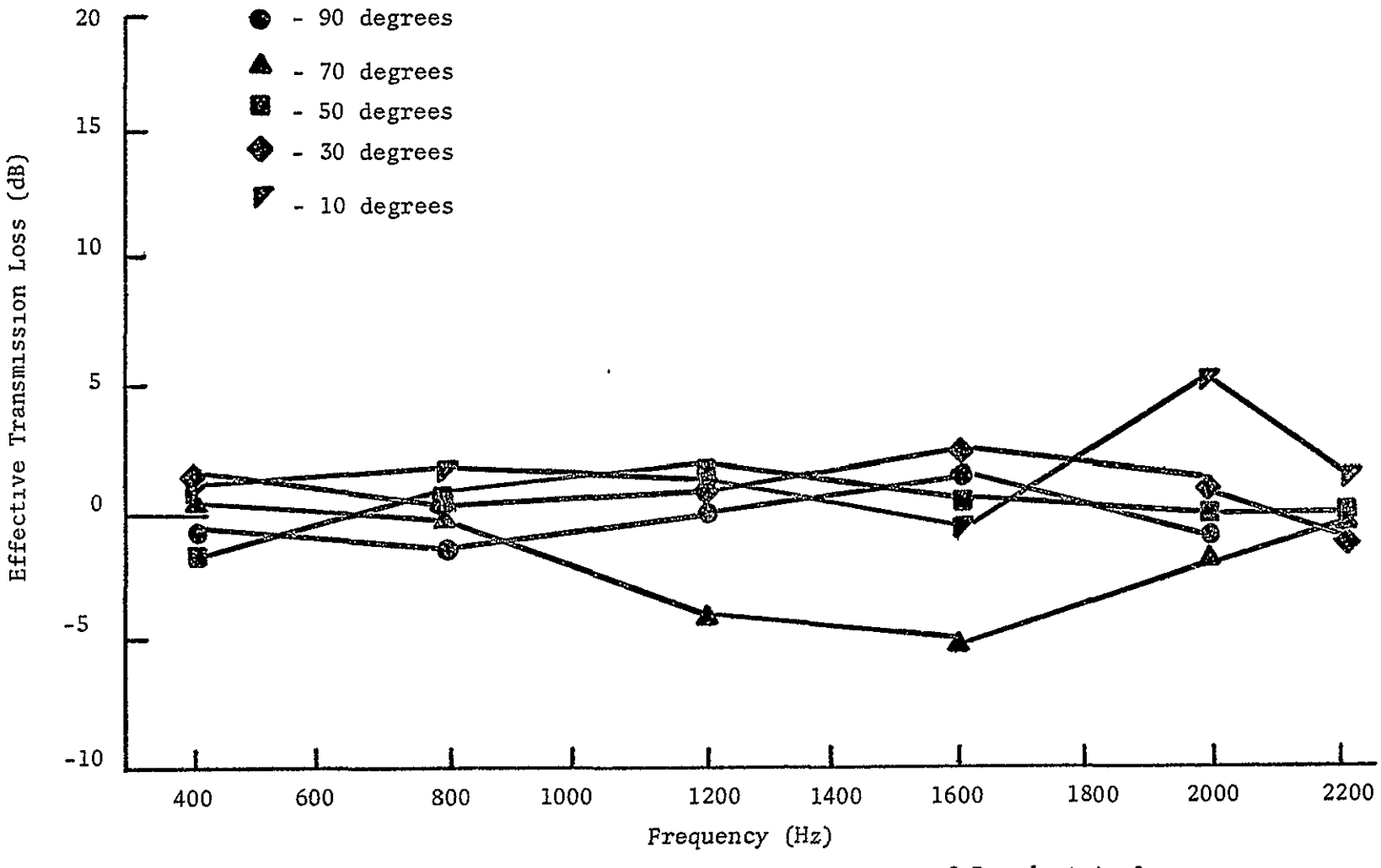

Figure 56 Grazing Absorption as a Function of Incident Angle. Feltmetal FM 123 With Solid Backing

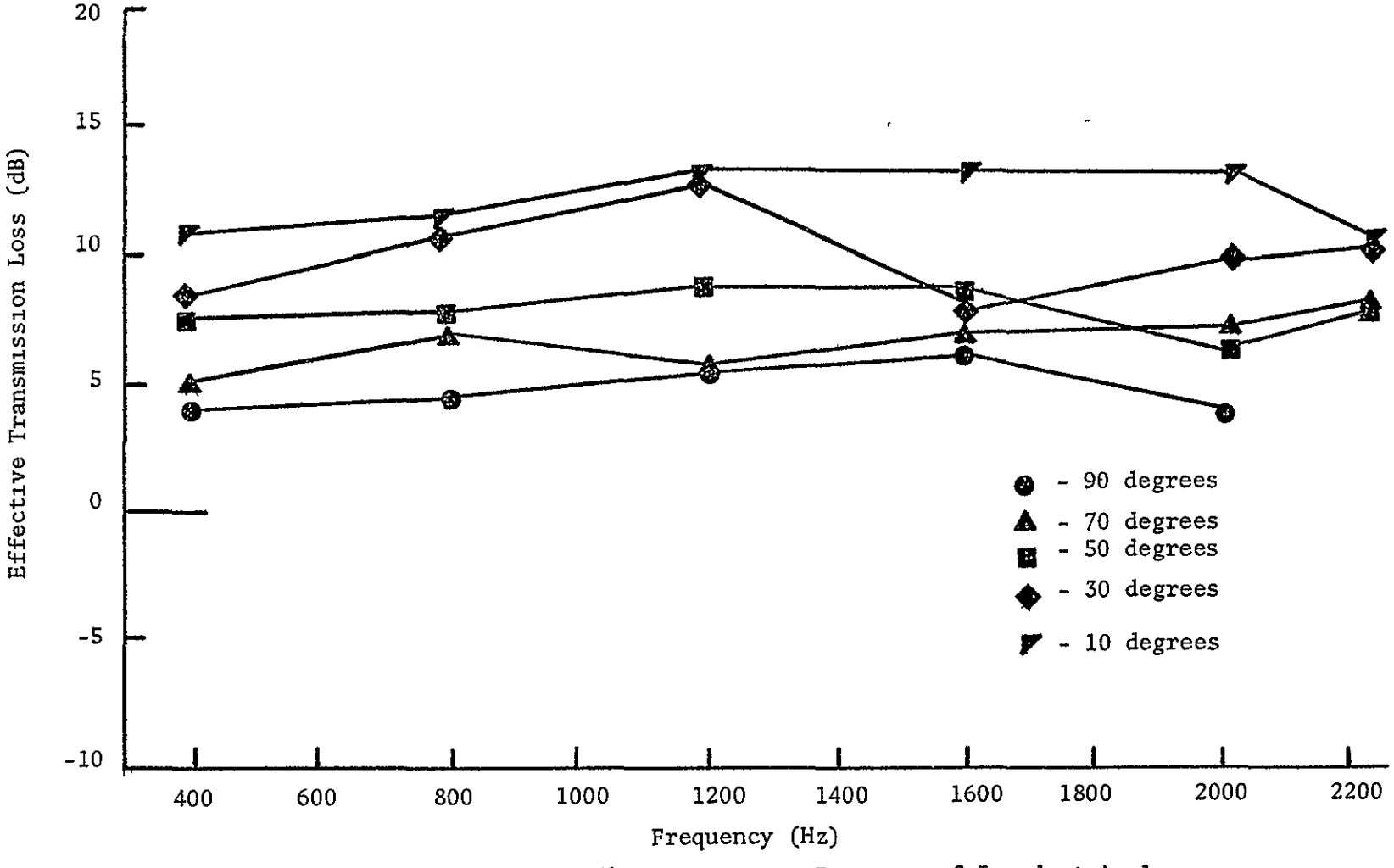

Figure 57 Grazing Absorption as a Function of Incident Angle. Feltmetal FM 123 With Air Backing

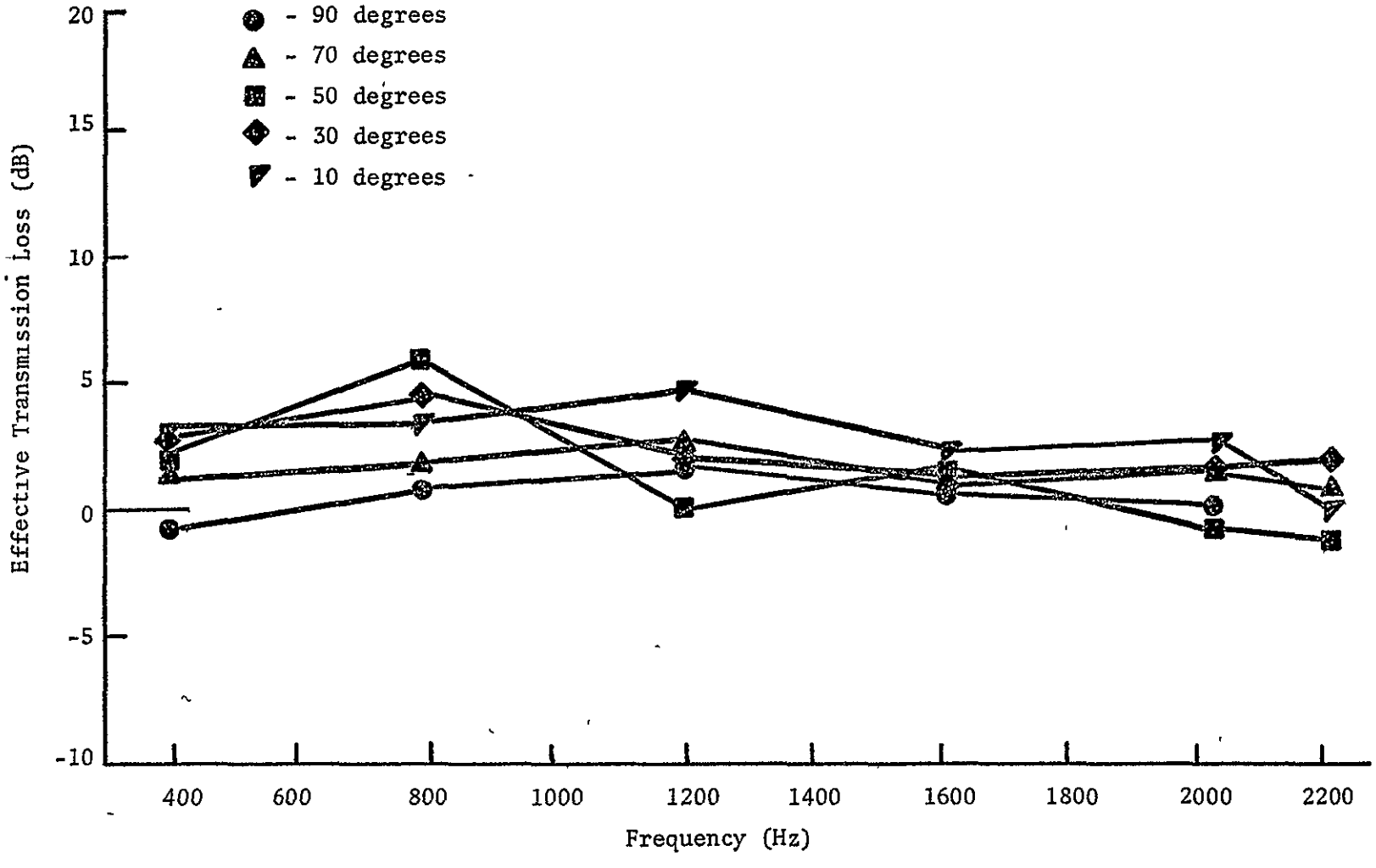

Figure 58 Grazing Absorption as a Function of Incident Angle. Perforated Facing With 1/2 Inch Air Backing

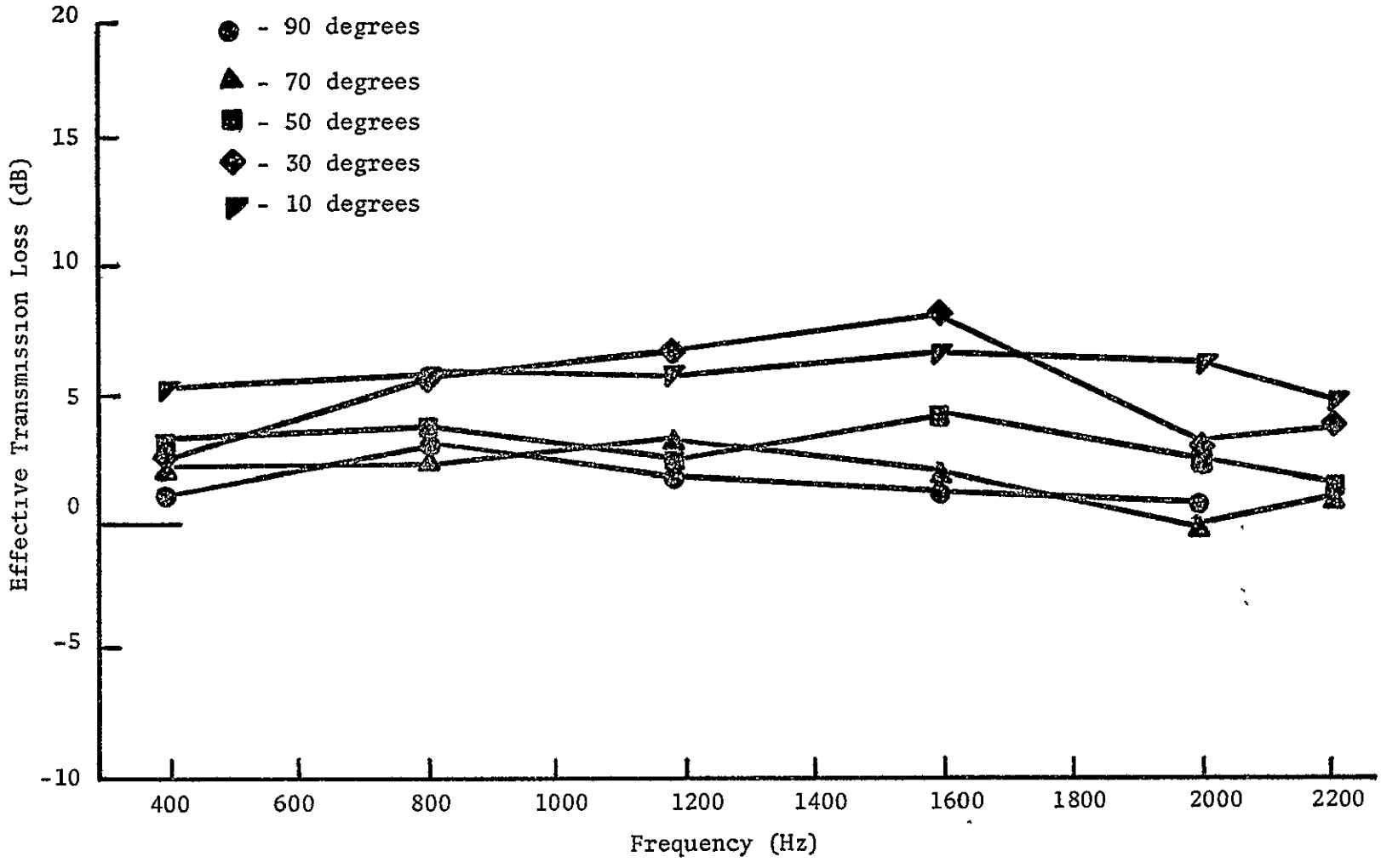

Figure 59 Grazing Absorption as a Function of Incident Angle. Perforated Facing With Scottfoam Core

4.5 Absorption Treatment Comparisons

To make the grazing incidence results easier to analyze, some of the effective transmission loss curves have been replotted so that the various acoustic configurations could be compared. Each of the results that follow have the effective transmission loss versus frequency plotted for an incidence angle of 10 degrees. The various configurations have been separated into five categories. The five comparison categories each contain the results of three related acoustic treatments.

Figure 60 shows the comparison of the three side branches using 80 pore per inch Scottfoam as a facing material. The results show that, at the 10 degree incidence angle, there is no advantage to be obtained by placing an air core behind a 1/2-inch thick sample. The results also indicate that very little is gained by increasing the thickness of the sample from 1/2 inch to 1 inch. This seems to give the ideal result for one can use the minimum amount of acoustic treatment to obtain the maximum result.

For the 100 pore per inch Scottfoam, Figure 61 indicates that the thicker sample is a better absorber, up to 1600 Hz, than the thinner sample. If one were interested in attenuating a 10 degree grazing incidence wave between 400 and 1600 Hz and he had 1 inch of available space for treatment, he would better serve his purpose by placing a 1-inch thick, 100 pore per inch Scottfoam sample in the space rather than the same material of 1/2-inch thickness with a 1/2-inch thick air core. However,

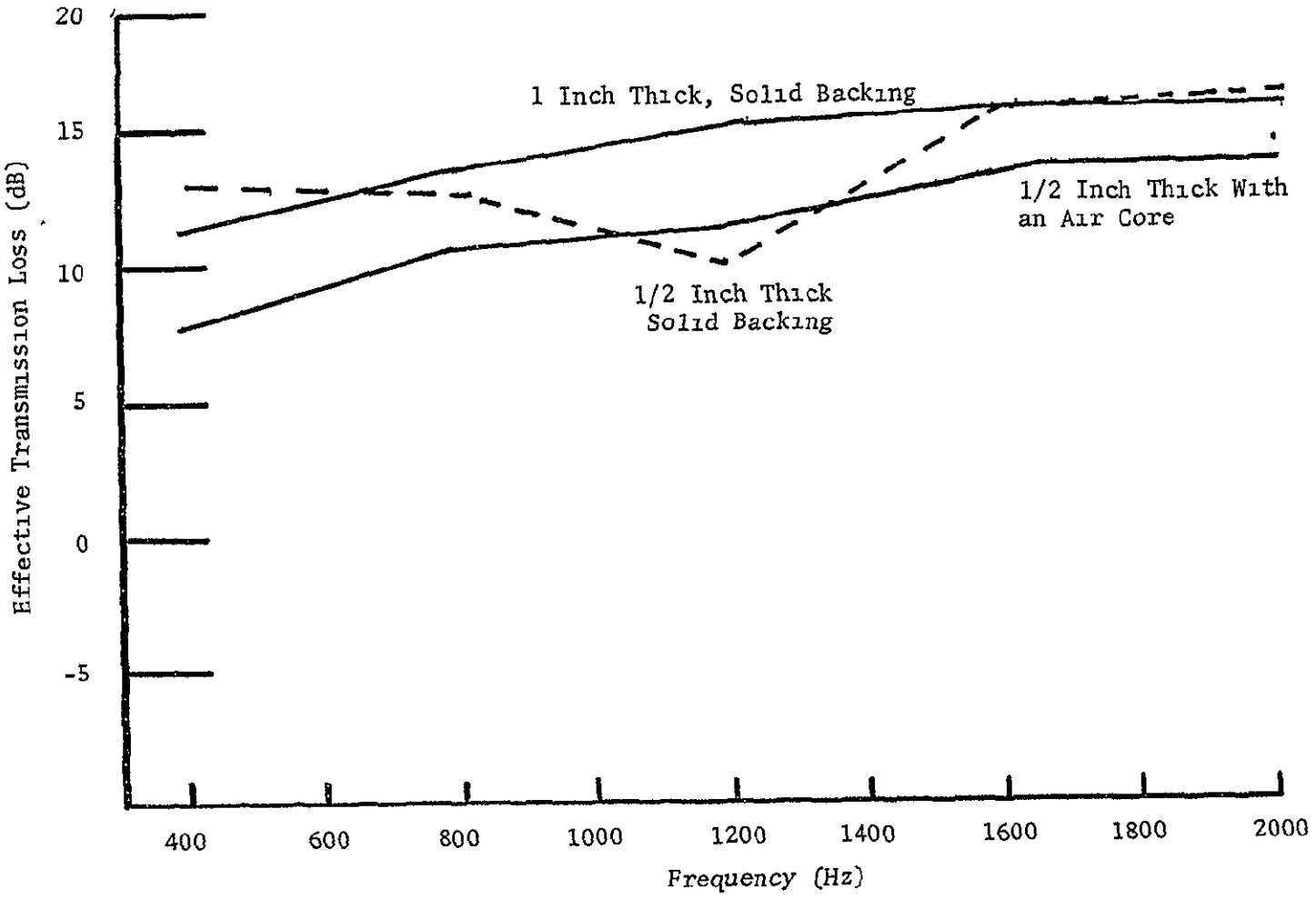

Figure 60 Effective Transmission Loss of Three Scottfoam Samples of 80 Pores/Inch

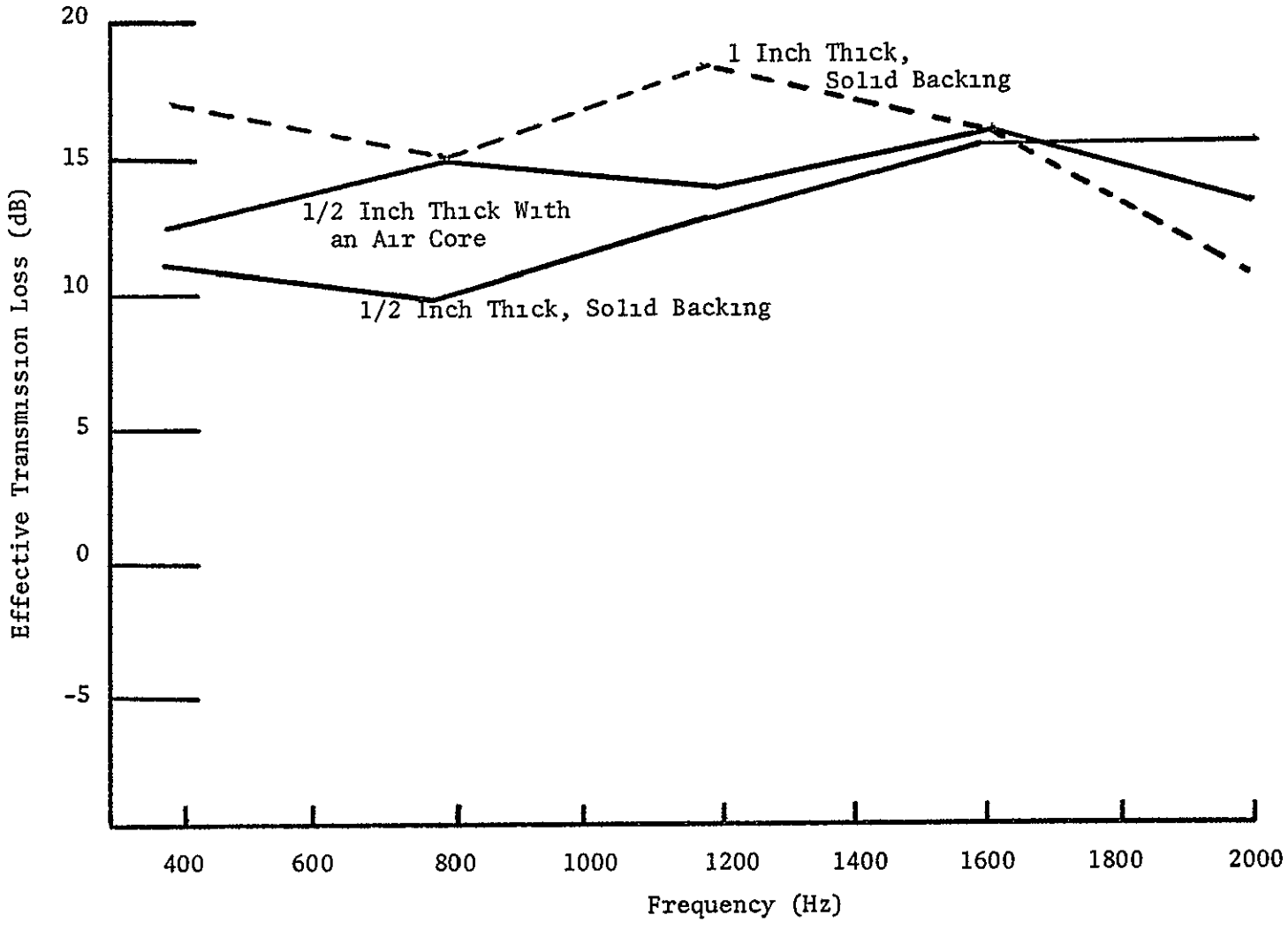

Figure 61 Effective Transmission Loss of Three Scottfoam Samples of 100 Pores/Inch

at the higher frequencies, the 1/2-inch thick 100 pore per inch sample proves to be the better absorber.

Figure 62 compares two 100 pore per inch samples with an 80 pore per inch sample. The 1-inch thick lower porosity sample is the better attenuator. This 80 pore per inch configuration averages 5 dB more effective transmission loss all the way to 1600 Hz. The 100 pore per inch configurations continuously increase with frequency until they cross the 80 pore per inch curve at approximately 1700 Hz. As a result of this, one could deduce that the lower porosities should be used to attenuate lower frequencies and higher porosities the higher frequencies.

Figures 63 and 64 show the comparison curves for the acoustic treatments using the two Feltmetal samples as facing materials. Figure 63 shows that the FM 134 Feltmetal is a better attenuator over the frequency range, 400 to 2000 Hz, than is FM 123 when both are backed by solid plates. This figure also indicates that the addition of an air core can significantly increase the grazing absorption properties of FM 134. Figure 64 shows the attenuation of FM 123 also being increased using an air core. This air backing increases the effective transmission loss by 10 dB over the whole frequency range. An interesting result from these two figures is, when FM 123 is backed by a solid plate, it is a very poor attenuator as compared to FM 134 backed by a solid plate. However, the air core placed on both samples makes the FM 123 plus air core a better attenuator than the FM 134 plus air core.

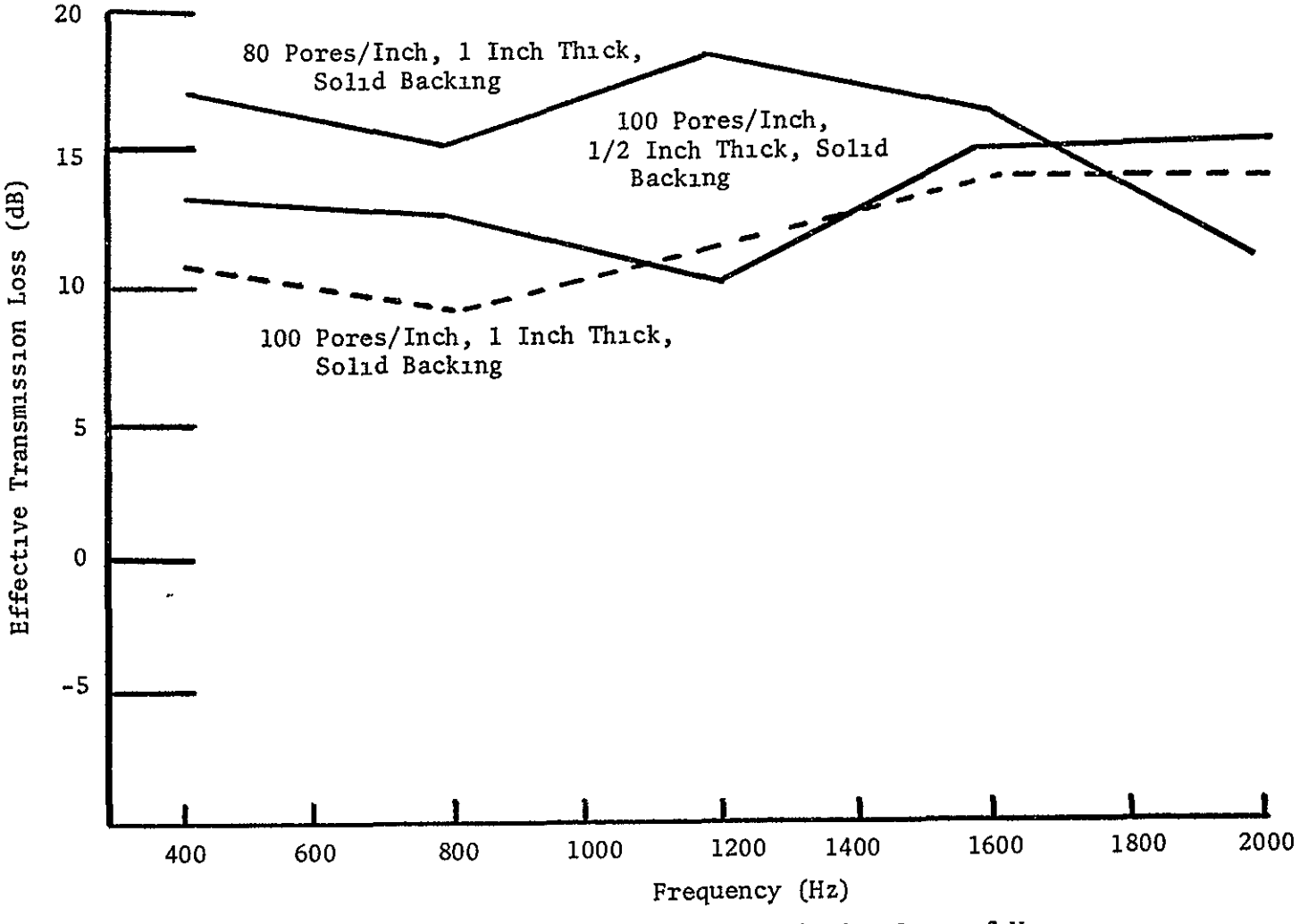

Figure 62 Effective Transmission Loss of Various Scottfoam Configurations

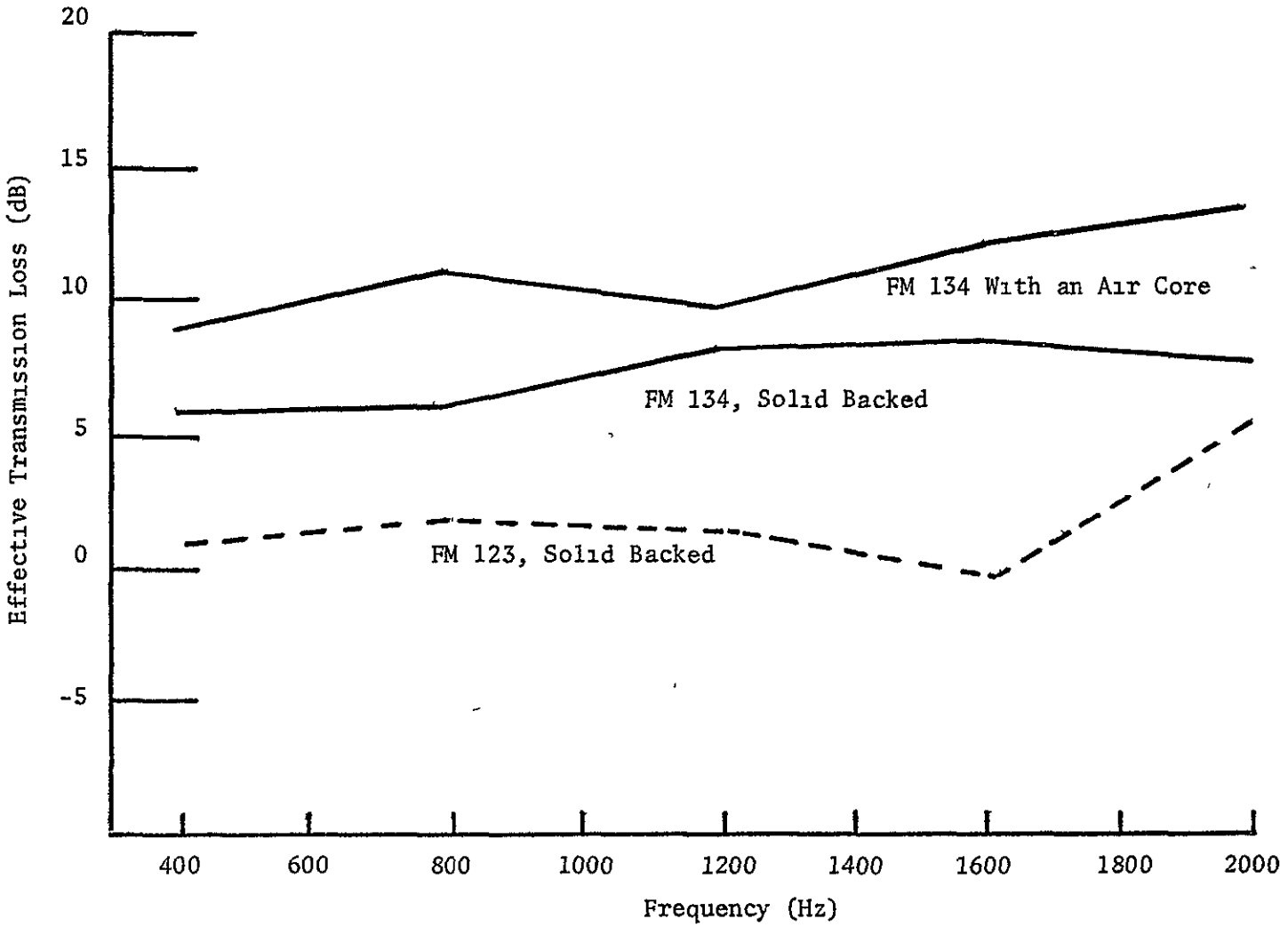

Figure 63 Effective Transmission Loss of Three Feltmetal Configurations

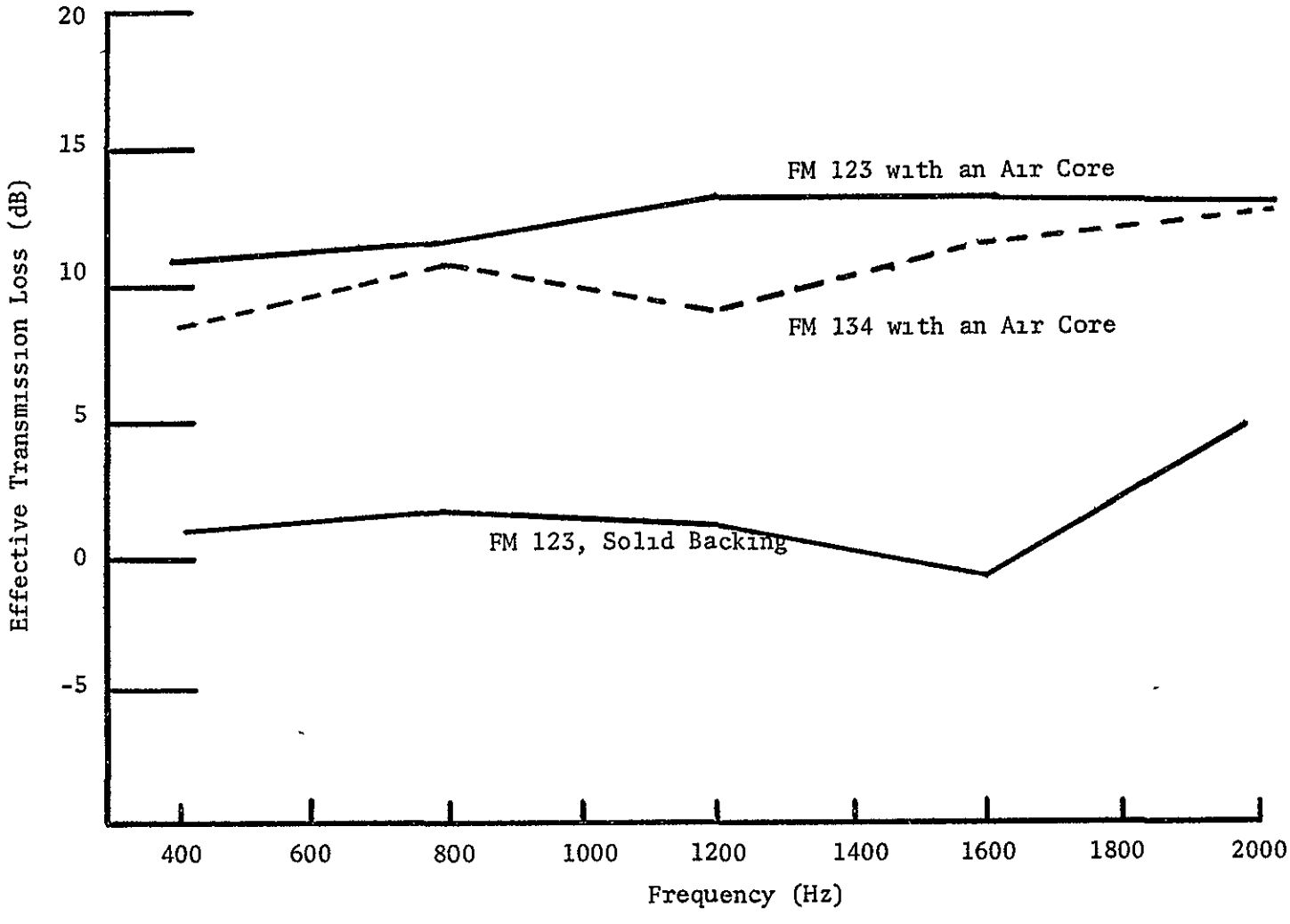

Figure 64 Effective Transmission Loss of Three Feltmetal Configurations

CHAPTER V

SUMMARY AND SUGGESTIONS FOR FUTURE RESEARCH

5.1 Statement of the Problem

The public concern over the high levels of noise produced by modern commercial and military jet aircraft has resulted in proposed federal standards for aircraft noise (1), and it has added impetus to research into new methods of suppressing and possibly eliminating fan noise radiated from the engine inlet. A promising approach to this problem is the reduction of the high frequency noise by noise suppression systems incorporated into the inlet of the engine. Most acoustic configurations are tested for their absorbing ability by propagating a plane wave either parallel or perpendicular to them. However, this is not a realistic approach to the problem because the inlet section of the engine has a helical spinning mode rather than a plane wave propagating through it and this spinning mode will impinge on a lining material at various angles of incidence.

Since the objective of this program has been to evaluate various acoustic configurations as absorbing devices and to subject these devices to a sound field which simulates the field in a jet engine environment, sound waves were directed toward a chosen acoustic configuration at various angles of incidence. These absorbing devices were then evaluated for the attenuating ability in the presence of this grazing incidence sound field.

Choosing an acoustical system to attenuate the sound required some knowledge of the basic acoustic properties of the materials used; however, there is no overall theory yet postulated that combines these properties into a simple program to obtain the best sound suppressor for a particular noise problem. Therefore, in order to shed some light on choosing the best materials to be used in the design of grazing incidence absorbers, a series of tests were conducted to determine the DC flow resistance and normal absorption coefficients of various configurations. We hoped that these basic properties used in conjunction with the configuration's grazing incidence attenuation would lead to a simplification in the designing of the acoustic systems.

5.2 Method of Approach

The design and development of laboratory equipment has been an important portion of this investigation. One of the two major pieces of equipment that have gone into the make up of this acoustic facility was a DC flow resistance device that was constructed to allow materials to be first evaluated for their flow resistance properties. The flow resistance of a pervious material can be directly related to the material's specific acoustic resistance, which is the real part of the acoustic impedance. This value is a basic acoustic property of the material and can be used to help predict the absorption characteristics of acoustic devices designed using the said material as one of its components.

The second important piece of equipment was a straight rectangular duct of constant cross section. Because the type of tests conducted in this duct is dependent upon its termination, an anechoic termination was designed to eliminate the reflections from the end of the duct and as a result to provide the traveling wave for attenuation measurements. The duct itself was then lined with the acoustic configuration of interest, and a sound wave was directed toward the sample with various grazing angles of incidence. The varying impingement angle of the traveling wave was obtained using a specially designed sound source box which contained a speaker mounted plate that could be varied from 0 to 90 degrees in relation to the duct axis.

5.3 Experimental Results

Normal absorption coefficient measurements were made on fourteen different sample configurations. These samples were placed at the end of the duct and subjected to normal incidence waves having varied frequencies from 400 to 2000 Hz. The standing wave technique was then used to find the absorption coefficient at each frequency. The normal absorption coefficient for the Scottfoam and Feltmetal absorbing configurations was continually increasing with frequency in the range tested. This could be expected because these pervious materials tend to have their resonant absorption point at a frequency higher than 2000 Hz. All porous samples have a maximum absorption at optimum values of porosity. The 100 pore

per inch material was closer to the optimum for Scottfoam than was the 80 pore per inch sample, while the FM 134 at these frequencies had the more optimum porosity of the Feltmetal samples. Of these materials, the most porous (100 pore per inch Scottfoam) had the highest value of absorption at every frequency and this value could be increased or decreased by varying the thickness of the material sample. The thicker samples offered more air pockets and resistive surfaces to dissipate the sound and consequently offer more absorption.

All of the porous samples, when tested with a solid backing, absorbed the incident sound below their maximum level, but the solid backed Feltmetal configurations tested were particularly low absorbers. This can be attributed to the high density effect of the mesh plus solid plate leaving very few air pores for pulsating dissipation. Of the two Feltmetal samples, the FM 134 mesh which had a higher porosity was the better performer of two solid backed samples.

For all the porous facing materials tested (Scottfoam and Feltmetal), the addition of an air core between the material and the backing resulted in an increase of absorption over the whole range of frequencies, however, though the values of normal absorption were increased by the air gap, none of the overall comparison trends between configurations changed, and this is worth noting because, in the grazing incidence tests to be mentioned later, the air core addition did have an effect on these trends. Two absorbing devices with perforated faces were

also tested for their normal absorption characteristics. The first configuration, a perforated face with partitioned air core, had its resonance within the frequency test band and, as a result, we were able to obtain the whole bell-shaped absorption curve. The second resonator configuration was simply a duplication of the first with a porous material core replacing the air core. This Scottfoam core had the effect of increasing the effective absorption bandwidth on the resonator; that is, the bell-shaped characteristics were spread out over a wider frequency range.

The DC flow resistance tests were conducted over a range of flow velocities that varied between 5 inches per second to a maximum of 93 inches per second obtained when the highest porosity Scottfoam was tested. As could be expected, the flow resistance varied as the air flow through the sample changed. For Feltmetal, the manufacturer quotes 50 Rayls and 35 Rayls as the acoustic resistance for FM 123 and FM 134, respectively. When our samples of these materials were flow tested, the results showed that the calculated average was in close agreement with the manufacturer's values, however, the individual values varied from this standard to a maximum deviation of 40 percent. The average value obtained for FM 123 was 50 Rayls which is the exact flow resistance the manufacturer quotes for this material. For FM 134, our tests indicate an average flow resistance of 40 Rayls or an approximate 14 percent deviation from the quoted value.

When Scottfoam was flow tested, it periodically gave irradic results. There seem to be problems associated with high velocity

testing of porous materials that were not originally anticipated because, for the very porous types, the structure breaks down at certain velocities so that the fiber construction is no longer indicative of the original material. Since we also found that as the flow velocity increased the thinner Scottfoam sample tended to buckle--a phenomenon that would distort the flow resistance characteristics--it is recommended that when using the curves in the previous chapter, the average value of flow resistance be calculated from the low velocity data. The most reliable Scottfoam flow resistance data was obtained for the lower porosity samples and these tests showed an increase in flow resistance as the thickness of the material increased. A 1/2-inch thick 80 pore per inch sample has an average flow resistance of 10 Rayls while the same material in a 1-inch thick section is 18 Rayls. The 100 pore per inch Scottfoam showed large fluctuations in resistance with flow velocity. The samples had more of a tendency to exhibit the buckling mentioned earlier and, consequently, the values of flow resistance are not as accurate. By averaging all the data, it was found that the measured flow resistance was approximately 9 Rayls for both the 1-inch thick sample and the 1/2-inch thick sample. However, if only low velocity data is considered, the 100 pore per inch Scottfoam also exhibits an increase in flow resistance with thickness.

In the grazing incidence tests, twelve different sample configurations were tested for their grazing absorption characteristics. Each of the samples were placed in the duct as

side branches and their effective transmission loss was measured as a function of frequency and incident angle. For every absorbing device tested, it was found that the effective transmission loss increased as the grazing incidence angle decreased and the test frequencies increased. When an air core was added to a facing material increasing its acoustic capacitance, there was an overall increase in transmission loss for each configuration tested. One result of particular interest was that the addition of an air core produced a greater transmission loss for the lower incidence angles than for the higher incidence angles. This result has particular ramifications and will be mentioned later in the concluding remarks.

The comparison results of the particular devices also showed some remarkable results For example, the perforated facing, which had been an effective normal incidence absorber, was a very poor attenuator of grazing incidence waves. By contrast, the Scottfoam samples plus solid backing which were not particularly good absorbers of waves with normal incidence showed very promising attenuation characteristics. The two Feltmetal samples, when backed by a solid wall, turned out to be poor absorbers in both series of tests. The air core alone improved the attenuation characteristics for all the porous samples. If you will recall, the addition of the air core in the normal incidence tests produced this same result; however, as side branches, the addition of the air core made the poorer attenuating FM 123 a better absorbing device than the FM 134 plus air core.

This result is interesting because it indicates that the addition of an air core not only increases the effective transmission loss of samples but also sometimes exhibits trends in attenuation that are not present when a material is backed just by a solid wall.

In the Scottfoam tests, the effectiveness of the material depended on the test frequency. As a general trend, the lower porosity (80 pore per inch) samples attenuated better at low frequencies, while the high porosity samples of 100 pore per inch Scottfoam attenuated better at high frequencies. As the thickness of the material increased the attenuation increased, and, as mentioned earlier, when an air core was placed behind the material, the effective transmission loss was significantly improved, particularly for the lower angles of incidence.

The results from these three sets of tests do not offer a clear cut path to the method of choosing an effective side branch absorber from its basic acoustic properties. In fact, just these data samples produced enough variation to question the feasibility of the approach. For example, Feltmetal FM 123 backed by a solid wall was a poor absorber of grazing incidence and normal incidence sound when compared to FM 134 backed by a solid wall. However, when both these materials were backed by an air core, the FM 123 plus air core turned out to be the better attenuator at grazing incidence but not the better absorber at normal incidence. We also noted that a resonator with high values of normal absorption did not exhibit good attenuation characteristics when compared to the lower absorbing porous materials. After

surveying the results one could conclude that a wider variety of data samples might help to illuminate some of these sought after trends. It is very probable that a correlation between basic acoustic properties of the facing material and the attenuating characteristics of devices using these materials exists; however, it will take a multitude of data to make these trends clear.

The grazing incidence results taken by themselves were very encouraging. The fact that the attenuation characteristics of an absorber increases as the grazing angle decreases can be used to add new assurance to the practice of using test stand designed absorbing devices in the actual jet engine ducts because, if an attenuating device is optimized in a duct with a plane wave propagating by it, the test results indicate that the grazing incidence of a wave propagating down the nacelle will be attenuated as well if not better than the wave in the duct. Another significant feature of these results is that the addition of the air core significantly increased the attenuation of the waves of lower grazing incidence. This allows one, if he knows the wave to have a low incidence angle, to place an air core on an absorbing device and be assured that he has optimized his configuration to all these low grazing waves. This should be particularly important for jet engines where weight is a design factor, for one could increase his attenuation of low grazing waves by reducing the configuration's thickness and substituting an air core for the cut away material. Thus, the

attenuation characteristics are improved and the weight of the engine reduced.

5.4 Suggestions for Further Research

The purpose of this program was to provide a preliminary engineering study of the design and performance of acoustically absorptive duct linings for jet engine inlets. The scope of the studies described herein has accomplished this objective; however, after observing the results obtained during this investigation, it is evident that these conclusions should serve as just the beginning of a program that could eventually lead to a thorough understanding of jet engine noise suppressors. One must now, using the results obtained from this program, extend the testing techniques to situations that are more representative of the environment in a jet engine duct. Also, as one reviews a study, he tends, through hindsight, to find various ways in which his procedural techniques could have been improved. In the section that follows, there is a discussion of the direction that suggested future research should take as a result of this study, and in what ways the experimental procedure used during these investigations could have been improved.

The experimental facilities were basic by nature and, consequently, left very little room for improvement. There were, however, two specific designs that could have been improved to increase the versatility of the set up. First, it is suggested that the sample holder on the flow resistance device by supplied

with some sort of brace that could securely fasten the very flexible porous samples. A brace of this type would eliminate the buckling effect mentioned earlier and allow the flow resistance device to be used for soft pervious blankets as well as for rigid materials. The second improvement that should be implemented is the acquisition of a larger variety of facing materials and the incorporation of these materials into different acoustic configurations. The problem involved in acquiring more samples is basically that of economics. Materials of the type that are applicable to engine ducts are very expensive and, consequently, cannot be ordered at random. However, I do think that selective types of materials have to be tested to realistically study some of the problems, such as air flow effects, associated with engine ducts.

At the conclusion of these tests, the results and trends obtained showed some dramatic results that could be very beneficial in the design of acoustic suppression devices for jet engines, however, before these results can actually be extrapolated, the trends must be tested under more representative conditions.

Because a liner in an engine duct is in the presence of moving air, the first suggestion would be to rerun these grazing incidence tests in the presence of a steady low velocity air flow to determine what effects, if any, this air flow has on the reported attenuation characteristics and trends of the various devices. If the trends found in the current study could be reproduced in the presence of air flow, one could devise a test

stand procedure that could be used for predicting the effectiveness of engine duct suppressors.

At the completion of the flow tests, the spinning mode synthesizer (6) should be coupled to the duct and a helical spinning wave propagated past the lining configurations. This would allow the determination of the attenuation characteristics for a wave very similar to that present in an engine duct.

As a final step in the overall understanding of how these suppressors would react in a jet engine duct, tests measuring the transmission loss in the presence of the spinning mode and air flow should be conducted. If a theoretical and experimental model can eventually be developed for this last case, one would have all of the necessary information needed for completely specifying this type of absorbing configuration that would be most effective for any particular jet engine noise suppression problem.

BIBLIOGRAPHY

1. "Noise Standards: Aircraft Type Certification, Notice of Proposed Rule Making," U.S. Department of Transportation, FAA, 14 CFR Parts 21 and 36, as Published in the Federal Register 34 F.R. 453 on January 11, (1969).

2. Lowson, M. V., "Reduction of Compressor Noise Radiation," Journal of Acoustical Society of America, 43.37-50, (1968).

3. Morfey, C. L., "A Review of the Sound Generating Mechanisms in Aircraft Engine Fans and Compressors," Proceedings of the AFOSR-UTIAS, pp. 291-331, (1968).

4. Blackman, A. W., "An Investigation of the Absorption Characteristics of Afterburner-Screech Liner Configurations," United Aircraft Corporation Research Report R-0597-10, (1957).

5. Tyler, J. M. and Sofrin, T. G., "Axial Flow Compressor Noise Studies," S.A.E. Transactions, pp. 309-332, (1961).

6. Seiner, J. M., "The Design and Development of a Spinning Mode Synthesizer," Master of Science Thesis, The Pennsylvania State University, (1969).

7. Beranek, L. L., Acoustic Measurements, John Wiley and Sons, New York, (1959).

8. Sperry, W. C., "Study and Tests to Reduce Compressor Sounds of Jet Aircraft," Quarterly Progress Report, Number 9, General Electric Company, (1967).

9. Taylor, H. O., "A Direct Method of Finding Values of Materials as Sound Absorbers," Physical Review, Volume 2, pp. 270-287, (1913).

10. Scott, R. A., "An Apparatus for Measurement of the Acoustic Impedance of Sound-Absorbing Materials," Proceedings of the Physical Society, Volume 58, pp. 253-265, (1946).

11. Marino, P. A., Bohn, N. and Garrison, G. D., "Measurement of Acoustic Resistance at Sound Pressure Levels to 171 dB," Journal of the Acoustical Society of America, Volume 41, pp. 1325-1327, (1967).

12. Morse, P. M. and Ingard, K. U., Theoretical Acoustics, McGraw-Hill Book Company, New York, (1968).

13. "Standard Method of Test for Impedance and Absorption of Acoustical Materials by the Tube Method," ASTM Standard, pp. 997-1009, (1961).

14. Meyers, G. H., "Development of an Anechoic Termination Design for an In-Duct Fan Sound Test Facility," Presented at the Acoustical Society of America Seventy-Eighth Meeting, November, (1969).

15. Beranek, L. L., Noise Reduction, McGraw-Hill Book Company, (1960).

16. Kreyzig, E., Advanced Engineering Mathematics, John Wiley and Sons, New York, (1964).

17. Rschevkin, S. N., A Course of Lectures on The Theory of Sound, Pergamon Press, New York, (1963).

18. Brennan, J. N., "A Precision Acoustic Impedance Tube," Master of Science Thesis, The Pennsylvania State University, (1949).

APPENDIX - A

Many analyses of the effect of dissipation in smooth rigid walled ducts have been conducted. (18) The attenuation in this type of apparatus is of importance not only because it affects the levels of pressure being measured, but also in the case of the standing wave, it will shift the position of the minima. The former effect is of particular interest here because it is a method of checking for appreciable dissipation by the tube walls. The investigation of this case considers the ratio of the maximum pressure amplitude to the minimum pressure amplitude when a rigid sample or perfect reflection is placed at the end of the duct. The procedure followed in this appendix was first outlined by Scott (10) and then improved by Brennan (18). For the pressure amplitude in the duct, one can write

$$P_z = A \sinh [\delta z + \psi + j(kz + \nu)] \quad , \qquad (A.1)$$

which, as Scott (10) shows, can be written

$$P_z = B[\cosh 2(\delta z + \psi) - \cos 2(kz + \nu)]^{1/2} \quad , \qquad (A.2)$$

from which he shows that the conditions for the maxima and minima are

$$2(kz + \nu) = 2n\pi - \frac{\delta}{k} \sinh 2(\delta z + \phi) \quad , \tag{A.3}$$

$$2(kz + \nu) = (2M + 1)\pi + \frac{\delta}{k} \sinh 2(\delta z + \psi) \quad , \tag{A.4}$$

where M and N are integers.

Using the identities

$$\cosh 2x = \cosh^2 x + \sinh^2 x \quad ,$$

and

$$\cosh^2 x = \sinh^2 x + 1 \quad , \tag{A.5}$$

Brennan (18) shows that the pressure P_z can be written as

$$P_z = A[2 \sinh^2 (\delta z + \psi) + 2 \sin^2 (kz + \nu)]^{1/2} \quad . \tag{A.6}$$

From Equation (A.3), Brennan (18) then shows that we can write

$$\sin (kz + \nu - N\pi) = \frac{\delta}{2k} \sinh (\delta z + \psi) \quad , \tag{A.7}$$

or

$$2 \sin^2 (kz + \nu) = \frac{\delta^2}{2k^4} \sinh^2 2(\delta z + \psi) \quad . \tag{A.8}$$

and the equation for the pressure amplitude at the minimum is

$$P_{min} = A\sqrt{2} \sinh (\delta z_n + \psi) \quad , \tag{A.9}$$

where z_n is the position of the minimum. The value of the pressure maxima is determined by writing Equation (A.2) as

$$P_z = A[2 \cosh^2 (\delta z + \psi) - 1 - \cos 2(kz + \nu)]^{1/2} \quad , \tag{A.10}$$

which can be rewritten as

$$P_z = A[2 \cosh^2 (\delta z + \psi) - \frac{\delta^2}{2k^4} \sinh 2 (\delta z + \psi)]^{1/2} \quad . \tag{A.11}$$

Here, the second term is negligible when compared with the first, and the equation can be rewritten as

$$P_{max} = A\sqrt{2} \cosh (\delta z_m + \psi) \quad , \tag{A.12}$$

where z_m is the discrete maxima location. The ratio of the amplitudes of the pressure maximum and pressure minimum is

$$\left| \frac{P_{max}}{P_{min}} \right| = \frac{\cosh (\delta z_m + \psi)}{\sinh (\delta z_m + \psi)} \quad . \tag{A.13}$$

For a rigid reflector, $\psi = 0$ and Equation (A.13) is rewritten

$$\left| \frac{P_{max}}{P_{min}} \right| = \frac{\cosh \delta z_m}{\sinh \delta z_m} \quad . \qquad (A.14)$$

Equation (A.14) is a function of three quantities. δ the attenuation constant for ducts given by

$$\delta = 38.2 \times 10^{-5} \sqrt{\frac{f}{s}} \quad , \qquad (A.15)$$

and the locations of the minimas and maximas given by

$$Z_n = \frac{N\lambda}{2} - \frac{\nu\lambda}{2} - \frac{\delta}{2k^2} \sinh 2(\delta z + \psi) \quad , \qquad (A.16)$$

and

$$Z_m = \frac{(m-1)}{2} \lambda - \frac{\nu\lambda}{2} + \frac{\delta}{2k^2} \sinh 2 (\delta z + \psi) \quad . \qquad (A.17)$$

Figure 11 shows the theoretical curve of how much higher the maximum pressure amplitude should be than the minimum pressure amplitude as a function of frequency. Also plotted in the graph in Figure 65 are the measured values of maximum and minimum pressure as a function of frequency taken in our duct. Our experimental investigation was conducted for frequencies between 100 Hz and 1500 Hz, and the difference in pressure ratios measured agreed remarkably well with those predicted by theory. All along the curve, any deviation from theoretical is negligible.

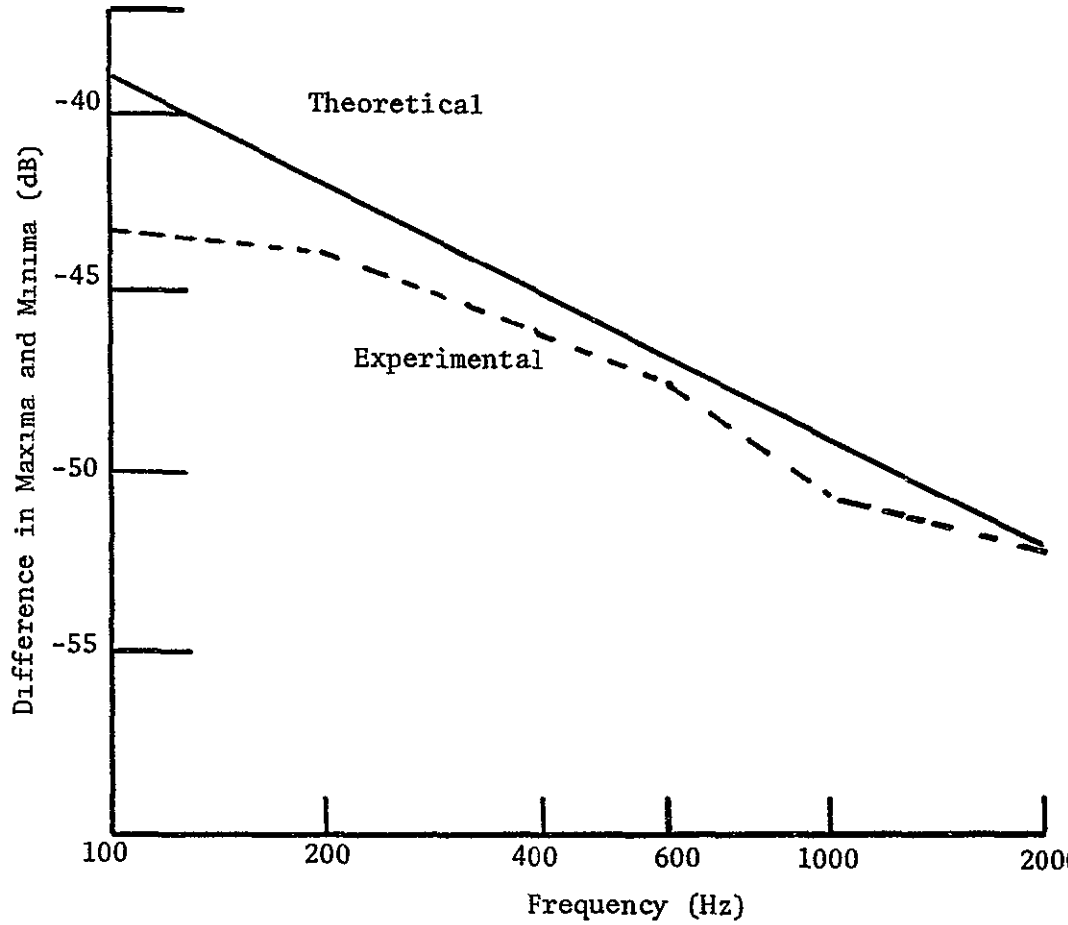

Figure 65 Pressure Amplitude Ratio

APPENDIX - B

As mentioned in Chapter II, if the probe used for the sound level measurements transmits a large amount of energy through its walls, it is highly probable that a significant amount of error can be introduced into the test results. Thus, the amount of transmission that can be tolerated without introducing a significant amount of error and how well our probe tube compared to these results will be investigated in this appendix. This theoretical study is similar to the one done by Brennan (18) in his probe tube design of a precision impedance tube.

If one takes a closed duct and sets up a standing wave, the pressure can be described by

$$P = \exp(j\omega t)\{\exp(-jkz) + T\exp[j(kz - 2\eta)]\} \quad . \quad (B.1)$$

To investigate the standing wave pattern in this duct, we are using a microphone connected to a rigid cylindrical probe tube. If we assume all the sound received by the microphone, including the sound radiated through the tube walls, can be interpreted as a standing wave, we can write an expression for this stray sound as

$$P_t = \Phi\{\exp(-jkz) + T\exp[j(kz - 2\eta + \kappa)]\}\exp(j\omega t) \quad , \quad (B.2)$$

where Φ as defined by Brennan (18) is the "coefficient of sound pick up." The resulting signal that this microphone will see is the sum of the standing wave, Equation (B.1), and the stray sound, Equation (B.2), which is

$$P_m = \Phi \{\exp(jkz) + T \exp[j(kz - 2\eta + \kappa)]\} +$$

$$\exp(-jkz) + T \exp[j(kz - 2\eta)] \exp(j\omega t) \quad . \qquad (B.3)$$

Now let us consider the case in which this stray sound will cause the maximum possible error, that is, when we are measuring a minimum. For this case, the phase angle $\eta = \frac{\pi}{2}$. Now, using the definitions of sine and cosine, we arrive at

$$P_m = \exp[j(\omega t - \beta)] [(1 + T)(\cos\beta - \Phi \sin\beta)$$

$$-j(1 - T)(\sin\beta + \Phi \cos\beta)] \quad , \qquad (B.4)$$

where $kz - \eta = \beta$. The intensity, I, of this wave is proportional to the square of the pressure, P_m. Therefore, we can show, after squaring Equation (B.4), that the intensity is given by

$$I = 1 + 2T \cos(2\beta) + T^2 - 4\Phi T \sin(2\beta)$$

$$+ \Phi^2 (1 - 2T \cos(2\beta) + T^2) \quad . \qquad (B.5)$$

Since we earlier set the phase angle η equal to 90 degrees, we can assume that the point we are measuring in the signal was at a minimum. In order to determine an expression for the minimum, Equation (B.5) is differentiated and set equal to zero. This gives as Brennan (18) shows

$$\tan 2\beta = \frac{-2\Phi}{(1 - \Phi^2)} \quad , \tag{B.6}$$

from which can be written

$$2\beta = n\pi - 2\Phi \quad . \tag{B.7}$$

In Equation (B.7), when n is odd, there is a minima and when n is even there is a maximum.

Using Equation (B.7), we can approximate that, when n is odd, the sin $2\beta = -2A$ and the cos $2\beta = -1$. Substituting these approximations into Equation (B.5), we get

$$I = (1 - T)^2 + \Phi^2 (1 + T)^2 - 8T\Phi^2 \quad . \tag{B.8}$$

At this juncture, it is normal procedure to make two simplifying assumptions. The first assumption is that the last term in Equation (B.8) is negligible when compared to the other two terms. The second assumption is that the stray sound is 90 degrees out of phase with the signal and can be represented by the diagram shown

in Figure 66. Upon making these assumptions, we will proceed to notice in Figure 66 that the maximum error will occur when the phase angle changes by 90 degrees. As a result of this, the maximum possible value of pressure amplitude is

$$P_{max} = \pm \Phi (1 - T) \quad . \qquad (B.9)$$

Equation (B.9) can never be greater than 2Φ. If we arbitrarily say that the magnitude of the error can be no more than 0.0025 of the maximum pressure, Brennan (18) has shown the Φ, the stray sound pick up, must be 52 dB below the maximum pressure level.

In order to determine how much intensity our probe tube picked up through the tube wall, a series of tests were conducted with the tip of the probe plugged. Table 1 shows how the level of intensity of the stray sound which was picked up from the plugged tube varied with frequency. The table also shows the difference in level at the microphone. These measurements were taken at three different positions in the duct. As seen in Figure 67, the error in measurements increases with frequency, but even at the highest frequency tested (2000 Hz), the intensity radiated in through the walls was 49 dB below the pressure level in the tube. By these results, we then concluded that any sound intensity transmitted through the probe tube walls could be considered negligible.

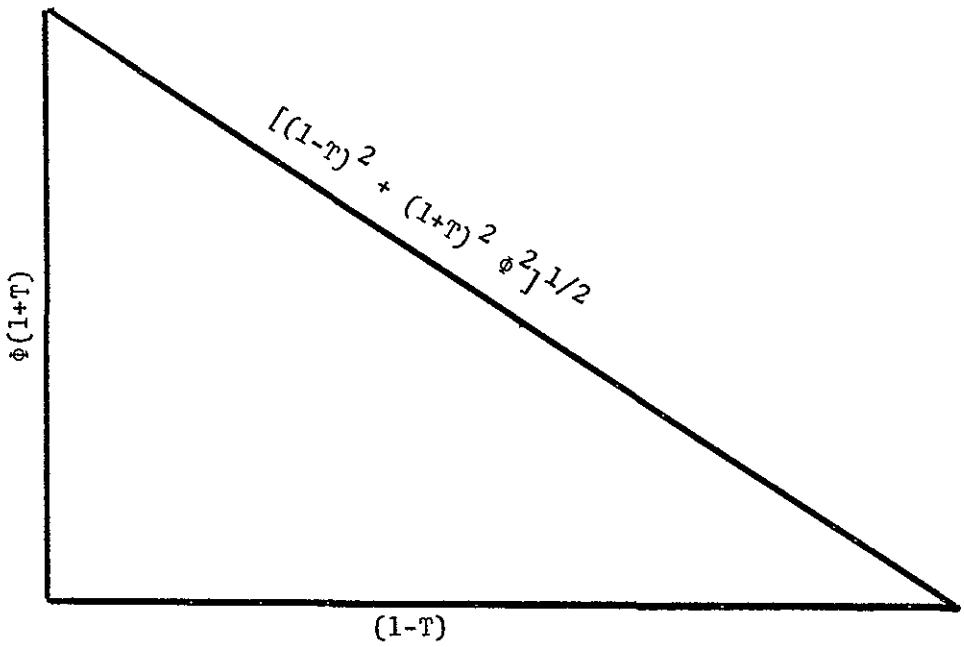

Figure 66 Stray Sound Vector Diagram

TABLE 1
SOUND RADIATED THROUGH THE WALLS OF THE PROBE TUBE

Position	Frequency (Hz)	Pressure Level (dB)	Stray Sound Level (dB)	Difference (dB)
1	200	108	52	56
2	200	108	52	56
3	200	108	53	55
1	400	110	51	59
2	400	110	52	58
3	400	110	54	56
1	600	110	55	55
2	600	110	58	52
3	600	110	55	55
1	800	109	50	59
2	800	109	51	58
3	800	110	54	56
1	1000	110	57	53
2	1000	110	57	53
3	1000	110	57	53
1	1200	99	49	50
2	1200	100	50	50
3	1200	100	49	51
1	1400	100	47	53
2	1400	100	49	51
3	1400	100	49	51
1	1600	98	49	49
2	1600	98	49	49
3	1600	98	49	49
1	1800	100	49	51
2	1800	100	49	51
3	1800	100	49	51
1	2000	100	51	49
2	2000	100	51	49
3	2000	100	51	49

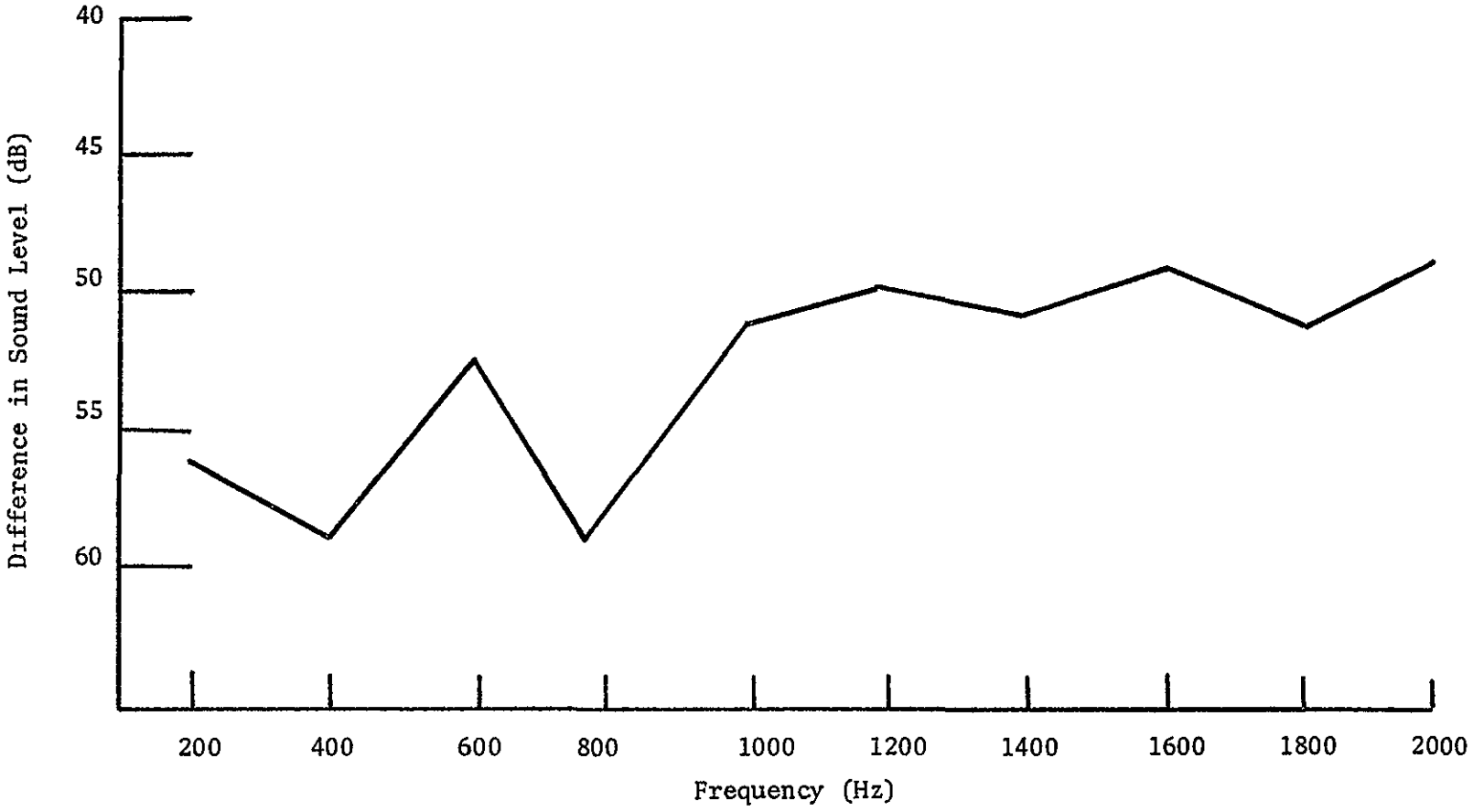

Figure 67 Sound Radiated Through the Walls of the Probe Tube